Gersonde, R., Hodell, D.A., Blum, P., et al., 1999
Proceedings of the Ocean Drilling Program, Initial Reports Volume 177

5. Site 1090[1]

Shipboard Scientific Party[2]

BACKGROUND AND OBJECTIVES

Site 1090 (proposed site TSO-3C) is located in the central part of the Subantarctic Zone on the southern flank of the Agulhas Ridge, where the topography of the ridge is more intricate than near Site 1088 to the northeast (see Figs. **F1**, p. 35; **F5**, p. 39; both in the "Leg 177 Summary" chapter). The water depth of Site 1090 (3702 m) places it near the boundary between North Atlantic Deep Water (NADW) and underlying lower Circumpolar Deep Water (CDW) (see Fig. **F2**, p. 36, in the "Leg 177 Summary" chapter). The water depth is above the calcium carbonate compensation depth and ensures preservation of calcareous microfossils during glacial and interglacial periods. Together with Site 1088 (2082 m) on the Agulhas Ridge to the northeast and Site 1089 (4620 m) in the Cape Basin, Site 1090 (3702 m) forms a depth transect that intersects most of the major water masses of the South Atlantic Ocean (see Fig. **F2**, p. 36, in the "Leg 177 Summary" chapter).

A geophysical survey of the area surrounding Site 1090 was conducted during *Thompson* Cruise TTN057 (Fig. **F1**). The seismic profile indicates a very thick (>1000 m) package of sediment overlying basement near magnetic Anomaly 34 (Upper Cretaceous) (Fig. **F2**). Two unconformities are evident in the seismic section at ~120 and 300 ms. The sedimentary succession bounded by these unconformities thickens to the southwest, and Site 1090 was selected to take advantage of maximum uniform thickness of these seismic stratigraphic units. Piston cores TTN057-6-PC4 and PS2489-2 from the vicinity of Site 1091 indicate sedimentation rates of 20–30 m/m.y. during the late Pleistocene. On the basis of this estimate, we predicted that a 200-m-deep hole at Site 1090 should penetrate late Miocene sediment. This prediction turned out to be a gross underestimate because of an unanticipated hiatus spanning ~15 m.y.

F1. Track line and shotpoints for the site survey of Site 1090, **p. 29.**

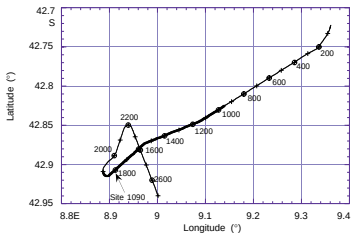

F2. Seismic line showing the location and penetration depth of Site 1090, **p. 30.**

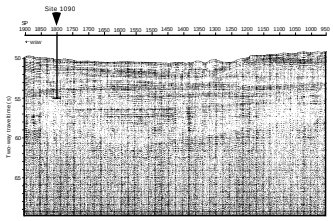

[1]**Examples of how to reference the whole or part of this volume.**
[2]**Shipboard Scientific Party addresses.**

Ms 177IR-105

The objective of Site 1090 was to recover a late Miocene–Pleistocene section at moderate temporal resolution to study (1) past migrations in the position of the Polar Front Zone; (2) changes in the mixing ratios of lower NADW and CDW in the Southern Ocean, and its relation to high-latitude climate change; and (3) the response of the Southern Ocean to orbital forcing, and the phase relationships (leads and lags) to climatic changes in the low and high northern latitudes. These objectives apply to the sedimentary record of the upper 70 meters composite depth (mcd) at Site 1090, which ranges from Holocene to late Pliocene in age. At ~70 mcd, a hiatus was encountered that documents the erosion and/or nondeposition of late Pliocene–early Miocene sediments. This unexpected hiatus presented the opportunity to recover older sediments than expected and to address the Cenozoic objectives that were not realized at Site 1088, where the recovered sedimentary section only documents a Pleistocene through middle Miocene interval and lacks a preserved signal of remanent magnetization. To recover the shallow-buried Paleogene record, we requested and received permission to deepen the holes at Site 1090 to a maximum depth of 400 meters below seafloor (mbsf).

The objectives for the early Miocene to middle Eocene part of the section below 70 mcd were to

1. Calibrate Paleogene and early Neogene biostratigraphic datums to the geomagnetic polarity time scale (GPTS) and to construct an astronomically tuned time scale for the late Paleogene–early Neogene based on the lithologic cycles observed at Site 1090. Such tuned time scales were previously obtained from sedimentary records of the Ceara Rise (Weedon et al., 1997);
2. Study marine proxies for the formation and stability of the Antarctic cryosphere during the Paleogene and early Neogene, where major differences exist in the interpretation of the extent and volume of the Antarctic ice sheet;
3. Investigate the establishment and expansion of the Antarctic Circumpolar Current during the late Paleogene and early Neogene and its implications for thermal isolation and cryospheric development on Antarctica;
4. Document changes in the production rates and chemistry of deep water in the Southern Ocean, and clarify the hypothesis of warm, saline deep-water production during the Paleogene (Kennett and Stott, 1990); and
5. Reconstruct the vertical movements of the Agulhas Ridge.

OPERATIONS

The 127-nmi transit to Site 1090 on the south flank of the Agulhas Ridge began in fair weather with a light northerly breeze that strengthened as the vessel approached the new drill site. The average transit speed was 11.0 kt. By the time the ship turned and maneuvered onto the site, however, the wind had reached gale force and large seas were building. A positioning beacon was dropped on 25 December at 1715 hr and the pipe trip began as soon as stable positioning had been achieved.

Hole 1090A

The winds continued to strengthen over the next few hours, with gusts reaching 50 kt and a large swell developing. The pipe trip was stopped (with 3305 m suspended) at 2300 hr as a result of violent pitch and heave motion that posed a hazard to personnel and the drill string. At midnight, the wind shifted from northerly to westerly but did not diminish in velocity. That caused both positioning and motion problems for the ship, with large swells at high angles to strong winds and seas. There was insufficient power to maintain station while on a minimum-roll heading, and the vessel was blown ~1.1 nmi off station to the east-northeast. Wind velocity and the northerly swell decreased slowly through the morning, and operations resumed after a weather delay of 13.25 hr. The pipe trip was completed in still marginal conditions, and the top drive and advanced hydraulic piston corer (APC) coring assembly were deployed.

Hole 1090A was spudded with an APC core shot from 3707 meters below rig floor (mbrf) at 1515 hr on 26 December. Pump pressure indicated a mechanical shear, casting considerable doubt on the quality of the mudline core. The core barrel contained 7.0 m of sediment, indicating a seafloor depth of 3709.5 mbrf. Because of the amount of scientific interest in the interface core and because of its probable poor quality, a second seafloor core was requested.

Hole 1090B

The second spud attempt was positioned 2 m higher than for Core 177-1090A-1H. Core 177-1090B-1H gave the same pressure indication, however, and recovered 4.2 m of sediment. Because of the operating conditions, no attempt was made to obtain core orientation or temperature data from Hole 1090B. APC coring continued to 185 mbsf, where the coring mode was switched to extended core barrel (XCB) because of the stiff, chalky nature of the sediment and the increasing frequency and severity of liner failures.

Excellent XCB core recovery was achieved in slowly improving weather and motion conditions. Hard drilling was encountered at 295 mbsf, and it was necessary to pull a short core and to install a hard-formation coring shoe. The thin, hard stratum was penetrated successfully by Core 33H, but the hard material was not recovered, probably because of a total core liner failure that limited recovery to less than 3 m. Subsequent cores recovered isolated thin layers of Eocene porcellanite. Core 42X reached the coring target depth at 397.5 mbsf, and the bit was then pulled back above the seafloor to end operations in Hole 1090B.

Hole 1090C

The initial core interval was positioned 3 m deeper (per drill string measurement) than that of Hole 1090B. After the rig had been offset 10 m laterally, the first core recovered an unexpectedly short 2.8 m of sediment, setting the seafloor depth at 3714.7 mbrf by convention. Seven additional APC cores were taken to a depth of 69.3 mbsf to cover the interval of primary interest. Given the unfavorable weather prognosis at that time, it was decided to pull out and start a new hole in the critical upper section before conditions could deteriorate.

Hole 1090D

The vessel was offset an additional 10 m in the direction of the positioning beacon. Again the core interval was adjusted 3 m deeper, and again a less-than-full core was recovered. The new seafloor depth was calculated to be 3713.1 mbrf. Continuous APC cores were taken to refusal, with azimuthal orientation beginning with Core 4H. Significant overpull of about 45 kips was noted on the third core beyond the point where XCB coring had began in Hole 1090B. The next core (24H) could not be freed with 100 kips overpull, and it was necessary to "drill over" with the main bit to free the APC barrel. Heave conditions allowed only about 6 m of drillover. Even then, 100 kips were required to free the core barrel, and APC refusal was acknowledged. Repeating the XCB-cored section from Hole 1090B was of secondary priority, and coring was terminated in Hole 1090D at 225.9 mbsf so that another APC section could be drilled.

Hole 1090E

Operational conditions and the available time allowed for a third hole to be drilled to the depth of APC refusal to provide complete stratigraphic coverage for that interval. The rig was offset back to the positioning coordinates of Hole 1090C, and the bit was positioned at 3714.5 mbrf for the initial core. The core recovered 8.7 m of sediment, placing the seafloor depth at 3715.3 mbrf by convention. Hole-to-hole correlation later indicated that the top of the core was taken from about 2 m below the seafloor (as planned) and that seafloor depth was near 3713 mbrf. Again, continuous APC cores were taken to refusal, with azimuthal orientation beginning with Core 4H. Weather and vessel-motion conditions began to deteriorate as operations began on Hole 1090E, and the effect on coring results was evident as core recovery was somewhat reduced in the upper portion of the section. Conditions moderated as operations progressed, but high heave continued to be a factor. Winds increased to more than 40 kt as APC coring approached refusal, but Core 25H was taken before overpull reached 90 kips and vessel motion threatened to force suspension of operations. Coring was thus completed at Site 1090, and the drill string and beacon were recovered. The *JOIDES Resolution* headed south at 1230 hr on 31 December.

LITHOSTRATIGRAPHY

Overview

Site 1090 was drilled to a total depth (TD) of 397 mbsf, recovering calcareous ooze and mud-bearing diatom and nannofossil ooze of Pleistocene to middle Eocene age (Fig. **F3**). A tephra layer and two chert layers were encountered. Carbonate and opal contents are highly variable, both ranging between 0 and ~80 wt%. The tephra layer was recovered in Cores 177-1090B-8H, 177-1090C-8H, 177-1090D-8H, and 177-1090E-7H. Above the tephra layer, a hiatus separates early Pliocene calcareous ooze from early Miocene mud-bearing diatom and nannofossil ooze (see **"Biostratigraphy,"** p. 8). Chert layers in the top of Section 177-1090B-32X-1 are apparently associated with discontinuities in interstitial water profiles (see **"Geochemistry,"** p. 19).

F3. Lithologic summary of Site 1090, **p. 31.**

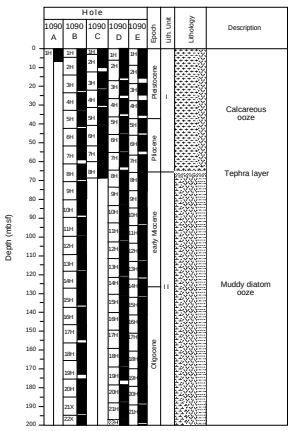

Nannofossils, diatoms, and mud comprise the major lithologic components at the site as indicated by smear-slide analyses (see the "Core Descriptions" contents list). Nannofossils are the dominant calcareous particles in smear slides, and their abundance tracks carbonate percentages downhole. Foraminifers are present in low abundance (<20%) below 70 mbsf (early Miocene to middle Eocene), and increase uphole above ~70 mbsf (Pleistocene to early Pliocene) to maximum abundances of 80%. The percentage of mud varies from a few percent to ~60% throughout most of the cores, and rarely to nearly 100%. Diatom proportions range from a few percentages to a maximum of ~90%, with highest abundances between ~100 and ~350 mbsf. Sediments between ~220 and 350 mbsf with high diatom abundances and high opal percentages were deposited with higher sedimentation rates (see "Biostratigraphy," p. 8) than the under- and overlying strata, and may indicate a period of high biologic productivity during the middle Eocene to early Oligocene.

Carbonate and nannofossil percentages covary with color reflectance (Fig. F4; see also "Physical Properties," p. 23). Smear-slide estimates of total calcareous particle, diatom, and mud abundance compare well with measurements of carbonate (by coulometry), opal (by X-ray diffraction [XRD]), and terrigenous sediment, indicating that the smear-slide data reliably characterize major downhole variations in lithology (Fig. F5).

Bioturbation is prevalent throughout the sedimentary succession and *Planolites*, Zoophycos, and *Chondrites* burrows are abundant (Figs. F6, F7).

Overall recovery at Site 1090 was 93.4% (see "Operations," p. 2). A complete splice covers approximately the upper 242 m of the section (see "Composite Depths," p. 8). Recovery averaged 92.3% below the splice in Hole 1090B (Fig. F3).

Description of Lithostratigraphic Units

Unit I

Intervals: 177-1090A-1H (0–6.87 mbsf; 0–6.87 mcd); 177-1090B-1H through 8H-4 (0–65.7 mbsf; 0.69.41 mcd); 177-1090C-1H through 8H-3 (0–62.1 mbsf; 0.5–69.91 mcd); 177-1090D-1H through 8H-1 (0–64.4 mbsf; 0.34–70.31 mcd); 177-1090E-1H through 7H-5 (0–61.0 mbsf; 3.38–69.55 mcd)
Age: Pleistocene to early Pliocene

This unit consists of Pliocene–Pleistocene meter-to-decimeter scale alternations between pale gray foraminifer nannofossil ooze and greenish gray mud- and diatom-bearing nannofossil ooze. Although the unit appears to have several hiatuses, it records lithologic variability on orbital time scales through at least the lower Jaramillo Subchron (see "Chronostratigraphy," p. 8). We have placed the lower boundary of Unit I at 70 mcd. This boundary marks a hiatus between lower Pliocene and lower Miocene strata, and appears 0.5 m above a tephra layer. The basal oozes (~69–70 mcd) of Unit I contain apparently reworked older components, indicated by mixed assemblages of Pliocene and Miocene microfossils (see "Biostratigraphy," p. 8). A few dispersed, and probably also reworked, manganese nodules are present as high as 2.5 m above the lower boundary of Unit I (Fig. F8).

F4. Variations in bulk-sediment composition at Site 1090, p. 33.

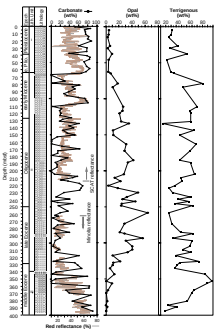

F5. Downhole lithologic abundances at Site 1090, p. 34.

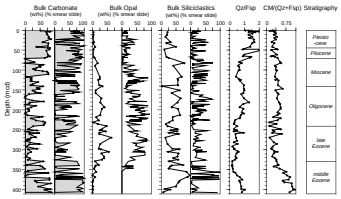

F6. Crosscutting *Zoophycos*, *Skolithos*, and *Planolites* burrows (interval 177-1090E-20H-1, 51–74 cm), p. 35.

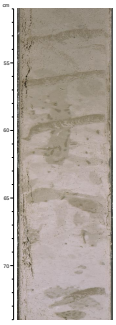

F7. *Chondrites* burrows (interval 177-1090D-17H-1, 69–97 cm), p. 36.

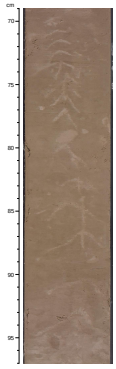

Unit II

Intervals: 177-1090B-8H-4 through 37X (65.7–339.6 mbsf; 69.41–351.59 mcd); 177-1090C-8H-3 through 8H-7 (62.1–69.3 mbsf; 69.91–77.11 mcd); 177-1090D-8H-1 through 24H (64.4–225.9 mbsf; 70.31–239.68 mcd); 177-1090E-7H-5 through 25H (61.0–236.7 mbsf; 69.55–258.14 mcd)
Age: early Miocene to early late Eocene

Unit II consists of mud-bearing diatom ooze, mud- and diatom-bearing nannofossil ooze, and chalk, between early Miocene and early late Eocene in age. The boundary between Units I and II corresponds to the Pliocene/Miocene hiatus at ~70 mcd and is associated with a lithologic change from the grayish foraminifer-bearing nannofossil ooze of Unit I to the pale reddish brown mud-rich nannofossil ooze of Unit II. Percentages of carbonate, though highly variable, are lower on average than in Units I and III. This variability is apparent in smear-slide estimates of nannofossil and diatom relative abundance, in color reflectance, and in opal abundance obtained from XRD analyses (Fig. **F5**).

Half a meter below the upper boundary of Unit II, a tephra sequence was encountered in Cores 177-1090B-8H, 177-1090C-8H, 177-1090D-8H, and 177-1090E-7H, that ranges between 34 and 70 cm in thickness. Figure **F8A** shows the relative stratigraphic position of the tephra sequence in standard ODP mbsf in the four cores, and Figure **F8B** shows the position of the tephra sequence in mcd units after adjustment on the basis of gamma-ray attenuation (GRA) bulk density and magnetic susceptibility data. The tephra sequence commences with a sharp erosional contact to the underlying ooze and consists of several graded layers of vitric volcanic ash admixed with variable amounts of hemipelagic biogenic and terrigenous particles (Fig. **F9**). Sedimentary structures and textural features, described in detail in the barrel sheets, suggest reworking and redeposition of the tephra components by turbidity currents.

A number of distinctive intervals of diatom ooze are present within the early Miocene and Oligocene–Eocene sediments at Site 1090. A prominent horizon of white to pale green diatom ooze was recovered in interval 177-1090B-22X-6, 147 cm, to 22X-7, 25 cm (base not recovered), in disrupted form in interval 177-1090D-22H-1, 91 cm, to 22H-2, 48 cm, and intact in interval 177-1090E-21H-5, 121 cm, to 21H-6, 18 cm. This bed consists of dominantly white diatom ooze with irregular green streaks and is mixed with the overlying reddish brown diatom mud. In intervals 177-1090D-20H-1, 80–90 cm, and 20H-4, 90–130 cm, burrows are filled with a distinctive white diatom ooze dominated by large *Coscinodiscus* sp. (see **"Biostratigraphy,"** p. 8). A further series of intermittently laminated diatom oozes is present in intervals 177-1090B-29X-2, 135 cm, to 29X-3, 42 cm; 29X-3, 137 cm, to 29X-4, 33 cm; 29X-5, 125–128 cm; 29X-6, 0–50 cm; 29X-6, 104–127 cm; 30X-6, 112–126 cm; and 32X-1, 6–24 cm. The diatom ooze in Section 177-1090B-32X-1 underlies a fragmented, dark green chert horizon that coincides with a major change in the interstitial water profile (see **"Geochemistry,"** p. 19). The dominant diatom genus in many of these lower intervals is *Pyxilla* (see **"Biostratigraphy,"** p. 8).

Unit III

Interval: 177-1090B-38X through 43X (339.6–397.5 mbsf; 351.59–409.49 mcd)

F8. Positions of tephra and manganese nodules in Holes 1090B–1090E, **p. 37.**

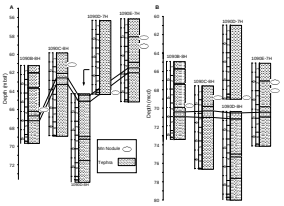

F9. Tephra sequence in Section 177-1090E-7H-4, **p. 38.**

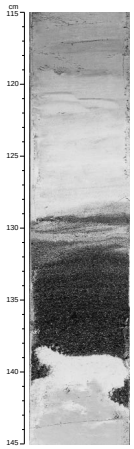

Age: early late Eocene to middle Eocene

This unit consists of middle Eocene mud-bearing nannofossil ooze, chalk, and two chert layers. Carbonate concentration shows high-amplitude fluctuations (0–80 wt%) in the upper part of this unit from ~340 to ~370 mbsf (~350–380 mcd), and higher but less variable abundances in the lower part of the unit from ~370 to 397 mbsf (~380–407 mcd). Calcareous microfossil abundance similarly rises downhole within Unit III and becomes the dominant lithologic component in the lower ~30 m of the hole. Diatom and opal abundances drop to near zero in this unit, and the highest mud abundance (from smear-slide estimates) in the hole is in the upper part of Unit III between ~340 and 397 mbsf (~350–407 mcd; Fig. **F5**). Clay abundance is also high relative to quartz and feldspar (see **"X-ray Diffraction Results,"** p. 7).

X-ray Diffraction Results

XRD measurements were made on the noncarbonate fraction of 81 samples (Table **T1**, also in ASCII format in the **TABLES** directory). Opal content of bulk sediment inferred from XRD measurements shows pronounced downhole fluctuations between 0 and 80 wt% (Fig. **F5**). Opal abundance was expressed as bulk sediment opal concentration (Fig. **F4**) using bulk carbonate concentrations (see **"Geochemistry,"** p. 19) at the same sample intervals to complete the sum of sedimentary components. Bulk opal contents in the carbonate-rich Pleistocene and Pliocene sediments of Unit I vary between 2 and 10 wt%. These values increase in early Miocene mud-rich sediments to average values of 20 wt%, with occasional peaks as high as 30 wt%. Highest average opal percentages and variability (between 15 and 65 wt%) are evident in the Oligocene and late Eocene sediments of Unit II and are associated with high variability in carbonate and terrigenous mud abundances. In the middle Eocene sediments of Unit III bulk opal concentrations drop to values <1 wt%.

T1. XRD estimates of opal and terrigenous sediment abundances for Site 1090, **p. 62.**

Quartz/feldspar and clay minerals/(quartz+feldspar) values show long-term variations at Site 1090. Quartz/feldspar values >1.0 and clay minerals/(quartz+feldspar) values <0.2 characterize the terrigenous fraction of Pliocene–Pleistocene sediments. Directly below the Miocene/Pliocene hiatus, quartz/feldspar values decrease to 0.5 whereas clay mineral/(quartz+feldspar) values slightly increase. This Neogene trend, also seen at Site 1088, may be caused by a shift in terrigenous grain size from silt to clay dominance. Both mineralogies covary downhole, probably because of changes in weathering. Periods of enhanced chemical weathering in source areas may strengthen feldspar hydrolysis and dissolution and enrich terrigenous debris in both quartz and pedogenic clay minerals.

Highest abundance of clay minerals, probably smectite and mixed-layer clay minerals (as indicated by a broad XRD reflection around 12 Å), is noted in middle Eocene sediments and is associated with low opal content and authigenic zeolite (clinoptilolite). The latter can be seen in carbonate-free smear slides as fine silt-sized euhedral crystal lathes exhibiting low birefringence. The mineralogical assemblage of smectite and zeolite could originate from diagenesis combining silicate dissolution and silica reaction with ion-rich interstitial water solutions leading to the formation of cation-rich minerals.

CHRONOSTRATIGRAPHY

Composite Depths

Multisensor track (MST) and color reflectance data (650–750 nm) collected from Holes 1090A–1090E were used to determine depth offsets in the composite section. Magnetic susceptibility, GRA bulk density, and color reflectance measurements were the primary parameters used for core-to-core correlation at Site 1090. GRA bulk density and magnetic susceptibility data were collected at 2-cm intervals on all APC cores recovered from Holes 1090A–1090D, and at 4-cm intervals on cores from Hole 1090E and Cores 177-1090B-21X through 43X. Color reflectance data were collected at 4- to 6-cm intervals on cores from Holes 1090A, 1090B, and 1090D and selected cores from Hole 1090E (see **"Physical Properties,"** p. 23, and **"Lithostratigraphy,"** p. 4, for details about MST and color reflectance data).

The data used to construct the composite section and determine core overlaps are presented on a composite depth scale in Figures **F10, F11,** and **F12**. The depth offsets that comprise the composite section for Holes 1090A–1090E are given in Table **T2** (also in ASCII format in the **TABLES** directory).

The composite data show that the cores from Site 1090 provide a continuous overlap to at least 212 mcd and possibly as deep as 245 mcd (base of Core 177-1090B-25X). The tie between the base of Core 177-1090E-22H and the top of Core 177-1090D-23H is not firm as it is supported only by an ambiguous correlation in magnetic susceptibility data between the two cores. Neither color reflectance data nor GRA bulk density data could confirm the overlap.

Stretching and compression of sedimentary features in aligned cores indicate distortion of the cored sequence. Because much of the distortion occurred within individual cores on depth scales of <9 m it was not possible to align every feature in the MST and color reflectance records accurately by simply adding a constant to the mbsf core depth. Core-scale changes will require postcruise processing to align smaller sedimentary features. Only after allowing variable adjustments of peaks within each core can an accurate estimate of core gaps be made.

Following construction of the composite depth section for Site 1090, a single spliced record was assembled for the aligned cores over the upper 245 mcd (base of Core 177-1090-25X) primarily by using cores from Holes 1090D and 1090E (Figs. **F13, F14**). The composite depths were aligned so that tie points between adjacent holes occurred at exactly the same depths in mcd. Intervals having significant disturbance or distortion were avoided when possible. The Site 1090 splice (Table **T3**, also in ASCII format in the **TABLES** directory) can be used as a sampling guide to recover a single sedimentary sequence between 0 and 212 mcd. If the splice tie between the base of Core 177-1090E-22H and the top of Core 177-1090D-23H is valid (see discussion above), the sampling splice continues until 245 mcd.

Biostratigraphy

Calcareous Nannofossils

Sediments recovered from Site 1090 provide a discontinuous Pleistocene through middle Eocene record. Pliocene–Pleistocene calcareous nannofossils are abundant to common, and good to medium preserva-

F10. Smoothed magnetic susceptibility data for Site 1090, **p. 39.**

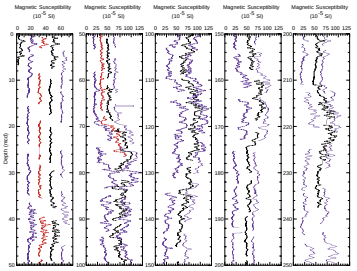

F11. Smoothed GRA bulk density data for Site 1090, **p. 40.**

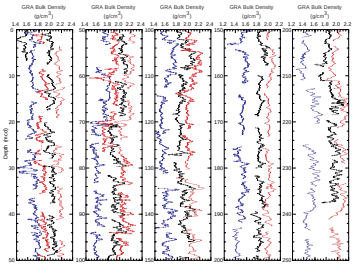

F12. Smoothed color reflectance data for Site 1090, **p. 41.**

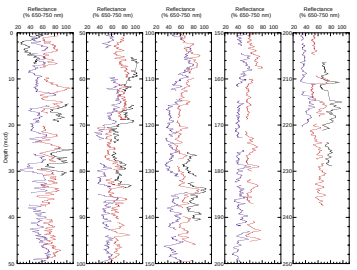

T2. Composite depths for Site 1090, **p. 64.**

tion is observed for this interval of time. Early Miocene assemblage abundances are rare to common, and no biostratigraphic marker species have been recognized. Eocene–Oligocene calcareous nannofossils are abundant to few, and preservation is moderate to poor. Some barren intervals are observed (Table T4, also in ASCII format in the TABLES directory). Besides the Martini (1971) and Okada and Bukry (1980) standard zonations, we have considered some additional events for the Pliocene–Pleistocene interval, according to Raffi et al. (1993) and Wei (1993). For the Oligocene–Eocene interval, some biostratigraphic events defined by Crux (1991) are included (see "Biostratigraphy," p. 10, in the "Explanatory Notes" chapter). For the Miocene–Eocene interval, the biochronology proposed by Berggren et al. (1995) is used.

Pleistocene

The Pleistocene sequence at Site 1090 extends from 0 to 45.0 mcd. The first occurrence (FO) of *Gephyrocapsa* medium (4–5.5 µm), between 44.05 and 43.35 mcd, is the nannofossil event that approximates the Pliocene/Pleistocene boundary (Fig. F15). The acme of *Emiliania huxleyi* defines the base of Subzone NN21b and is recognized between 2.80 and 4.20 mcd. The FO of *E. huxleyi* is tentatively placed between 56.5 and 6.0 mcd, defining the base of Subzone NN21a. The last occurrence (LO) of *Pseudoemiliania lacunosa* is present between 16.75 and 115.85 mcd, and defines the base of Zone NN20. The top and base of the small *Gephyrocapsa* acme (see "Biostratigraphy," p. 10, in the "Explanatory Notes" chapter) are not recognized from the samples analyzed; closer sampling and quantitative analyses could elucidate this acme whose occurrence has been recognized in both Sites 1088 and 1089. The LO and FO of *Reticulofenestra asanoi* are recognized at Site 1090 from 29.01 to 30.01 mcd and from 35.02 to 36.66 mcd, respectively. The reentrance of *Gephyrocapsa* medium is present between 33.51 and 35.02 mcd. The proximity between the reentrance of *Gephyrocapsa* medium and the FO of *R. asanoi* suggests the presence of a short hiatus (Fig. F15). The LO of large *Gephyrocapsa* (>5.5 µm) is observed from 36.66 to 37.61 mcd, whereas the FO of this morphotype is present from 39.61 to 40.41 mcd. The LO of *Calcidiscus macintyrei* is identified between 42.31 and 43.31 mcd (Tables T4, T5, both also in ASCII format in the TABLES directory).

Pliocene

Characteristic upper Pliocene assemblages are observed in Hole 1090B, and they allow us to identify Zones NN19 (LO *Discoaster brouweri,* 44.81–45.1 mcd) and NN18 (LO *Discoaster pentaradiatus,* 53.10–53.44 mcd). Typical markers of Zones NN16 and NN15 are absent or are extremely rare. Well-diversified and preserved assemblages are observed in Sample 177-1090B-8H-2, 140 cm (67.81 mcd), where *Reticulofenestra pseudoumbilicus* is dominant and *P. lacunosa* is absent. The lowest presence of the latter species (FO?) is recorded at 66.11 mcd, within Zones NN14–NN15, in agreement with Rio et al. (1990b) (4.0 Ma according to Gartner, 1990). *R. pseudoumbilicus* is absent at this depth. Previous workers reported a co-occurrence of *R. pseudoumbilicus* and *P. lacunosa* within Zones NN14–NN15, so we cannot exclude a hiatus between Samples 177-1090B-8H-2, 140 cm (67.81 mcd), and 8H-1, 120 cm (66.11 mcd).

A poorly preserved Miocene assemblage is observed in Hole 1090B, below 71.21 mcd. This material, comprised essentially of poorly preserved specimens of *Discoaster deflandrei* gr. and *Cyclicargolithus flori-*

F13. Spliced record of magnetic susceptibility at Site 1090, p. 42.

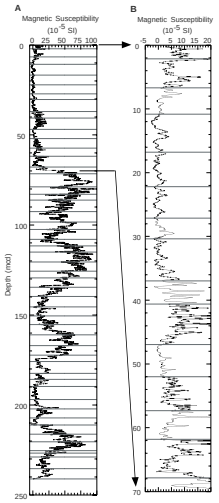

F14. Spliced record of GRA bulk density at Site 1090, p. 43.

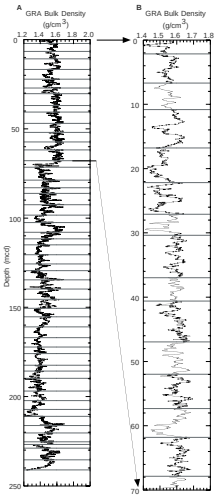

T3. Site 1090 splice tie points, p. 66.

T4. Main calcareous nannofossil species in Hole 1090B, p. 67.

danus, marks a hiatus from early Pliocene Zone NN15(?) to early Miocene Zones NN1–NN2(?).

Miocene

The presence of long-ranging species and the absence of index species prevent the identification of biozones. *Sphenolithus belemnos* and intermediate forms between *S. belemnos* and *Sphenolithus dissimilis* (Rio et al., 1990a), as well as the presence of *Calcidiscus* sp. in a few samples, indicate an early Miocene age (Zones NN1–NN2[?]) (Table **T4**).

The Miocene interval is represented in Hole 1090B between 71.21 and ~140.00 mcd. The Oligocene/Miocene boundary at Site 1090 can be placed on the basis of the LO of *Reticulofenestra bisecta* (Zones NN1–NP25) between 175.49 and 179.49 mcd.

Oligocene

The events recognized within the Oligocene interval at Site 1090 include the LO of *Reticulofenestra umbilica* (Zone NP23) from 220.70 to 221.70 mcd, and the LO of *Ismolithus recurvus* (Zone NP22) between 221.70 and 222.16 mcd (Table **T4**).

The base of the Oligocene interval is not clearly defined in Hole 1090B because the LO of *Reticulofenestra oamaruensis,* the nannofossil event that approximates this boundary, is not recognized. In fact, this species is very rare and the poor preservation of the assemblages generally prevents the identification of this marker. Other nannofossil events approximate the Eocene/Oligocene boundary in Hole 1090B: the LO of *Discoaster saipanensis* (Zone NP20) from 262.09 to 262.69 mcd, and the acme of *Clausicoccus* spp. (Zone NP21) from 232.06 to 233.86 mcd (Table **T5**; Fig. **F15**).

Eocene

A continuous record from the Eocene/Oligocene boundary (Zone NP21) to the middle Eocene (top of Zone NP15) is observed in Hole 1090B. The LO of *Discoaster saipanensis* (Zone NP21) is present between 262.69 and 262.09 mcd. Characteristic markers from Zone NP20 are not identified. The FO of *Ismolithus recurvus* (Zone NP19) is found between 301.49 and 302.99 mcd. In most cases, *Chiasmolithus* is not identified at the species level because of poor preservation; therefore, Zone NP18, whose base is defined by the FO of *Chiasmolithus oamaruensis,* is not recognized. The FO of *R. bisecta* (Zone NP17) is placed between 361.11 and 362.49 mcd and is coincident with the late/middle Eocene boundary. Between 309.39 and 361.11 mcd, *Reticulofenestra reticulata,* which is commonly in Zones NP16 through NP18, is recognized. The LO of *Nannotetrina cristata* is found between 384.57 and 390.39 mcd. The disappearance of genus *Nannotetrina* is commonly used to approximate the NP15/NP16 boundary (Table **T4**). Calibration of the above-mentioned events shows a very important diachronism (sometimes of million of years) between low and high latitudes (Berggren et al., 1995).

Planktic Foraminifers

The sediments recovered at Site 1090 span two different time intervals. In the upper cores, from the sedimentary surface to ~74 mcd, the planktic foraminifer fauna is characterized by a Pliocene–Pleistocene assemblage. Below this depth, Miocene, Oligocene, and Eocene forms were recorded only occasionally (Table **T6**, also in ASCII format in the **TABLES** directory). In the Pliocene–Pleistocene sequences, planktic foraminifers are abundant and dominate the >63-µm fraction, and the

F15. Bio- and magnetostratigraphic correlations and age designations for Site 1090, **p. 44.**

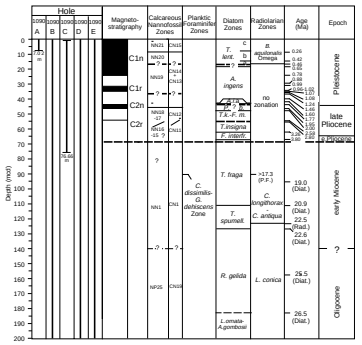

T5. Biostratigraphic age assignments for Site 1090, **p. 70.**

T6. Major planktic foraminifer species at Site 1090, **p. 76.**

preservation of planktic foraminifers is generally good to moderate. A slight decrease in preservation, which is marked by an increase in fragmentation and a decrease in the abundance of microperforate species, was recorded downhole. In general, *Neogloboquadrina pachyderma* (sinistral) is the dominant species, but *Globigerina bulloides* is often almost as abundant as *N. pachyderma* (sinistral) in the most well-preserved core-catcher (CC) samples. In addition to these two species, the planktic foraminifer fauna consists of *Globigerina quinqueloba, Globigerinita glutinata, Globigerinita uvula, Globorotalia puncticulata,* and *Globorotalia puncticuloides*. *Globorotalia inflata* was only recorded in the uppermost one or two cores in each hole. In addition, small, microperforate species (not shown in Table T6), mainly in the 63- to 150-µm fraction, make a significant contribution to the planktic foraminifer fauna. The abundance of microperforate species is lower in samples with a higher degree of fragmentation.

At Site 1090, the population of *G. puncticuloides* includes two distinct forms characterized by differences in the morphology of the last chamber. In addition to the more abundant form, which exhibits compressed margins (see Scott et al., 1990, their fig. 48), the Pliocene–Pleistocene assemblage at Site 1090 often contains relatively large specimens with a more broadly rounded final chamber. In this form the resemblance with *G. puncticulata* is stronger. The existence of different four-chambered morphotypes of *G. puncticuloides* in Pleistocene sequences from the mid- and high-latitude Southern Hemisphere gives rise to taxonomic confusion between this species and *G. puncticulata,* making it hard to establish the temporal distribution of these two species in different regions (e.g., Berggren, 1992).

Below the inferred hiatus, only rare occurrences of planktic foraminifers were recorded in the studied CC samples, and many of the samples were barren. In the Paleogene and late Neogene sediments, the preservation of planktic foraminifers was poor to moderate. In the poorly preserved CC samples many tests were partially broken or severely etched. The few specimens recorded can be divided into two groups: a lower Miocene assemblage characterized by the presence of *Catapsydrax dissimilis, C. stainforthi, Globigerina woodi,* and *Globorotalia miozea*; and a middle Eocene assemblage characterized by the presence of a few *Acarinina* species, *Chiloguembelina cubensis, Mozozovella spinulosa, Pseudohastigerina micra, Subbotina angiporoides, S. brevis, S. linaperta,* and *Truncorotaloides* spp. (Table **T6**). Because of the low abundance of planktic foraminifers and the low temporal resolution of the samples examined it is difficult to further divide the assemblages into any zonations. However, the co-existence of *C. dissimilis* and *Globoquadrina dehiscens* in Sample 177-1090D-9H-CC, 7–12 cm (90.48 mcd), suggests an early Miocene age for this sample if the warm subtropical zonation scheme by Jenkins and Srinivasan (1986) is applied (no Subantarctic or Antarctic zonation schemes use *C. dissimilis* as a marker species) (Fig. **F15**). Berggren et al. (1995) suggested a last appearance datum of *C. dissimilis* at 17.3 Ma. Furthermore, the presence of both *Acarinia primitiva* and *P. micra* in Sample 177-1090B-39X-CC, 12–22 cm (370.77 mcd) indicates that this sample belongs to Zone AP9 or AP10 in the zonal scheme of Stott and Kennett (1990) and that it is of middle Eocene age (Fig. **F15**). Future quantitative high-resolution studies of the Paleogene and late Neogene planktic foraminifer fauna at Site 1090 may provide important paleoceanographic information, especially if combined with stable isotopic studies and census counts of nannofossils. The abundance of planktic foraminifers varies markedly downhole (narrow bands of fora-

minifer sand are present), and meaningful biostratigraphic and paleoceanographic interpretations will only be possible from high-resolution sampling.

Benthic Foraminifers

Benthic foraminifers at Site 1090 are highly variable, both in abundance and preservation. Above the lithologic transition that marks the early Miocene–Pliocene unconformity, benthic foraminifers generally constitute between 5% and 10% of the total foraminifer fauna from the >63-µm fraction; these values increase to >50% in most early Miocene–Eocene samples. Absolute foraminifer abundances are variable and exhibit a clear trend toward higher values above ~67 mcd in Hole 1090B, reaching a maximum of 220 specimens/cm³ in Sample 177-1090B-3H-CC, 13–18 cm. An increase in foraminifer abundance is also observed below 361.11 mcd in Hole 1090B, notably in Sample 177-1090B-41X-CC, 0–5 cm, where 170 specimens/cm³ were recorded (Table **T7**, also in ASCII format in the **TABLES** directory; Fig. **F16**). Preservation above ~67 mcd is moderate to good and generally improves uphole. Two significant barren intervals are present in Samples 177-1090B-20H-CC through 22H-CC and 33X-CC through 35X-CC, within the Oligocene and late Eocene, respectively. Although carbonate abundances are generally low throughout these intervals, they remain highly variable (see **"Geochemistry,"** p. 19), and the low temporal resolution of the CC samples examined may have resulted in missed intervals containing foraminifers. Quantitative estimates of relative species abundance were made from Hole 1090B, with counts of up to 200 specimens per sample. Species richness is variable, with a maximum of 38 taxa recorded in Sample 177-1090B-2H-CC, 0–10 cm, and a minimum of four taxa in Samples 177-1090B-28X-CC, 16–21 cm, and 32X-CC, 13–18 cm. Some of this variability can be accounted for by sample size (see **"Biostratigraphy,"** p. 10, in the "Explanatory Notes" chapter), but the consistently low values from ~150 to 350 mcd represent an interval of generally poor preservation that corresponds to generally lower carbonate abundances.

Although certain intervals of the cored sequence appear to be far from ideal for high-resolution benthic foraminifer studies of the Paleogene/Neogene transition, the near-ubiquitous presence of extremely well-preserved specimens of *Oridorsalis umbonatus* at Site 1090 suggests that there is good potential for establishing a long benthic stable isotopic record here.

Assemblage 1: Pliocene–Pleistocene

Assemblage 1 is present in Samples 177-1090B-1H-CC through 7H-CC, from the mudline to 65.59 mcd. Biostratigraphic differentiation of the Pliocene–Pleistocene at Site 1090 is limited to the LO of *Stilostomella lepidula* in Sample 177-1090B-4H-CC, 12–17 cm, which supports a late Pleistocene age above 35.02 mcd in Hole 1090B (e.g., Thomas, 1987). This depth is below the LO of *A. ingens* (0.64 Ma) at a depth of 23.45 mcd in Hole 1090B (see **"Diatoms,"** p. 13). The benthic foraminifer assemblages of the Pliocene–Pleistocene sequence (Table **T7**) are the most diverse at Site 1090 (average number of species = 30) and are dominated by *Alabaminella weddellensis, Epistominella exigua, Melonis pompilioides,* and *Pullenia quinqueloba*. Additional taxa which are constrained to Assemblage 1 include *Pyrgo murrhiana, Stainforthia loeblichi, Triloculina trihedra,* and *Uvigerina hispidicostata*. As noted at Site 1089, these

T7. Benthic foraminifers in Hole 1090B, **p. 79.**

F16. $CaCO_3$ vs. number of specimens/cm3, number of species, and agglutinated/calcareous taxa at Hole 1090B, **p. 46.**

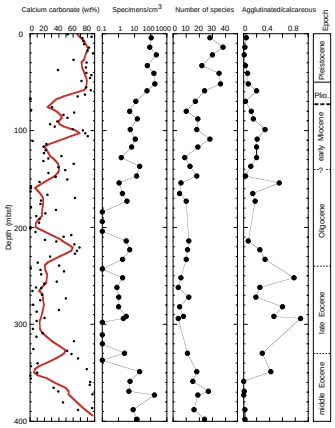

taxa, notably *E. exigua* and *A. weddellensis,* are known to respond to changes in phytodetritus supply within the flocculent layer of the ocean floor (Gooday, 1988). Because of the low temporal resolution of the CC samples examined, however, it has not been possible to establish the assemblage response through the glacial–interglacial cycles of the Pliocene–Pleistocene.

Assemblage 2: early Miocene–late Eocene

Assemblage 2 is present in Samples 177-1090B-8H-CC through 37X-CC, from 73.34 to 349.15 mcd. The benthic foraminifer assemblages are rather poor and generally very low in species diversity (average number of species = 12), suggesting that certain intervals may have been influenced by carbonate dissolution (see **"Planktic Foraminifers,"** p. 10). Low species richness and high agglutinated (noncalcareous) to calcareous benthic foraminifer ratios throughout the upper Eocene–Oligocene sequence, from ~150 to 350 mcd in Hole 1090B, suggest that this interval has, indeed, been influenced by carbonate dissolution. The most abundant taxa are *O. umbonatus, Pullenia* spp., *Stilostomella* spp., and *Ophthalmidium* spp. The LO of *Alabamina dissonata* in Sample 177-1090B-31X-CC, 27–32 cm (303.43 mcd), which ranges from the late Paleocene to latest Eocene, is of limited biostratigraphic value, but it generally supports the assignment of this interval to Zone NP19 (>36 Ma). The LO of *Nuttallides truempyi* in Sample 177-1090B-36X-CC, 26–34 cm (342.11–342.19 mcd), which is considered by Berggren and Aubert (1983) to provide a useful marker of the Eocene/Oligocene boundary, may have been influenced by the barren intervals above and is not considered a reliable event. It is possible that detailed postcruise sampling throughout this sequence may provide information on the diachroneity of this LO from the late middle Eocene to latest Eocene reported by Tjalsma and Lohman (1983).

Assemblage 3: middle Eocene

Assemblage 3 is present in Samples 177-1090B-38X-CC through 43X-CC, from 361.11 mcd to the bottom of the hole. Benthic foraminifers are moderately well preserved, with no evidence of calcite overgrowths, and both total abundances and diversity are higher in this interval (average number of species = 20), coinciding with higher carbonate abundances. The dominant taxon is *N. truempyi*, together with common occurrences of *A. dissonata, Bulimina semicostata, Cibicidoides praemundulus,* and *Stilostomella subspinosa*. The presence of *Aragonia aragonensis* in Sample 177-1090B-42X-CC, 22–27 cm (389.49 mcd), provides a potentially valuable indication of latest middle Eocene age.

Diatoms

The sediments recovered in four holes at Site 1090 consist of a Pleistocene to middle Eocene record that is disrupted by a hiatus around 69–70 mcd. The hiatus spans the lower Pliocene to lower Miocene. A few decimeters below this hiatus is a volcanic ash layer described in **"Lithostratigraphy"** (p. 4). Other hiatuses have been identified in the lower Pleistocene and upper Pliocene sequence (Fig. **F15**). To obtain a reliable biostratigraphy and to accurately identify hiatuses, we examined smear slides from Holes 1090B and 1090E in addition to the CC samples (Tables **T5, T8,** both also in ASCII format in the **TABLES** directory). In the Pliocene–Pleistocene sequence, we observed moderately preserved diatoms that generally range from few to com-

T8. Diatom, silicoflagellate, ebridian, *Actiniscus*, sponge spicule, and phytolith occurrence, Site 1090, **p. 83.**

mon in occurrence. The sediments from a few meters above and ~10–13 m below the lower Pliocene/lower Miocene hiatus bear only trace to rare diatoms, and some intervals are barren. Between ~85 and 340 mcd, diatom assemblages are generally moderately to well preserved and are common to abundant in smear slides. A distinct abundance maximum of biosiliceous components, mainly diatoms, is present between 250 and 320 mcd in the upper Eocene sequence, as also indicated by opal measurements (see **"Lithostratigraphy,"** p. 4). Middle Eocene sediments below 340 mcd are barren of siliceous microfossils. However, the presence of clinoptilolite in this interval indicates the former presence of biogenic opal that has been diagenetically transformed.

For the establishment of diatom biostratigraphic zonations at Site 1090 we used the zonations proposed by Gersonde and Bárcena (1998) and Gersonde et al. (1998) for Pleistocene to late Pliocene and Pliocene to Oligocene sediments, respectively. The stratigraphic age assignment for the Eocene was based on the zonation proposed by Fenner (1984) (see **"Biostratigraphy,"** p. 10, in the "Explanatory Notes" chapter). The diatom stratigraphic information from the four holes was combined and converted to the mcd scale. Events were placed at the midpoint of the investigated sample depth (Tables **T5, T8**).

Diatom Biostratigraphy

The base of the upper Pleistocene *Thalassiosira lentiginosa* Zone, marked by the LO of *Actinocyclus ingens,* can be placed at 18.30 mcd (Table **T9,** also in ASCII format in the **TABLES** directory; Fig. **F15**). The *T. lentiginosa* Subzone b, which ranges from the base of marine isotope Stage (MIS) 11 to the top of MIS 7 is between 7.23 and 14.58 mcd. *Thalassiosira elliptipora,* which is a marker of the *A. ingens* Subzone c, could not be identified below the *T. lentiginosa* Zone. *Fragilariopsis barronii,* which is present in the *A. ingens* Subzone a, was only observed in one sample at 44.81 mcd (177-1090B-5H-6, 130 cm), near the top of a ~2.5-m-thick interval with normal polarity (see **"Paleomagnetism,"** p. 17) interpreted to represent the Olduvai Subchron (C2n) (Fig. **F15**). This interpretation is based on the occurrence of assemblages typical of the *Proboscia barboi* Zone identified in Samples 177-1090B-5H-1, 70 cm, 5H-CC, 14–19 cm, 177-1090E-5H-1, 70 cm, and 5H-2, 70 cm, between 45.01 and 47.69 mcd. This zone stratigraphically coincides with the Olduvai Subchron. The apparent lack of most of the *A. ingens* Subzone a indicates a hiatus at or close to the top of the Olduvai Subchron and the *P. barboi* Zone. This hiatus may have removed a time record ranging minimally from 1.3 to 1.8 Ma, and may also include the upper portion of the Olduvai Subchron. The sediment in the magnetically reversed interval below the Olduvai Subchron (between ~47.7 and 56 mcd) belongs to the *Thalassiosira kolbei/Fragilariopsis matuyamae* Zone, indicated by the co-occurrence of few to common *P. barboi* and *F. matuyamae*. The nominate taxon of this zone, *T. kolbei*, was encountered only in trace amounts. From 56 to 61.8 mcd, diatom assemblages are marked by few to common *Fragilariopsis weaveri* and the absence of *Thalassiosira insigna. T. insigna* is known to have an acme in the upper portion of the Gauss Chron in southern high latitudes (Burckle et al., 1990). This indicates an age range between 2.8 and 3.26 Ma in the lower portion of the *T. insigna* Zone. The top of this interval is marked by the LO of *F. weaveri* around 2.8 Ma, occurring in Subchron C2An.1n of the Gauss Chron, whereas the LO of *T. insigna* defines the top of the *T. insigna* Zone at the top of the Gauss Chron. The absence of the nominate taxon of the *Thalassiosira vulnifica* Zone (~2.5 to 2.63 Ma) and the

T9. Control points used to calculate sedimentation rates at Site 1090, **p. 89.**

absence of *T. insigna* indicate a hiatus lasting between 2.5 and 2.8 Ma during the lowermost portion of the Matuyama to upper Gauss Chrons. The absence of both taxa cannot be explained by paleoenvironmental conditions that would exclude their presence at Site 1090, as both taxa have been reported in few to common numbers in Subantarctic waters (Fenner, 1991). Below the sediments assigned to the *T. insigna* zone, we note the presence of the nominate species of the *Fragilariopsis interfrigidaria* Zone at 62.32 mcd, whereas *F. weaveri* that has its FO in the uppermost portion of the *F. interfrigidaria* Zone is absent. The *F. interfrigidaria* Zone ranges from 3.26 to 3.8 Ma, spanning the lower portion of the Gauss and upper Gilbert Chrons. At ~67.5 mcd, we found *F. praeinterfrigidaria,* the evolutionary precursor of *F. interfrigidaria*. This indicates that sediments between ~67.5 mcd and the lower Pliocene/lower Miocene hiatus are somewhat older than 3.8 Ma (Table **T9**; Fig. **F15**).

The lower Pliocene/lower Miocene hiatus around 69–70 mcd is marked by a mixture of Pliocene and lower Miocene diatom species and is underlain by sediments that contain poorly preserved lower Miocene assemblages that do not allow a distinct age assignment. Moderately to well-preserved diatoms were recovered in Samples 177-1090E-9H-1, 70 cm, and 9H-5, 70 cm, at 85.81 and 91.81 mcd, respectively. Few to common occurrences of *Thalassiosira fraga* place this sediment in the early Miocene *T. fraga* Zone, which ranges from 17.7 to 20.8 Ma. The absence of *Thalassiosira spumellaroides,* a taxon co-occurring with *T. fraga* in the middle and lower portions of the *T. fraga* Zone, suggests that sediments below the hiatus belong to this zone (<19 Ma). Co-occurrence of both taxa was found between 95.29 and 111.4 mcd, which indicates an age between 19 and 20.8 Ma for this interval. Assemblages of the underlying *T. spumellaroides* Zone were recovered to a depth of 126.5 mcd (Table **T9**; Fig. **F15**). Rare to few occurrences of *Rocella gelida* place the underlying interval to a depth of 182.6 mcd in the *R. gelida* Zone, which ranges from 22.58 to 26.5 Ma and straddles the early Miocene/late Oligocene boundary. The co-occurrences of *Rocella vigilans* and *R. gelida* place the sediments between 157.6 and 182.6 mcd in the lower portion of the *R. gelida* Zone, between 25.5 and 26.5 Ma. The diatom biostratigraphic zonation thus indicates that the Miocene/Oligocene boundary, at 23.8 Ma (Berggren et al., 1995), is present between 126.5 and 157.6 mcd. This is consistent with the age assignments based on radiolarians (Table **T9**; Fig. **F15**). Diatom assemblages belonging to the *Lisitzinia ornata* and the *Azpeitia gombosii* Zones (early late Oligocene) have been found between 192 and 211.3 mcd.

Paleoenvironmental Implications

The early late and late early Pliocene assemblages between ~60 mcd and the hiatus are composed of diatoms that indicate rather warm sea-surface temperatures (SSTs). Taxa such as *Azpeitia nodulifer, Azpeitia tabularis, Hemidiscus cuneiformis, Fragilariopsis fossilis, F. reinholdii, Thalassionema nitzschioides, Thalassiosira oestrupii,* and *T. eccentrica* are prominent, whereas typical Antarctic taxa, such as *F. barronii* and *Thalassiosira inura* that are present in high numbers in mid-Pliocene sediments in more southern latitudes than Site 1090 (Abelmann et al., 1990; Gersonde and Burckle, 1990), are rare or absent. This supports Dowsett et al.'s (1996) conclusion based on a global survey that mid-Pliocene SSTs were higher than modern. Site 1090 was probably located north of an oceanographic system that separated more southerly cold waters from warmer waters in the north during the mid-Pliocene, comparable to the present Subtropical Front.

Radiolarians

Radiolarian biostratigraphy at Site 1090 is based on the examination of 39 CC samples (Table T10, also in ASCII format in the TABLES directory). Radiolarians are abundant to common and generally well preserved in Site 1090 sediments, except for the lower part of Hole 1090B (Samples 177-1090B-38X-CC, 8–18 cm, 39X-CC, 12–22 cm, and 43X-CC, 29–39 cm; below 349.12 mbsf [361.20 mcd]) where radiolarians are absent. Preliminary investigations indicate that at least two stratigraphic units are present throughout the recovered sequence.

T10. Main components of the radiolarian assemblage at Site 1090, p. 91.

The upper unit which is between Samples 177-1090C-1H-CC, 14–19 cm (2.80 mbsf, 3.16 mcd), and 1090D-7H-CC, 17–22 cm (62.90 mbsf, 68.98 mcd), is Pleistocene to late Pliocene in age. The four Samples 177-1090B-1H-CC, 20–25 cm (4.20 mbsf, 4.25 mcd), 1090C-1H-CC, 14–19 cm (2.80 mbsf, 3.35 mcd), 1090D-1H-CC, 12–17 cm (7.37 mbsf, 7.76 mcd), and 1090E-1H-CC, 8–13 cm (8.65 mbsf, 12.08 mcd), are correlative with the mid-latitude *Botryostrobus aquilonalis* Zone and high-latitude Omega Zone based on the absence of *Stylatractus universus*. The precise stratigraphic positions of other samples are not well understood because of the absence of index species, but Samples 177-1090B-7H-CC, 12–17 cm (59.29 mbsf, 65.64 mcd), 1090C-7H-CC, 8–13 cm (58.88 mbsf, 66.75 mcd), and 1090D-7H-CC, 17–22 cm (62.90 mbsf, 69.03 mcd), are older than 2.61 Ma based on the first appearance datum (FAD) of *Cycladophora davisiana*. Radiolarian assemblages from the upper unit are similar to known Antarctic fauna, but application of Antarctic radiolarian zonations appears to be hampered by the transitional character of the species composition.

The lower unit below the hiatus ranges in age from early Miocene to late Eocene. All Miocene samples contain *Lychnocanoma conica,* and some are correlative with the lower Miocene *Cyrtocapsella longithorax* Zone or underlying *Cycladophora antiqua* Zone. The distinction of the two zones at Site 1090 is impossible because the FAD of *C. longithorax,* which defines the base of the *Cyrtocapsella longithorax* Zone (Abelmann, 1990, 1992), seems to be below the Miocene/Oligocene boundary as suggested by Caulet (1991). Samples 177-1090B-8H-CC, 18–23 cm (69.63 mbsf, 73.39 mcd), 1090C-8H-CC, 0–5 cm (68.80 mbsf, 76.66 mcd), and 1090D-8H-CC, 17–22 cm (73.97 mbsf, 79.93 mcd), whose horizons are probably situated immediately below the hiatus, contain reworked radiolarians in moderate number. The Miocene/Oligocene boundary can be placed below Sample 177-1090B-13H-CC, 0–5 cm (117.12 mbsf, 122.60 mcd), based on the FAD of *Cyrtocapsella tetrapera* (Takemura and Ling, 1997). The Antarctic Paleogene radiolarian zones established by Takemura (1992) (i.e., *Eucyrtidium spinosum, Axoprunum irregularis,* and *Lychnocanoma conica* Zones in ascending order) are recognized in Hole 1090B. The boundary between the upper Oligocene *Lychnocanoma conica* Zone and lower to upper Oligocene *Axoprunum irregularis* Zone can be identified between Samples 177-1090B-21X-CC, 15–25 cm (194.09 mbsf, 202.20 mcd), and 22X-CC, 0–10 cm (203.69 mbsf, 211.40 mcd). This boundary is also recognized in Holes 1090D and 1090E. The boundary between the *Axoprunum irregularis* Zone and the upper Eocene to lowest Oligocene *Eucyrtidium spinosum* Zone is not well recognized yet. At present, it is certain that Sample 177-1090B-27X-CC, 13–18 cm (251.53 mbsf, 263.60 mcd), and the interval below are correlative with the *Eucyrtidium spinosum* Zone. As a whole, the assemblages from the lower unit are very similar to those reported by

Abelmann (1990, 1992), Takemura (1992), and Takemura and Ling (1997).

Paleomagnetism

Archive halves of APC and XCB cores recovered at Site 1090 were measured using the shipboard pass-through magnetometer. Measurements were made at 5-cm intervals. Sections obviously affected by drilling disturbance were not measured. Hole 1090A (Cores 177-1090B-1H through 20H) and Hole 1090D were measured after alternating-field demagnetization at peak fields of 0 (natural remanent magnetization [NRM]), 5, 10, 15, and 20 mT. Cores 177-1090B-21X through 40X were measured at peak fields of 0, 10, 20, and 25 mT. Cores 177-1090E-1H through 14H were measured at peak fields of 0, 10, and 20 mT. Cores 177-1090E-15H through 25H were measured at peak fields of 0 and 20 mT. Cores 177-1090D-4H through 24H and 177-1090E-5H through 24H were oriented using the Tensor tool, except for Cores 177-1090D-18H and 19H and 177-1090E-10H, 11H, and 17H, which were not oriented because of technical difficulties.

At Site 1090, NRM intensities vary with lithologic unit (see **"Lithostratigraphy,"** p. 4). In Unit I, the white calcareous oozes above the prominent tephra layer at ~65 mbsf in Hole 1090B (see **"Lithostratigraphy,"** p. 4) have NRM intensities between 4×10^{-2} and 1×10^{-4} A/m. In Unit II, the upper Eocene to lower Miocene red/brown oozes below the tephra layer have NRM intensities between 2×10^{-2} and 8×10^{-2} A/m. In Unit III, comprising middle Eocene oozes at the base of the recovered section, the intensities are generally $>1 \times 10^{-1}$ A/m.

Above the tephra layer at ~65 mbsf within lithologic Unit I in Hole 1090B (see **"Lithostratigraphy,"** p. 4), the inclinations of magnetic remanence (after 20-mT peak field demagnetization) indicate identifiable polarity zones (Fig. **F17**; Table **T9**). The inclination records from the three holes are, however, highly discontinuous because of poor recovery and/or drilling disturbance. The polarity interpretation given in Table **T9** and Figures **F15** and **F17** is based on the record from Hole 1090C. The two normal polarity zones within the Matuyama Chron are interpreted as the Jaramillo and Olduvai Subchrons. Correlations from Hole 1090C to the other holes imply offsets of several mbsf, which should be reconciled when the data are converted to the mcd scale.

Below 70 mbsf in Holes 1090B, 1090D, and 1090E, the inclination records indicate clearly defined polarity zones for the APC sections from Holes 1090D and 1090E, and for the APC and XCB sections from Hole 1090B (Fig. **F18**). Close to the top and base of the XCB section in Hole 1090B, at ~185 and ~340 mbsf, respectively, inclination values are highly scattered because of drilling-induced core deformation; however, the inclination pattern in the rest of the XCB section is coherent and allows polarity zones to be identified. Correlation of polarity zones to the GPTS is ambiguous because of the lack of distinctive "fingerprints" in the polarity zone pattern. The correlation must, therefore, await detailed postcruise biostratigraphy.

Stratigraphic Summary

A 397-m-thick sedimentary section spanning the interval from the Pleistocene through the middle Eocene was recovered at Site 1090. The base of Site 1090 lies at about the boundary of calcareous nannofossil

F17. Inclination of the remanent magnetization after AF demagnetization of 0–70 mbsf at Holes 1090B–1090E, **p. 47.**

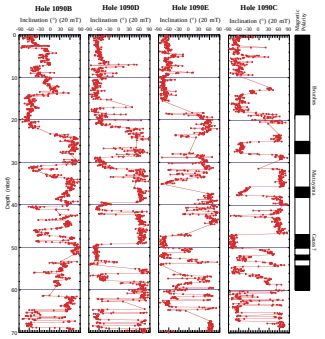

F18. Inclination of the remanent magnetization after AF demagnetization of 60–370 mbsf at Holes 1090B, 1090D, and 1090E, **p. 48.**

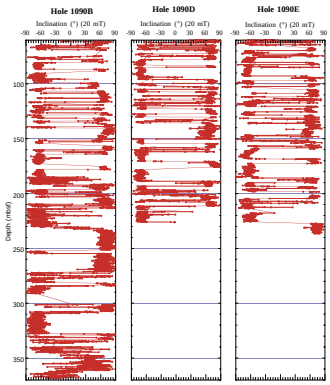

Zones NP16/NP15 of Martini (1971) or the lowermost Zone CP14 of Okada and Bukry (1980). Therefore, the basal age at Site 1090 is between 43 and 44 Ma according to the Berggren et al. (1995) time scale. The stratigraphic record is interrupted by a major hiatus at ~70 mcd, which separates lower Pliocene from upper Miocene sediments and spans ~14 m.y. Other hiatuses may occur in the Pleistocene and upper Pliocene sections of Site 1090 (Figs. **F15, F19**).

Holes 1090A–1090E were cored with the APC to 7, 173, 69, 226, and 237 mbsf, respectively. Hole 1090B was drilled with the XCB to a TD of 397 mbsf (Fig. **F15**). The combined MST and color reflectance data indicate that a continuous sedimentary section was recovered to 212 mcd and possibly as deep as 245 mcd at the base of Core 177-1090B-25X (Figs. **F10, F11, F12**).

Age assignment and calculation of sedimentation rates for Site 1090 are based on calcareous nannofossil, diatom, and radiolarian biostratigraphy, as well as measurements of geomagnetic polarity reversals (Table **T9;** Figs. **F15, F19**).

The uppermost 44 mcd corresponds to the Pleistocene. All biostratigraphic datums yield consistent age assignments to the base of the Jaramillo Subchron at ~35 mcd. Sedimentation rate averages ~35 m/m.y. (Fig. **F19B**). A combination of physical properties variations and biostratigraphic data allows the identification of MISs 4 to 12 in the upper 18 mcd (Figs. **F10, F11, F12**). The proximity of two stratigraphic datum levels, the LO of *P. lacunosa* (0.46 Ma at ~16.30 mcd) and the top of the *A. ingens* Zone (0.65 Ma at ~18.30 mcd) (Table **T9**), indicates a short hiatus during this interval (Figs. **F15, F19**). Cyclicity in color reflectance and GRA bulk density records documents the shift from the "100-k.y.-world" to the "40-k.y.-world" around 30 mcd at Site 1090 (Figs. **F13, F14**). We observe a mismatch between the diatom and nannofossil age assignments between ~35 and 43 mcd, and thus between the Jaramillo and Olduvai Subchrons within the Matuyama Chron. Diatom ages indicate continuous high sedimentation rates of ~33 m/m.y. below the Jaramillo Subchron, followed by a hiatus at ~43 mcd that spans the time interval between ~1.3 and 1.8 Ma. In contrast, calcareous nannofossil datums show a drop in sedimentation rates below the Jaramillo Subchron and a possible hiatus at ~38.5 mcd (Figs. **F15, F19B**). However, this disagreement could be related to inaccurate age calibration of the microfossil data. Improvement of the age calibrations will be possible only after integration of all Pliocene–Pleistocene stratigraphic data obtained during Leg 177.

The upper Pliocene sequences have been deposited at sedimentation rates of ~10–12 m/m.y. (Fig. **F19B;** Table **T9**). Diatom data indicate another hiatus at ~55 mcd, which approximately spans the time interval between 2.5 and 2.8 Ma. The lowermost portion of the Pliocene, below ~3.8 Ma, is missing because of a hiatus present at 70 mcd. This hiatus is underlain by a tephra layer (see **"Lithostratigraphy,"** p. 4).

The youngest sediments below the hiatus are early Miocene in age and were assigned to the *T. fraga* diatom Zone and *C. longithorax–C. antiqua* radiolarian Zone, which indicate an age of ~19 Ma or slightly younger for this interval. On the basis of diatom and radiolaria occurrences, it is estimated that the Miocene/Oligocene boundary is at ~150 mcd. Calcareous nannofossil and radiolarian data place the Oligocene/Eocene boundary at ~230 mcd. The late/middle Eocene boundary was interpreted to be at ~360 mcd. This age interpretation results in sedimentation rates of ~10 m/m.y. in the early Miocene, Oligocene, and middle Eocene, whereas calculated average sedimentation rates are ~30 m/m.y. in the late Eocene

F19. Age-depth relationship integrating biostratigraphic and geomagnetic polarity data at Site 1090, **p. 49.**

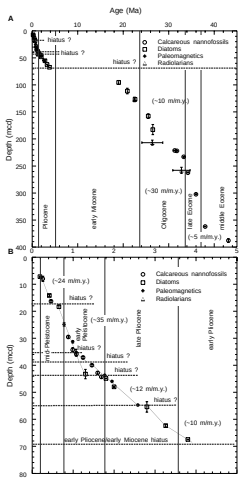

(Fig. F19A; Table T9). However, the upper Miocene to middle Eocene biostratigraphic age assignments are very preliminary because not all available stratigraphic data points have yet been identified and included in the age model. The same is true for the paleomagnetic polarity record, which displays clearly defined polarity zones in the APC as well as in the XCB sections. More detailed combined biostratigraphic and paleomagnetic studies will allow the establishment of a well-defined age model for the early Miocene to middle Eocene interval. The preliminary data hold much promise for correlating calcareous and siliceous zonations to the GPTS, which will considerably improve our knowledge of early Miocene to middle Eocene stratigraphy in southern high latitudes.

GEOCHEMISTRY

Volatile Hydrocarbons

As part of the shipboard safety and pollution program, volatile hydrocarbons (methane, ethane, and propane) were measured in the sediments of Site 1090 from every core in Hole 1090B using the standard ODP headspace sampling techniques (Table T11; Fig. F20). Headspace methane concentrations were generally low (2–9 parts per million by volume [ppmv]) throughout the sedimentary sequence at Site 1090. Ethane, propane, and other higher molecular weight hydrocarbons were not observed.

T11. Concentrations of methane at Site 1090, p. 93.

F20. Concentration of methane vs. depth at Site 1090, p. 50.

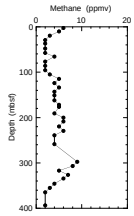

Interstitial Water Chemistry

Shipboard chemical analyses of the interstitial water from the sediments at Site 1090 followed the procedures for Sites 1088 and 1089. The results from the shipboard analyses (Table T12; Fig. F21) were obtained from 34 interstitial water samples from Hole 1090B to a depth of 392 mbsf. Generally, interstitial water samples were taken from every core to 259 mbsf (Core 177-1090B-28X). However, Cores 177-1090B-27X, 29X, and 30X were moderately to severely disturbed; the whole rounds taken from these cores were considered unacceptably contaminated and, therefore, were not squeezed. In Core 177-1090B-31X, the core liner was fractured and no interstitial water sample was taken. Fragments of chert were found in Section 177-1090B-31X-CC and the top of Core 177-1090B-32X at ~290 mbsf. Below 326 mbsf, an interstitial water sample was taken from every other core. A second chert layer was recovered in Section 177-1090B-38X-1 at ~340 mbsf (see "Lithostratigraphy," p. 4, and the "Core Descriptions" contents list for core images).

The interstitial water profiles determined by shipboard analyses for most of the chemical species at Site 1090 show relatively modest gradients downhole to 259 mbsf. Below 290 mbsf, however, there is a significant offset in nearly all of the profiles (Fig. F21). Although we have no interstitial water samples in the interval from 259 to 293 mbsf, the lack of any detectable transitional gradients either above or below this interval suggests that an impermeable layer (presumably the chert layer found in Core 177-1090B-32X) was a barrier to diffusion in interstitial waters. Thus, the interstitial water gradients above the chert layer at 290 mbsf have evolved independently of the interstitial water gradients below this layer since the formation of the impermeable barrier. This unique circumstance may permit insight into the processes controlling

T12. Interstitial water chemistry at Site 1090, p. 94.

F21. Interstitial water chemistry profiles vs. depth at Site 1090, p. 51.

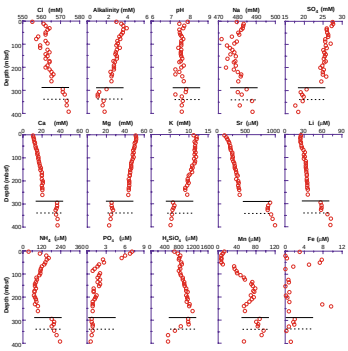

the behavior of several dissolved species. There may also be a smaller offset in some profiles below the second chert horizon at 340 mbsf (Fig. F21) but, because of low data density below 290 mbsf, the following discussion will be limited to those profiles that do not show obvious effects of the second chert layer observed at 340 mbsf.

The trends in some of the species would be nearly identical to those observed in Site 1088 if it were not for the chert layer at ~290 mbsf (Fig. F22), whereas other trends are not affected by the layer. In the uppermost part of the profile, chlorinity increases from 555 mM at 2.5 mbsf to 564 mM at 29 mbsf, similar to the increase in chlorinity seen at Site 1088. This trend is clearly not influenced by the deep diffusional barrier, for the reasons discussed in previous chapters (the downward diffusion of Cl^- with a glacial signature). However, the chloride concentration reaches a relatively constant value of ~564 mM at Site 1090, which is lower than the value of ~568 mM at Site 1088 (Fig. F22). This characteristic probably is related to the chert layer, because the water mass bathing the two sites (and diffusing into the interstitial waters) cannot have been much different.

As at Site 1088, Ca^{+2} and Mg^{+2} show an inverse behavior at Site 1090, and Sr^{+2} increases with Ca^{+2}. Above the chert layer at 290 mbsf in Site 1090, the downhole increase of Ca^{+2} and Sr^{+2} and the accompanying decrease of Mg^{+2} are less pronounced than at Site 1088 (Fig. F22); below the layer, however, the values of these cations conform to the trends extrapolated from Site 1088. In fact, the Mg/Ca values throughout the section at Site 1090 are nearly identical to those observed at Site 1088. These similarities suggest that similar processes govern the sources and sinks of these cations. They also suggest that, after the sources and sinks were restricted by the chert layer at Site 1090, the downward diffusion of seawater acted to smooth out the profiles.

Figure F23 shows a partial comparison of the major cation chemistries at Sites 1088 and 1090. The plot of Mg^{+2} vs. Ca^{+2} shows that the trends are reasonably linear suggesting conservative behavior over the sampled intervals (i.e., the major processes responsible for the gradients in Ca^{+2} and Mg^{+2} are occurring at depths deeper in the sediment column). Both Sites 1088 and 1090 also show similar $\Delta Mg/\Delta Ca \approx -1.1$ and similar Mg/Ca values with depth, suggesting that the same diagenetic processes are operating at both sites. At least three major processes have been recognized to be important in influencing Ca^{+2} and Mg^{+2} concentrations in interstitial waters: (1) seawater alteration of basalts that typically produces a $\Delta Mg/\Delta Ca \approx -0.5$ (McDuff, 1981), (2) diagenetic alteration of silicic basement or volcanic ash with a $\Delta Mg/\Delta Ca \approx -2$ (Baker, 1986), and (3) dissolution of calcite and recrystallization as dolomite, which, in the case of increasing Ca^{+2} and decreasing Mg^{+2}, would produce a $\Delta Mg/\Delta Ca \approx -1$ (Shipboard Scientific Party, 1988a); although this occurs only in very high C_{org} sediments found in continental margin settings. From the shipboard data alone, it is not possible to determine uniquely the combination of these (or other) processes controlling Ca^{+2} and Mg^{+2} concentrations at Sites 1088 and 1090; the interstitial water Sr^{+2} concentrations, however, may offer some insight.

The lower panels in Figure F23 show the Sr^{+2} vs. Ca^{+2} and Sr^{+2} vs. Mg^{+2} plots for Sites 1088 and 1090. It is possible, of course, that Sr^{+2} is governed by processes independent of those that dictate Mg^{+2} and Ca^{+2}. But the Mg^{+2} vs. Ca^{+2}, Sr^{+2} vs. Ca^{+2}, and Sr^{+2} vs. Mg^{+2} trends for Site 1090 are all relatively linear and continuous suggesting that, at least at this site, the concentration profiles of all three elements are related. At first glance it appears that Sr^{+2} diagenesis is quite different at the two sites, but at

F22. Comparison of interstitial water profiles from Sites 1088 and 1090, p. 52.

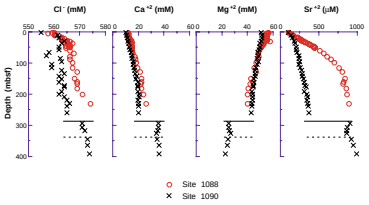

F23. Relationships among Ca^{+2}, Mg^{+2}, and Sr^{+2} at Sites 1088 and 1090, p. 53.

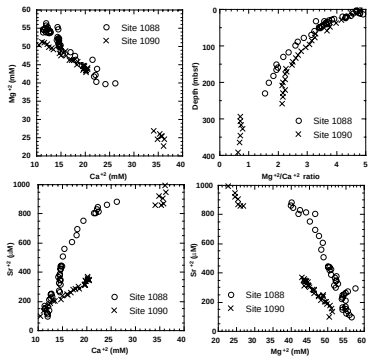

least some of the differences between the sites likely were caused by diffusional smoothing that has occurred at Site 1090 as a result of the chert layer at 290 mbsf. (It is important to note that the Sr^{+2} gradient is several times greater than either the Ca^{+2} or Mg^{+2} gradients.) Downhole Sr^{+2} increases almost always result from dissolution of biogenic carbonates and recrystallization of authigenic carbonates (Gieskes, 1983; Baker, 1986). The absolute value of the plateau in Sr^{+2} probably reflects celestite solubility (Baker, 1986; Baker et al., 1982), but there is no evidence for a decrease in Sr^{+2}, which might be expected from basalt interactions (Gieskes et al., 1986). Basement at Site 1088 is at ~1300 mbsf, and it is impossible to draw any firm conclusions about basement interaction. At Site 1090, basement is at ~800 mbsf. Thus, the 400-m section should show some evidence of basement influence on interstitial Sr^{+2} concentrations if this were an important process.

Therefore, the $\Delta Mg/\Delta Ca$ slope and the Sr^{+2} behavior suggest that carbonate diagenesis at depths greater than 400 mbsf is the primary factor responsible for the observed gradients in Ca^{+2}, Mg^{+2}, and Sr^{+2} at Site 1090. Still, it will be necessary to model these data with interstitial water $\delta^{18}O$ (and possibly also Sr isotopes) to sort out the relative importance of various processes affecting Ca^{+2}, Mg^{+2}, and Sr^{+2} concentrations. At the very least, it is clear that the gradients in the upper 290 m of the section at Site 1090 were much greater prior to formation of the chert layer at 290 mbsf.

The K^+ and Li^+ profiles also suggest a deep sink and source, respectively, below the chert layer. Presumably, interstitial waters are exchanging K^+ and Li^+ with basement or basalts deeper in the sediments below the diffusion barrier, whereas diffusional smoothing occurs above the layer. Silicate increases quite gradually to values near opal saturation above the chert layer; it then decreases below the chert layer for reasons not entirely clear, although the decrease could be related to the observation of zeolite at the base of the section (see **"Lithostratigraphy,"** p. 4).

The redox chemistry of Site 1090 can be characterized generally as suboxic, with sulfate reduction occurring at very low rates, perhaps only in narrow horizons or microenvironments, as evidenced by the relatively small decreases in sulfate with depth. A small, 1- to 2-mM, decrease in sulfate together with small peaks in alkalinity and ammonium at 30 mbsf suggest that sulfate reduction may be somewhat more important near this interval. A small peak in dissolved Fe^{+2} of ~8 µM at 40–50 mbsf may be the result of dissolved Fe^{+2} diffusing away from organic-rich bands that had previously concentrated iron by localized reducing conditions. It may also be related to a peak in magnetic susceptibility (see **"Physical Properties,"** p. 23). More detailed solid phase analyses in this section are required to identify the sources of this dissolved iron. Downhole, Mn^{+2} begins increasing at ~58 mbsf, with a broad peak of ~75 µM between 150 and 200 mbsf. The jump in Mn^{+2} from 9 to 33 µM between 58 and 66 mbsf may be related to a 10- to 15-cm-thick tephra layer observed just below this level at ~67 mbsf in Section 177-1090B-8H-4 (see **"Lithostratigraphy,"** p. 4). The broad peak in Mn^{+2} from ~150 to 200 mbsf suggests that relic, solid phase oxidized Mn has survived burial and is actively being reduced. Intact manganese nodules were observed at shallower depths (Cores 177-1090B-8H, 177-1090C-8H, 177-1090D-7H, and 177-1090E-7H; see **"Lithostratigraphy,"** p. 4, and the **"Core Descriptions"** contents list for core images), indicating that Mn-oxides do survive burial to significant depths at this site. A second dissolved Fe^{+2} peak of ~10 µM is observed at ~235 mbsf.

This peak is less well defined, and interpretation is hampered by having only one sample below this depth and the chert layer. However, if the explanation for the broad Mn^{+2} peak is correct, the Fe^{+2} peak at ~235 mbsf likely represents the standard diagenetic sequence for reduction of potential electron acceptors for organic-matter oxidation in marine sediments. Thus, Mn-oxides are reduced before Fe-oxides by virtue of the higher free energy available for oxidation of organic carbon by Mn-oxides vs. Fe-oxides (Froelich et al., 1979):

$$O_2 \rightarrow NO_3^- \rightarrow Mn^{+4} \text{ (as } MnO_2) \rightarrow Fe^{+3} \text{ (as FeOOH)} \rightarrow SO_4^{-2} \rightarrow HCO_3^-.$$

Taken together, these data suggest that the downhole gradient in sulfate may be the remnant of diffusional gradients that were in place before the formation of the chert layer, and may not be the result of sulfate reduction in the upper 250 m of the section. It is likely that some sulfate reduction is occurring or has occurred in these sediments, but it has never become pervasive enough to clear the sedimentary column of reactive Mn- and Fe-oxides. Thus, the gradients in all the major cations and anions, even the biologically active sulfate ion, appear to reflect processes occurring deep in the sedimentary column.

Solid Phase Analysis

The shipboard solid phase analysis at Site 1090 consisted of measurements of inorganic carbon, total carbon (TC), total nitrogen (TN), and total sulfur (TS) (for methods see **"Geochemistry,"** p. 18, in the "Explanatory Notes" chapter). The results of Hole 1090B are presented in Table **T13** and Figure **F24**. Calcium carbonate ($CaCO_3$) contents in Hole 1090B range from 0.6 to 90.7 wt%, with an average value of 39.3 wt%. In the Pliocene–Pleistocene sequence above ~65 mbsf (see **"Lithostratigraphy,"** p. 4), $CaCO_3$ shows relatively stable and high values averaging ~76 wt%, whereas, below 65 mbsf, $CaCO_3$ shows high-amplitude short-term fluctuations. These high-amplitude fluctuations in $CaCO_3$ content correspond to the alternations of light nannofossil ooze and nannofossil-poor terrigenous sediment. Long-term fluctuations in $CaCO_3$ content, which are shown smoothed with a 7-point running mean in Figure **F24**, might also be linked to changes in biogenic opal concentrations (see **"Lithostratigraphy,"** p. 4). These data suggest that the sedimentary sequence in the late Eocene is characterized by low $CaCO_3$ and high opal content.

Total organic carbon (TOC) contents vary between 0 and 0.61 wt%, with an average value of 0.19 wt%. Most TOC concentrations, measured as the difference between TC and carbonate carbon, are below 0.5 wt%. Many samples have TOC concentrations below the detection limits of the technique, with the difference between TC and carbonate carbon yielding negative values. TN contents are generally low (0.04–0.12 wt%). TS values are also generally low (nearly zero) from 0 to 100 mbsf and from 310 mbsf to the bottom of Hole 1090B. However, slightly higher sulfur contents are observed from 180 to 310 mbsf, corresponding to a late Eocene–Oligocene opal-rich interval (see **"Lithostratigraphy,"** p. 4). These data may suggest that the environment of deposition tended toward anoxia because of increased productivity and/or restricted deep-water ventilation in this region during the late Eocene and Oligocene. TOC/TN values vary between 0.4 and 10.7, indicating a predominance of marine organic material. Relatively high TOC/TN values are observed in the lower section below 290 mbsf. Pyrolysis analyses

T13. Concentrations of IC, $CaCO_3$, TC, TOC, TN, TS, and TOC/TN at Site 1090, **p. 96.**

F24. $CaCO_3$, TOC, TN, TS, and TOC/TN vs. depth at Site 1090, **p. 54.**

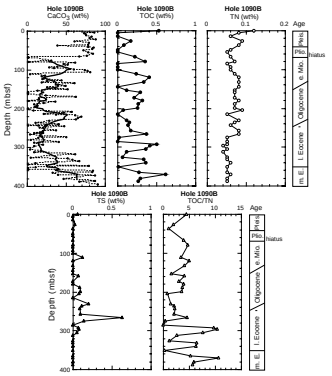

were not made because of the organic-carbon-poor nature of the sediments.

PHYSICAL PROPERTIES

GRA bulk density, magnetic susceptibility, natural gamma-ray (NGR) emission, and *P*-wave velocity were measured with the MST on whole-core sections recovered from Site 1090 (Table T14). Color reflectance and resistivity were measured on the working half of all split APC cores using the Oregon State University Split Core Analysis Track (OSU-SCAT) (see "Lithostratigraphy," p. 5, in the "Explanatory Notes" chapter). Color reflectance was also measured with the Minolta CM-2002 spectrophotometer on cores from Hole 1090B (Table T14). Other physical properties measurements conducted on discrete core samples included moisture, density, and *P*-wave velocity. Measured parameters were initial wet bulk mass (M_b), dry mass (M_d), and dry volume (V_d). Velocity was measured on split-core sections using the *P*-wave velocity sensor 3 (PWS3). Table T14 summarizes the physical properties measurements performed and their sampling frequency.

Multisensor Track and Density

There is good agreement between discrete-sample (determined using the moisture and density [MAD] method) and GRA bulk densities (Figs. F25, F26, F27). Densities range between 1.2 and 1.8 g/cm³. The trend in bulk density at Site 1090 is mainly controlled by downhole variations in carbonate vs. biogenic opal concentrations. Highest densities are associated with carbonate oozes in the top 70 and bottom 100 m, and lowest densities occur between 250 and 320 mcd, corresponding to an interval that is particularly rich in diatom ooze. There is a sharp drop in density across a disconformity that occurs around 70 mcd, below which biogenic opal becomes a significant component of the sediment and carbonate content decreases (see "Lithostratigraphy," p. 4). GRA bulk density generally covaries with magnetic susceptibility and NGR records. The dominant period of this cyclicity is approximately 50–60 m, and superimposed on this signal is a higher frequency cyclicity with a period of ~5 m.

In the uppermost 40 mcd, resistivity, GRA bulk density, NGR emission, and reflectance show a cyclicity with a period of ~5 m (Fig. F26), which is not well represented in the magnetic susceptibility record. Reflectance and NGR show an inverse correlation, probably as a result of dilution of the more radiogenic terrigenous minerals by carbonate (i.e., low NGR emission and high reflectance). The low porosity of the carbonate results in the high resistivity and GRA bulk density observed.

There is one notable exception to the otherwise good correlation between resistivity, GRA bulk density, magnetic susceptibility, and NGR below 350 mcd, where the magnetic susceptibility record becomes particularly noisy, possibly related to large fluctuations in carbonate content or introduction of gravel contamination during the drilling process (see "Lithostratigraphy," p. 4).

P-wave Velocity

P-wave velocities measured with the PWS3 velocimeter were slightly greater on average than those logged by the *P*-wave logger (PWL) of the

T14. Physical properties measurements conducted at Site 1090, p. 98.

F25. Site 1090 porosity, resistivity, *P*-wave velocity, bulk density, magnetic susceptibility, and NGR, p. 55.

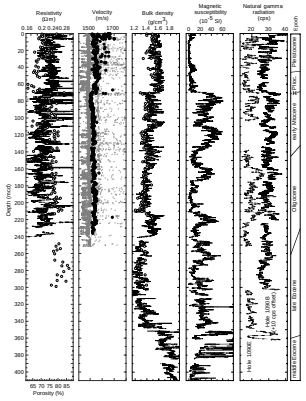

F26. Covariance between resistivity, density, magnetic susceptibility, NGR, and reflectance in the upper 70 mcd, p. 56.

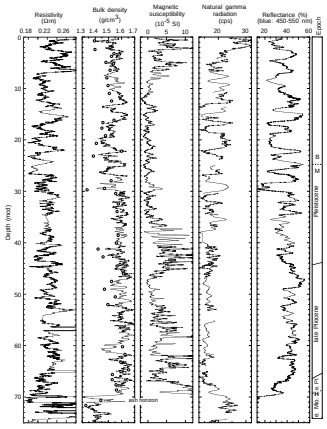

F27. Relationship between GRA and MAD bulk density at Site 1090, p. 57.

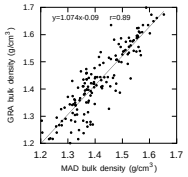

MST. In both records, velocities were fairly constant with depth (Fig. F25). The greater scatter in PWL data is probably an artifact of the quality of the contact between the core liner and the sediment or of a wrong threshold setting (see "Physical Properties," p. 21, in the "Explanatory Notes" chapter). This may result in a lower signal level and the second rather than first wavelet being auto-picked by the PWL. This leads to longer traveltimes and lower velocities being recorded.

Resistivity and Porosity

Porosity determined gravimetrically on discrete samples (MAD method) ranged from 87% to 62% at Site 1090. Porosities were actually greatest in the deeper part of the hole between 250 and 300 mcd (Fig. F25), the same interval in which bulk densities were smallest. This reflects the greater water content of siliceous ooze as well as the lower grain density of biogenic opal, as compared with carbonate. Resistivity shows the expected inverse relationship with porosity, with the greater average values (0.224 Ωm) that are associated with high carbonate concentration occurring within the upper 70 mcd. Resistivity decreases sharply below this depth, with the exception of discrete spikes of ~2 Ωm within the tephra layer at 71 mcd (Figs. F25, F26). Below the tephra layer, resistivity values range from 0.1 to 0.5 Ωm, with average values around 0.2 Ωm.

Diffuse Spectral Reflectance

Diffuse reflectance of APC recovered sediments from Site 1090 was measured with the OSU-SCAT system at 4- to 6-cm resolution. The XCB sediments from Hole 1090B were scanned with the handheld Minolta CM-2002 spectrophotometer at a nominal resolution of 5 cm to avoid fractures and coring disturbance. For comparison with the OSU-SCAT data, averages in the blue (450–550 nm) and red (650–700 nm) bands were calculated.

Sediments from Site 1090 exhibit rhythmic variations in reflectance on depth scales ranging from decimeters to several meters (see Fig. F4). Down to the hiatus at 70 mcd, cyclic changes in sediment color are reminiscent of classic Southern Ocean carbonate stratigraphic sections such as those recovered at ODP Site 704 (Shipboard Scientific Party, 1988b). Below the hiatus, there is evidence of cyclic color variability in both the APC (see Fig. F4) and XCB (Fig. F28) sediments recovered, although postcruise analysis with firm age control will be required to elucidate the exact nature of this variability.

Comparison of OSU-SCAT blue and red reflectance to carbonate measurements (see "Geochemistry," p. 19) indicates a clear relationship (Fig. F29). This pattern is similar in character to that observed in North Atlantic sediments at ODP Site 984 (Shipboard Scientific Party, 1996) and is observed for Pliocene–Pleistocene sediments from Sites 1088–1090, as well as early Miocene sediments below the hiatus at Site 1090. Interestingly, whereas red reflectance and carbonate data from Pliocene–Pleistocene sediments plot along a single trajectory, lower Miocene to middle Eocene sediments from Site 1090 are systematically redder. This increase in red reflectance is presumably caused by the downhole increase in red-clay content as indicated by visual observation and XRD analysis (see "Lithostratigraphy," p. 4). This systematic behavior can be clearly seen in a plot of blue and red reflectance vs.

F28. Minolta spectral reflectance in the red band from Hole 1090B, p. 58.

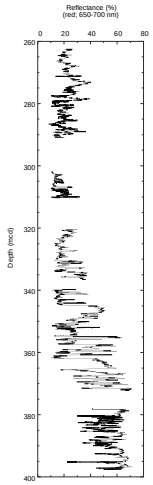

F29. Comparison of OSU-SCAT reflectance to carbonate measurements from Sites 1088–1090, p. 59.

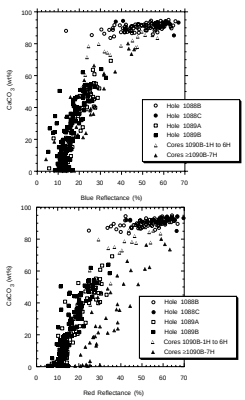

depth. Sediments above the hiatus exhibit a smaller red/blue contrast than those below (Fig. F30).

Thermal Conductivity

A total of 166 thermal conductivity measurements were made on cores from three holes at Site 1090 (Table T15, also in ASCII format in the TABLES directory; Fig. F31). The measured values range from 0.65 to 1.22 W/(m·K). The highest values (>1.15 W/[m·K]), measured from the bottom of the hole, are associated with the highest carbonate values. The lowest values measured (<0.7 W/[m·K]) correlate with distinct diatom ooze layers. Therefore, the first peak mode in the distribution of thermal conductivity values at 0.8 W/(m·K) appears to represent lithologies dominated by siliceous oozes, and the second peak mode at 1.0 W/(m·K) is associated with calcareous oozes (Fig. F31). Thermal conductivity is expected to be controlled mainly by interstitial water content and grain density, and the measurements from this site exhibit a significant linear relationship between thermal conductivity and bulk density measurements, yielding a correlation coefficient of 0.88 (Fig. F31).

F30. Site 1090 blue and red reflectance, p. 60.

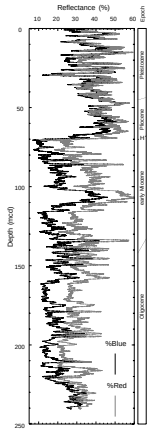

T15. Thermal conductivity measurements at Site 1090, p. 99.

F31. Thermal conductivity measurements at Site 1090, p. 61.

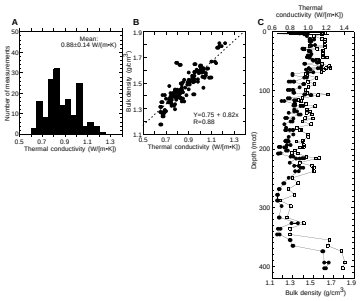

REFERENCES

Abelmann, A., 1990. Oligocene to middle Miocene radiolarian stratigraphy of southern high latitudes from Leg 113, Sites 689–690, Maud Rise. *In* Barker, P.F., Kennett, J.P., et al., *Proc. ODP, Sci. Results,* 113: College Station, TX (Ocean Drilling Program), 675–708.

————, 1992. Early to middle Miocene radiolarian stratigraphy of the Kerguelen Plateau, Leg 120. *In* Wise, S.W., Jr., Schlich, R., et al., *Proc. ODP, Sci. Results,* 120: College Station, TX (Ocean Drilling Program), 757–783.

Abelmann, A., Gersonde, R., and Spiess, V., 1990. Pliocene-Pleistocene paleoceanography in the Weddell Sea: siliceous microfossil evidence. *In* Bleil, U., and Thiede, J. (Eds.), *Geologic History of the Polar Oceans: Arctic Versus Antarctic:* NATO ASI Ser., Ser. C, 308:729–759.

Baker, P.A., 1986. Pore-water chemistry of carbonate-rich sediments, Lord Howe Rise, Southwest Pacific Ocean. *In* Kennett, J.P., von der Borch, C.C., et al., *Init. Repts. DSDP,* 90: Washington (U.S. Govt. Printing Office), 1249–1256.

Baker, P.A., Gieskes, J.M., and Elderfield, H., 1982. Diagenesis of carbonates in deep-sea sediments: evidence from Sr^{2+}/Ca^{2+} ratios and interstitial dissolved Sr^{2+} data. *J. Sediment. Petrol.,* 52:71–82.

Berggren, W.A., 1992. Neogene planktonic foraminifer magnetobiostratigraphy of the southern Kerguelen Plateau (Sites 747, 748, and 751). *In* Wise, S.W., Jr., Schlich, R., et al., *Proc. ODP, Sci. Results,* 120 (Pt. 2): College Station, TX (Ocean Drilling Program), 631–647.

Berggren, W.A., and Aubert J., 1983. Paleogene benthonic foraminiferal biostratigraphy and bathymetry of the Central Coast Ranges of California. *In* Brabb, E.E. (Ed.), *Studies in Tertiary Stratigraphy of the California Coast Ranges*. Geol. Surv. Prof. Pap. U.S., 1213:4–21.

Berggren, W.A., Kent, D.V., Swisher, C.C., III, and Aubry, M.-P., 1995. A revised Cenozoic geochronology and chronostratigraphy. *In* Berggren, W.A., Kent, D.V., Aubry, M.-P., and Hardenbol, J. (Eds.), *Geochronology, Time Scales and Global Stratigraphic Correlation*. Spec. Publ.—Soc. Econ. Paleontol. Mineral. (Soc. Sediment. Geol.), 54:129–212.

Burckle, L.H., Gersonde, R., and Abrams, N., 1990. Late Pliocene-Pleistocene paleoclimate in the Jane Basin regions: ODP Site 697. *In* Barker, P.F., Kennett, J.P., et al., *Proc. ODP, Sci. Results,* 113: College Station, TX (Ocean Drilling Program), 803–809.

Caulet, J.-P., 1991. Radiolarians from the Kerguelen Plateau, Leg 119. *In* Barron, J., Larsen, B., et al., *Proc. ODP, Sci. Results,* 119: College Station, TX (Ocean Drilling Program), 513–546.

Crux, J.A., 1991. Calcareous nannofossils recovered by Leg 114 in the subantarctic South Atlantic Ocean. *In* Ciesielski, P.F., Kristoffersen, Y., et al., *Proc. ODP, Sci. Results,* 114: College Station, TX (Ocean Drilling Program), 155–177.

Dowsett, H., Barron, J., and Poore, R., 1996. Middle Pliocene sea surface temperatures: a global reconstruction. *Mar. Micropaleontol.*, 27:13–25.

Fenner, J., 1984. Eocene-Oligocene planktic diatom stratigraphy in the low latitudes and the high southern latitudes. *Micropaleontology,* 30:319–342.

Fenner, J.M., 1991. Late Pliocene-Quaternary quantitative diatom stratigraphy in the Atlantic sector of the Southern Ocean. *In* Ciesielski, P.F., Kristoffersen, Y., et al., *Proc. ODP, Sci. Results,* 114: College Station, TX (Ocean Drilling Program), 97–121.

Froelich, P.N., Klinkhammer, G.P., Bender, M.L., Luedtke, N.A., Heath, G.R., Cullen, D., Dauphin, P., Hammond, D., Hartman, B., and Maynard, V., 1979. Early oxidation of organic matter in pelagic sediments of the eastern equatorial Atlantic: suboxic diagenesis. *Geochim. Cosmochim. Acta,* 43:1075–1090.

Gartner, S., 1990. Neogene calcareous nannofossil biostratigraphy, Leg 116 (Central Indian Ocean). *In* Cochran, J.R., Stow, D.A.V., et al., *Proc. ODP, Sci. Results,* 116: College Station, TX (Ocean Drilling Program), 165–187.

Gersonde, R., and Bárcena, M.A., 1998. Revision of the late Pliocene–Pleistocene diatom biostratigraphy for the northern belt of the Southern Ocean. *Micropaleontology*, 44:1–15.

Gersonde, R., and Burckle, L.H., 1990. Neogene diatom biostratigraphy of ODP Leg 113, Weddell Sea (Antarctic Ocean). *In* Barker, P.F., Kennett, J.P., et al., *Proc. ODP, Sci. Results,* 113: College Station, TX (Ocean Drilling Program), 761–789.

Gersonde, R., Spiess, V., Flores, J. A., Hagen, R., and Kuhn, G., 1998. The sediments of Gunnerus Ridge and Kainan Maru Seamount (Indian sector of Southern Ocean). *Deep-Sea Res. Part I,* 45:1515–1540.

Gieskes, J.M., 1983. The chemistry of interstitial waters of deep-sea sediments: interpretation of deep-sea drilling data. *In* Riley, J.P., and Chester, R. (Eds.), *Chemical Oceanography* (Vol. 8): London (Academic), 221–269.

Gieskes, J.M., Elderfield, H., and Palmer, M.R., 1986. Strontium and its isotopic composition in interstitial waters of marine carbonate sediments. *Earth Planet. Sci. Lett.,* 77:229–235.

Gooday, A.J., 1988. A response by benthic foraminifera to the deposition of phytodetritus in the deep sea. *Nature,* 332:70–73.

Jenkins, D.G., and Srinivasan, M.S., 1986. Cenozoic planktonic foraminifers from the equator to the sub-antarctic of the southwest Pacific. *In* Kennett, J.P., von der Borch, C.C., et al., *Init. Repts. DSDP,* 90: Washington (U.S. Govt. Printing Office), 795–834.

Kennett, J.P., and Stott, L.D., 1990. Proteus and Proto-oceanus: ancestral Paleogene oceans as revealed from Antarctic stable isotopic results: ODP Leg 113. *In* Barker, P.F., Kennett, J.P., et al., *Proc. ODP, Sci. Results,* 113: College Station, TX (Ocean Drilling Program), 865–880.

Martini, E., 1971. Standard Tertiary and Quaternary calcareous nannoplankton zonation. *In* Farinacci, A. (Ed.), *Proc. 2nd Int. Conf. Planktonic Microfossils Roma:* Rome (Ed. Tecnosci.), 2:739–785.

McDuff, R.E., 1981. Major cation gradients in DSDP interstitial waters: the role of diffusive exchange between seawater and upper oceanic crust. *Geochim. Cosmochim. Acta,* 45:1705–1713.

Okada, H., and Bukry, D., 1980. Supplementary modification and introduction of code numbers to the low-latitude coccolith biostratigraphic zonation (Bukry, 1973; 1975). *Mar. Micropaleontol.,* 5:321–325.

Raffi, I., Backman, J., Rio, D., and Shackleton, N.J., 1993. Plio-Pleistocene nannofossil biostratigraphy and calibration to oxygen isotopes stratigraphies from Deep Sea Drilling Project Site 607 and Ocean Drilling Program Site 677. *Paleoceanography,* 8:387–408.

Rio, D., Fornaciari, E., and Raffi, I., 1990a. Late Oligocene through early Pleistocene calcareous nannofossils from western equatorial Indian Ocean (Leg 115). *In* Duncan, R.A., Backman, J., Peterson, L.C., et al., *Proc. ODP, Sci. Results,* 115: College Station, TX (Ocean Drilling Program), 175–235.

Rio, D., Raffi, I., and Villa, G., 1990b. Pliocene-Pleistocene calcareous nannofossil distribution patterns in the Western Mediterranean. *In* Kastens, K.A., Mascle, J., et al., *Proc. ODP, Sci. Results,* 107: College Station, TX (Ocean Drilling Program), 513–533.

Scott, G.H., Bishop, S., and Burt, B.J., 1990. *Guide to Some Neogene Globotalids (Foraminiferida) from New Zealand*. New Zealand Geol. Surv. Paleontol. Bull., 61; New Zealand Geological Survey DSIR, Lower Hutt.

Shipboard Scientific Party, 1988a. Site 679. *In* Suess, E., von Huene, R., et al., *Proc. ODP, Init. Repts.,* 112: College Station, TX (Ocean Drilling Program), 159–248.

————, 1988b. Site 704. *In* Ciesielski, P.F., Kristoffersen, Y., et al., *Proc. ODP, Init. Repts.,* 114: College Station, TX (Ocean Drilling Program), 621–796.

————, 1996. Site 984. *In* Jansen, E., Raymo, M.E., Blum, P., et al., *Proc. ODP, Init. Repts.,* 162: College Station, TX (Ocean Drilling Program), 169–222.

Stott, L.D., and Kennett, J.P., 1990. Antarctic Paleogene planktonic foraminifer biostratigraphy: ODP Leg 113, Sites 689 and 690. *In* Barker, P.F., Kennett, J.P., et al., *Proc. ODP, Sci. Results,* 113: College Station, TX (Ocean Drilling Program), 549–569.

Takemura, A., 1992. Radiolarian Paleogene biostratigraphy in the southern Indian Ocean, Leg 120. *In* Wise, S.W., Jr., Shlich, R., et al., *Proc. ODP, Sci. Results,* 120: College Station, TX (Ocean Drilling Program), 735–756.

Takemura, A., and Ling, H.Y., 1997. Eocene and Oligocene radiolarian biostratigraphy from the Southern Ocean: correlation of ODP Legs 114 (Atlantic Ocean) and 120 (Indian Ocean). *Mar. Micropaleontol.*, 30:97–116.

Thomas, E., 1987. Late Oligocene to Recent foraminifers from Deep Sea Drilling Project Sites 608 and 610, northeastern North Atlantic. *In* Ruddimann, W.F., Kidd, R.B., Thomas, E., et al., *Init. Repts. DSDP,* 94: Washington (U.S. Govt. Printing Office), 997–1031.

Tjalsma, R.C., and Lohmann, G.P., 1983. Paleocene-Eocene bathyal and abyssal benthic foraminifera from the Atlantic Ocean. *Micropaleontol. Spec. Publ.,* 4.

Weedon, G.P., Shackleton, N.J., and Pearson, P.N., 1997. The Oligocene time scale and cyclostratigraphy on the Ceara Rise, western equatorial Atlantic. *In* Shackleton, N.J., Curry, W.B., Richter, C., and Bralower, T.J. (Eds.), *Proc. ODP, Sci. Results*, 154: College Station, TX (Ocean Drilling Program), 101–114.

Wei, W., 1993. Calibration of Upper Pliocene-Lower Pleistocene nannofossil events with oxygen isotope stratigraphy. *Paleoceanography,* 8:85–99.

Figure F1. Track line and shotpoints for the site survey of Site 1090 conducted during *Thompson* Cruise TTN057. The bold portion of the track line corresponds to the segment of the seismic profile displayed in Figure F2, p. 30.

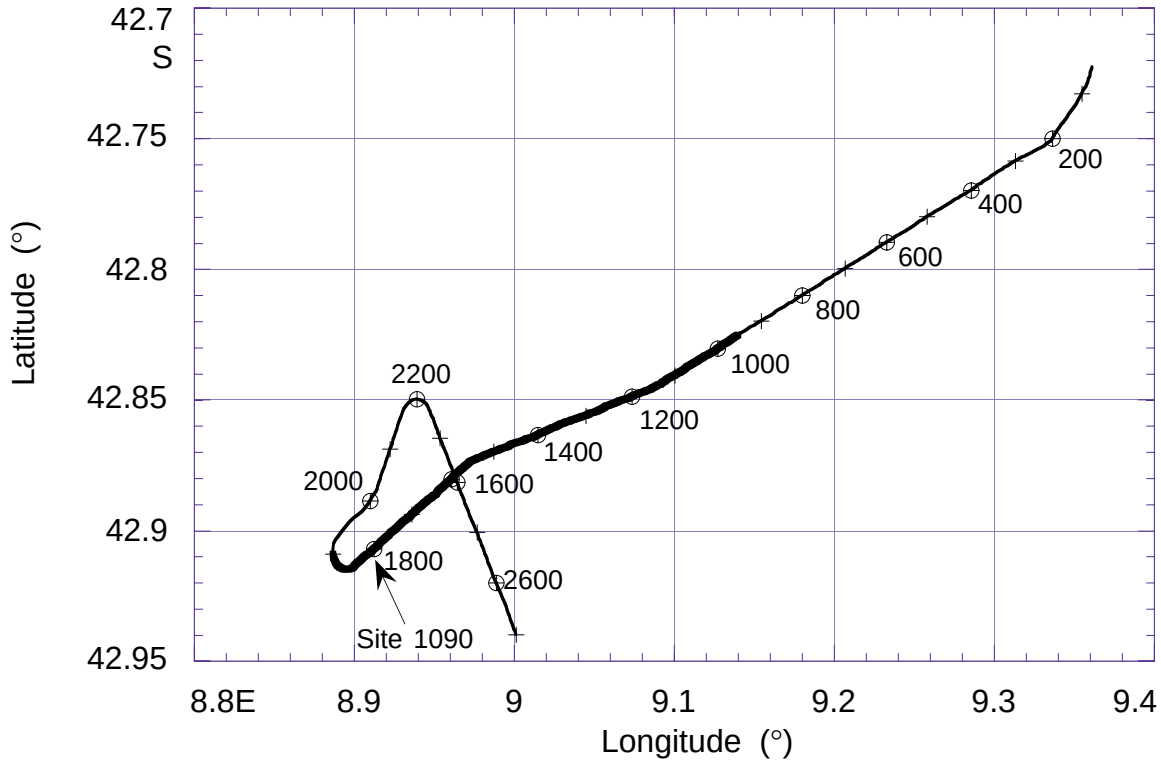

Figure F2. Single-channel seismic line collected during site-survey *Thompson* Cruise TTN057 showing the location and penetration depth of Site 1090. SP = shotpoint

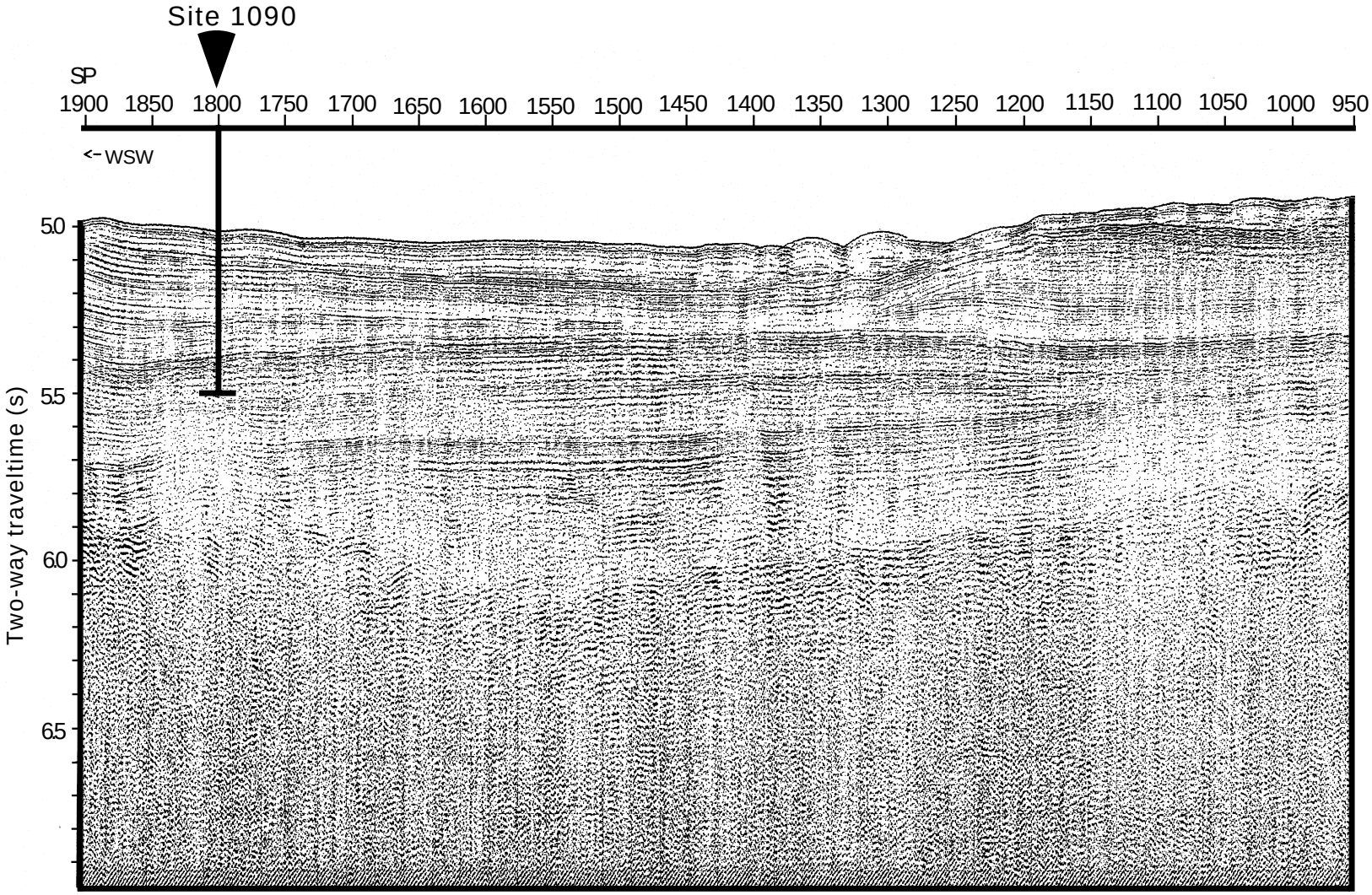

Figure F3. Lithologic summary showing core recovery, lithologic unit, and graphic lithology in the five holes drilled at Site 1090. Positions of lithostratigraphic/biostratigraphic boundaries refer to Hole 1090B. (Continued on next page.)

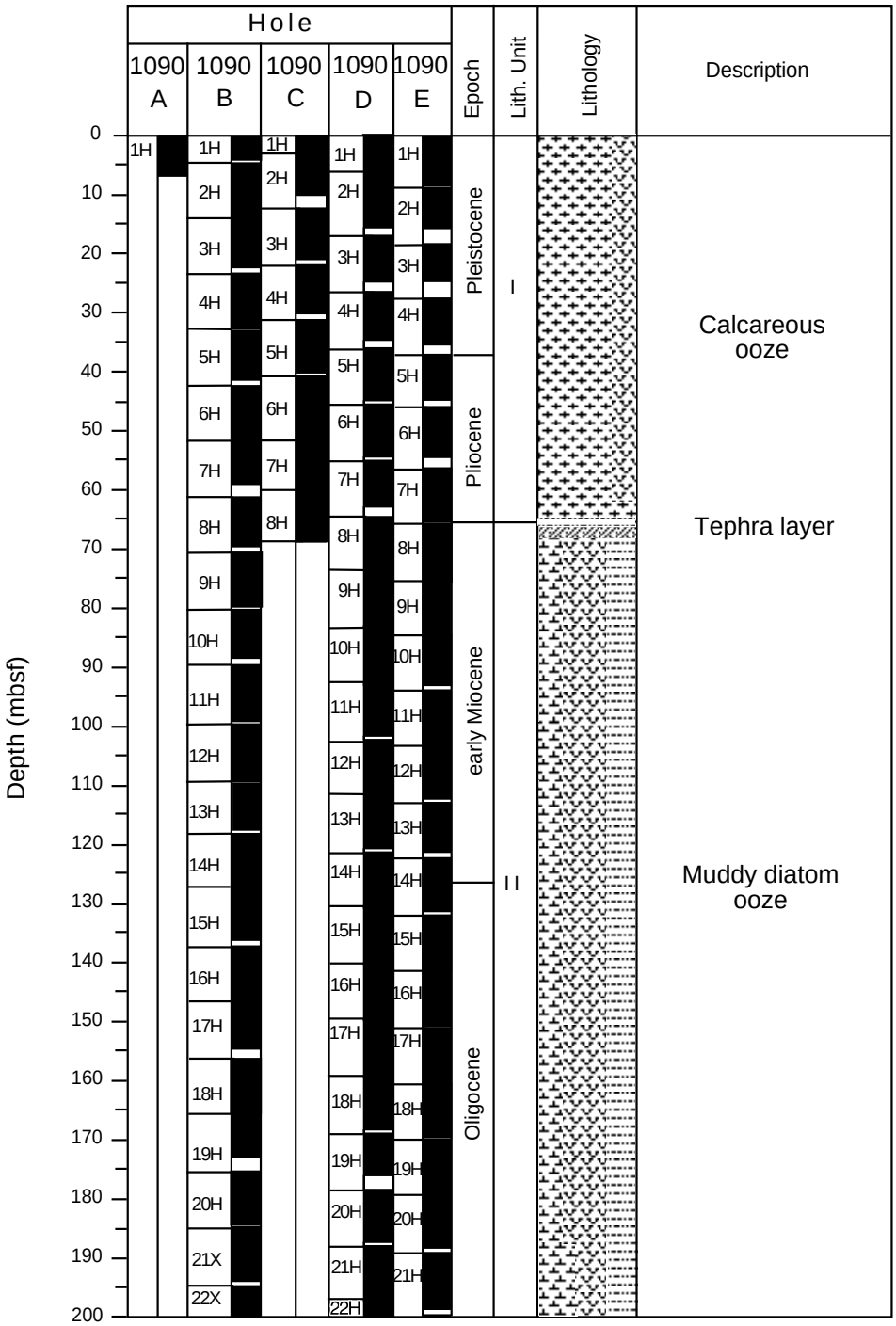

Figure F3 (continued).

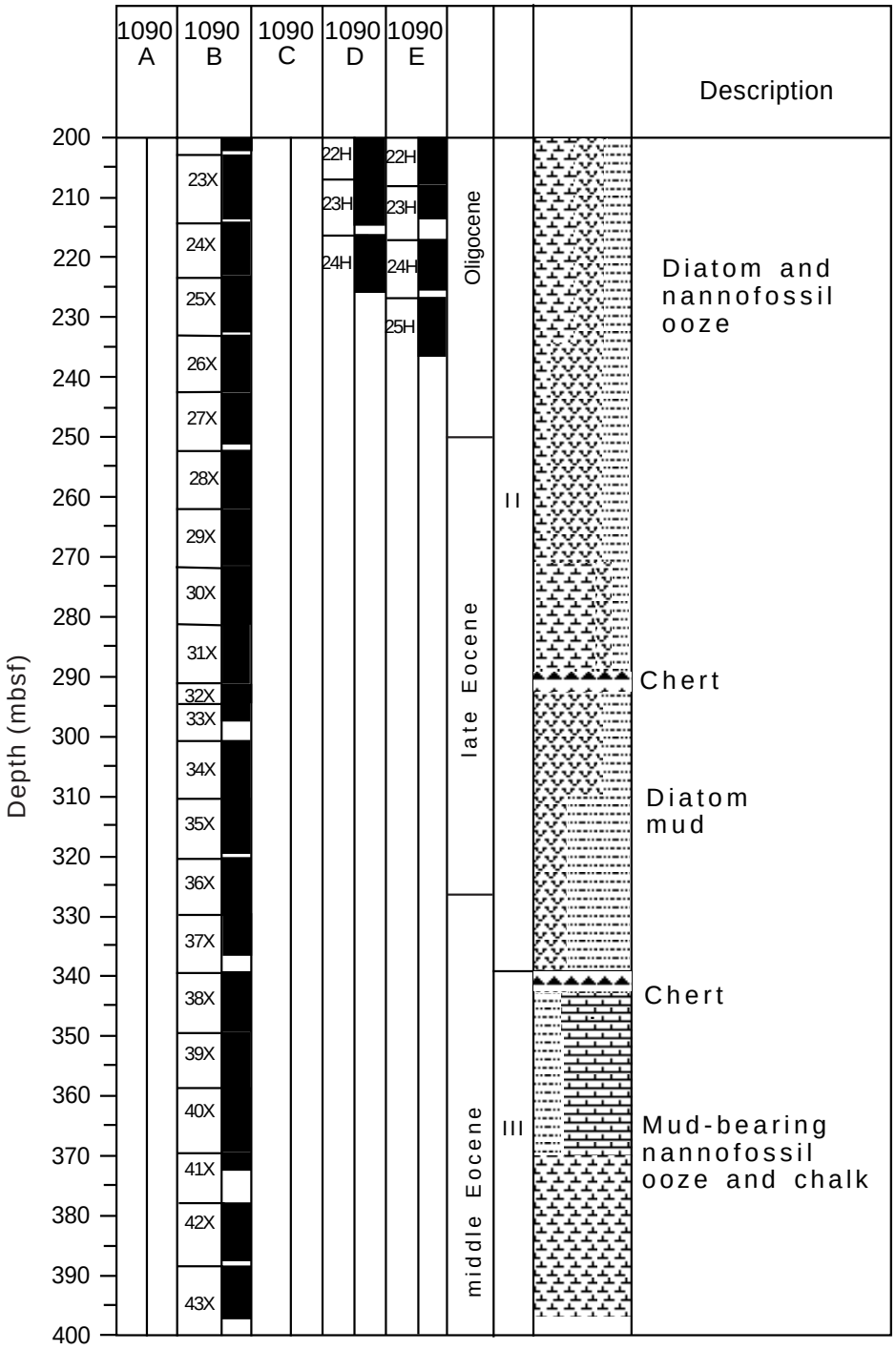

Figure F4. Graphic lithology and variations in bulk-sediment composition as indicated by calcium carbonate (see "Geochemistry," p. 19), red color reflectance, opal (from XRD), and terrigenous mud. Note that reflectance in the upper 210 m of the section was measured with the OSU-SCAT system and below 260 mbsf with the Minolta CM-2002 spectrophotometer (see "Physical Properties," p. 23). All data and lithologic unit boundaries refer to Hole 1090B.

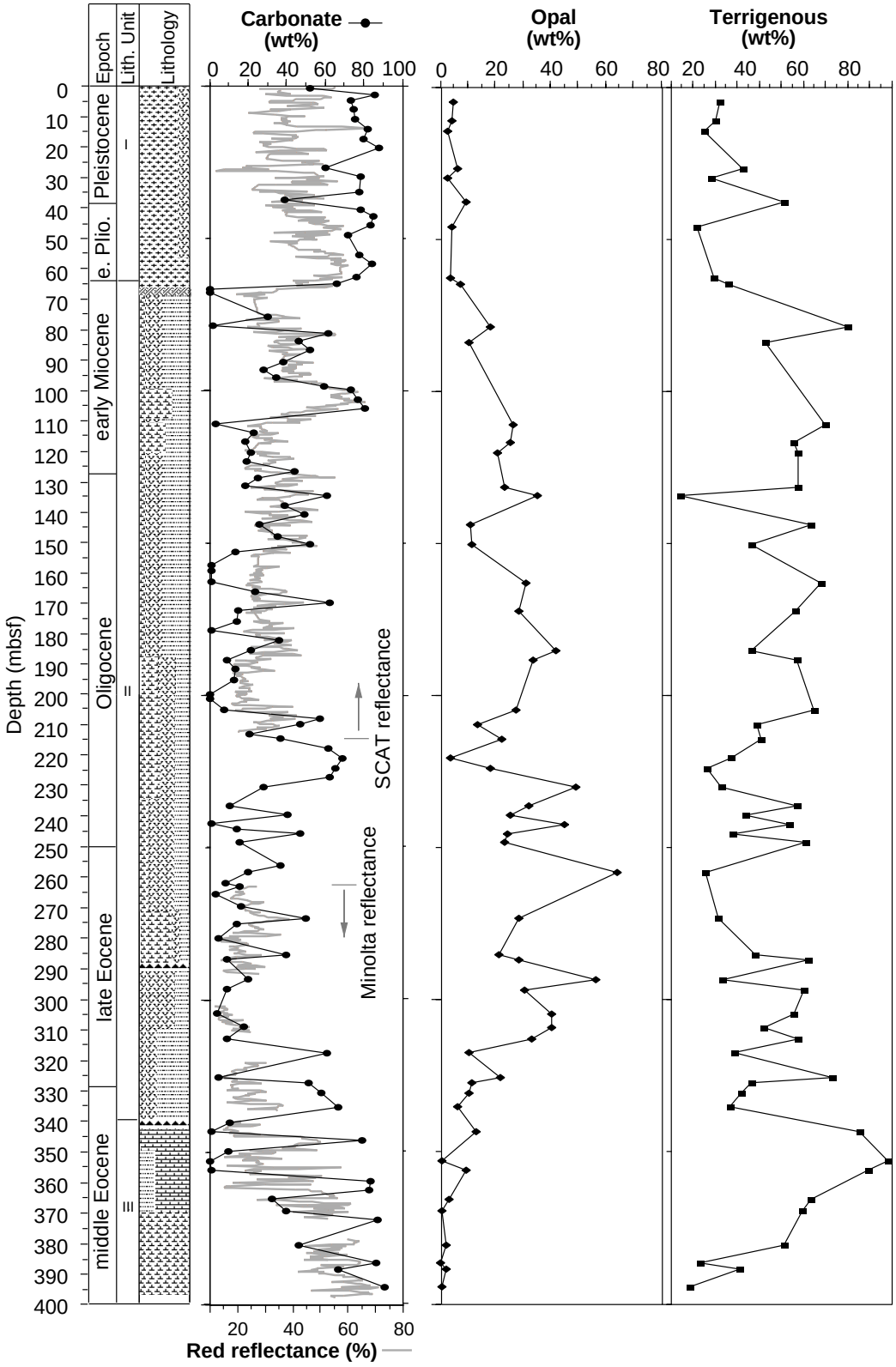

Figure F5. Comparison of downhole variations of abundances of lithologic components by smear-slide (% area), coulometry (calcium carbonate), and XRD (opal) estimates. Percent terrigenous sediment is estimated by difference. Frames from left to right: coulometric and smear-slide estimates of carbonate abundance (nannofossils + foraminifers on smear slides); opal and diatom abundance; mud and terrigenous sediment content; quartz/feldspar; clay minerals/(quartz+feldspar); and stratigraphy. Qz = quartz, Fsp = feldspar, CM = clay minerals.

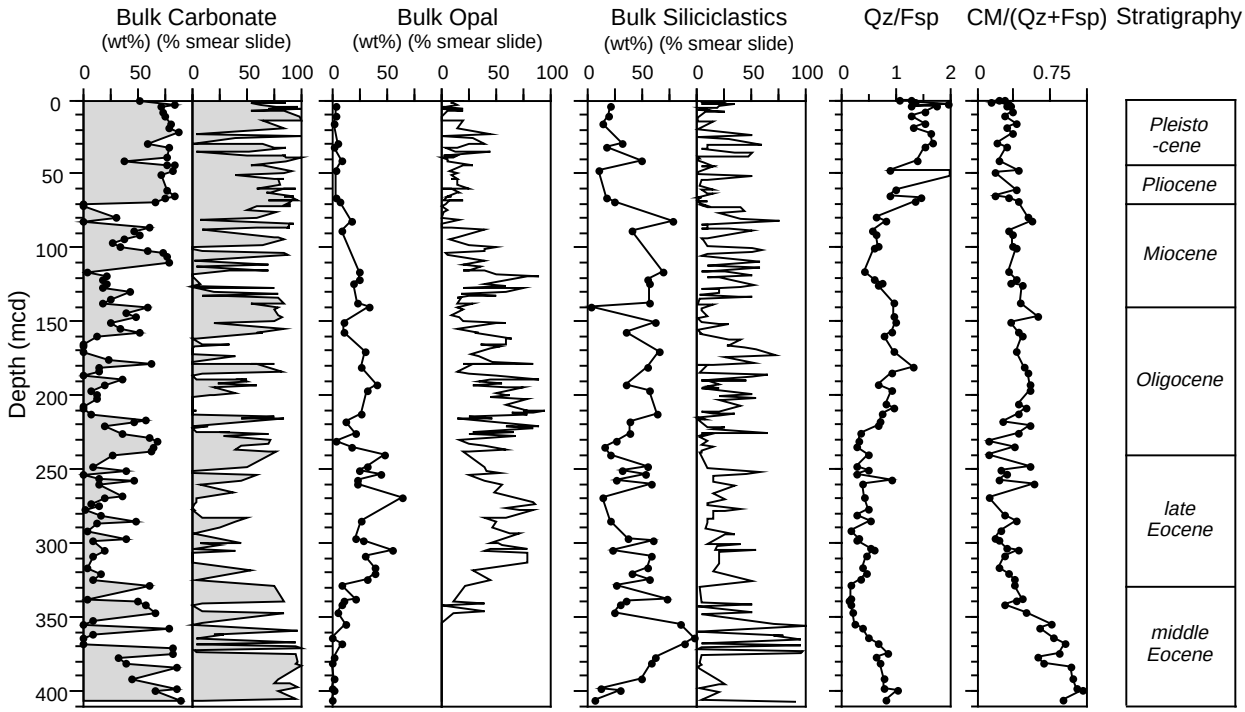

Figure F6. Crosscutting *Zoophycos*, *Skolithos*, and *Planolites* burrows (interval 177-1090E-20H-1, 51–74 cm).

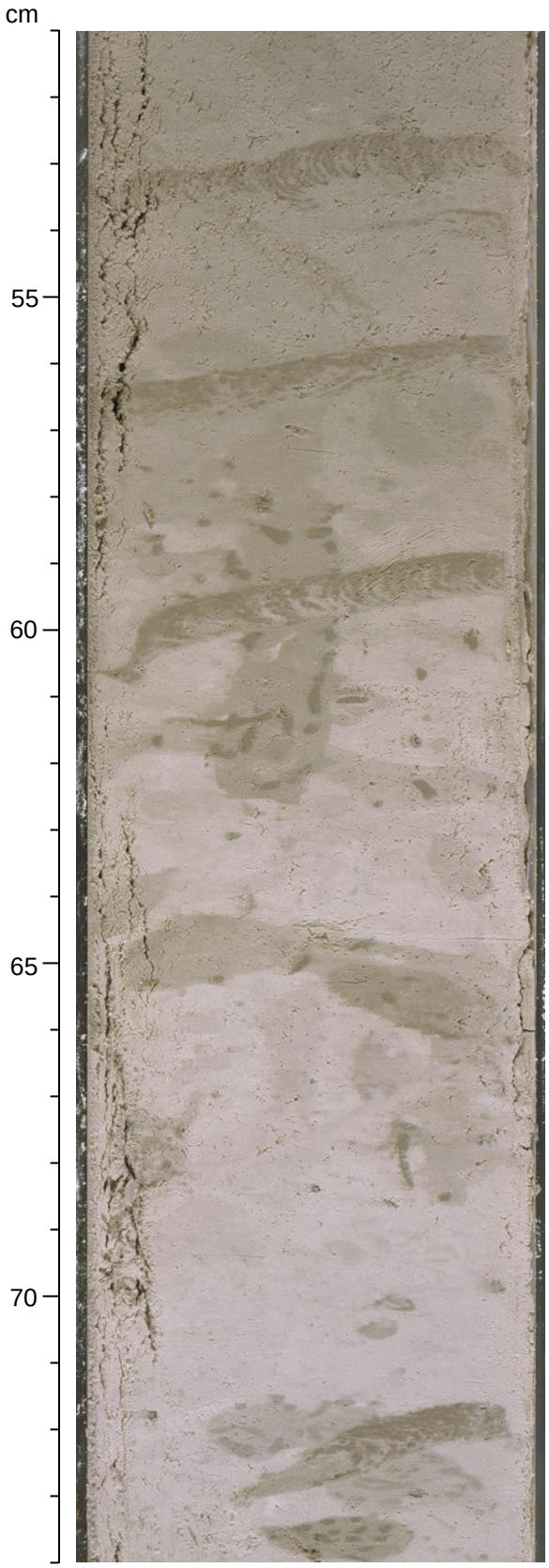

Figure F7. *Chondrites* burrows (interval 177-1090D-17H-1, 69–97 cm).

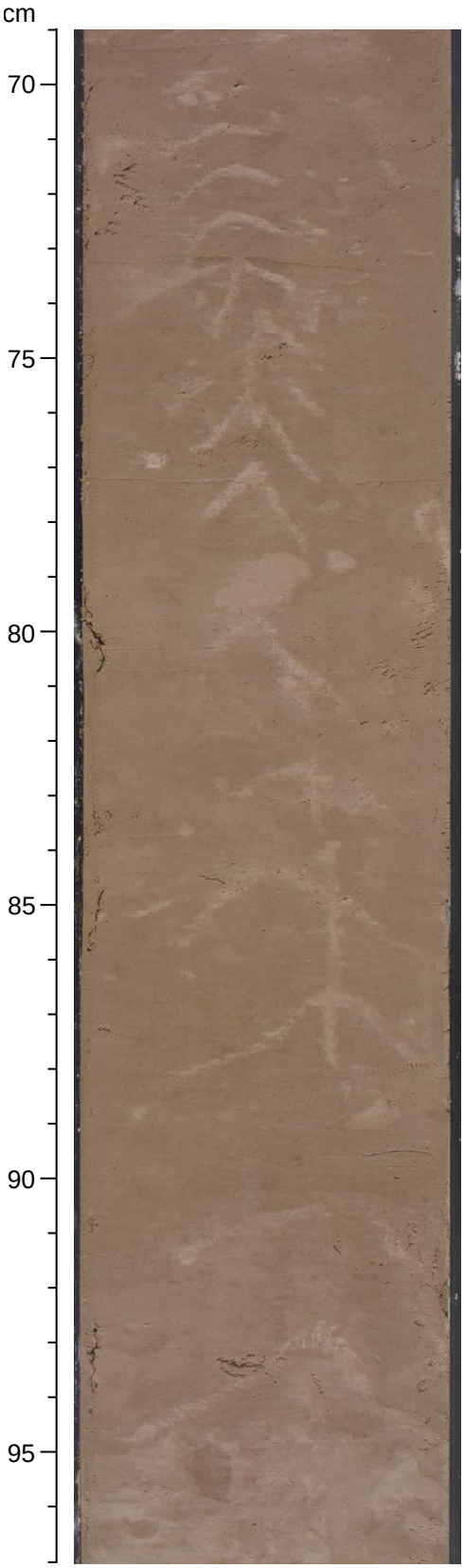

Figure F8. Positions of tephra and manganese nodules in Holes 1090B–1090E in **(A)** standard ODP mbsf depth and **(B)** mcd units after adjustment based on GRA bulk density and magnetic susceptibility data.

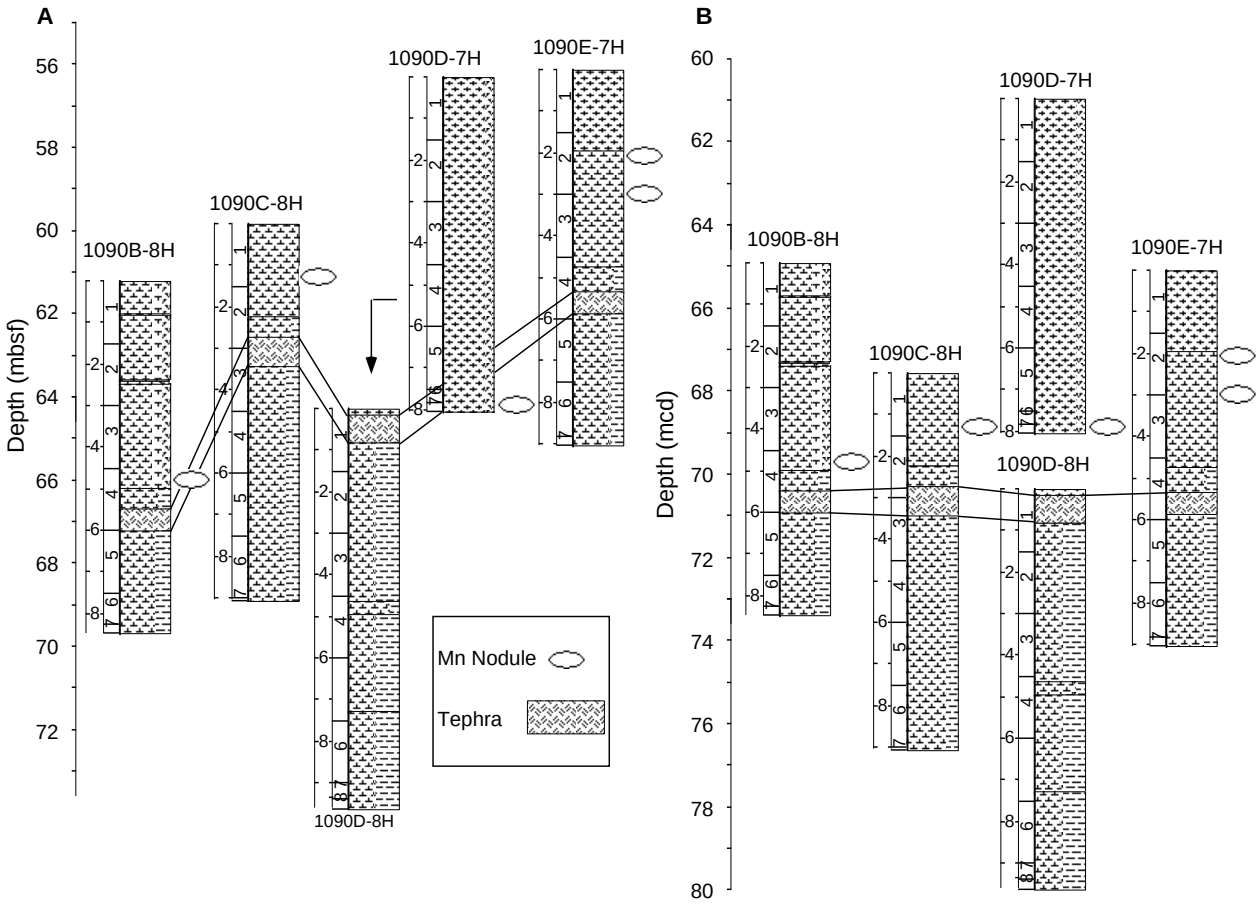

Figure F9. Lower part of the tephra sequence in Section 177-1090E-7H-4 (interval 177-1090E-7H-4, 115–145 cm).

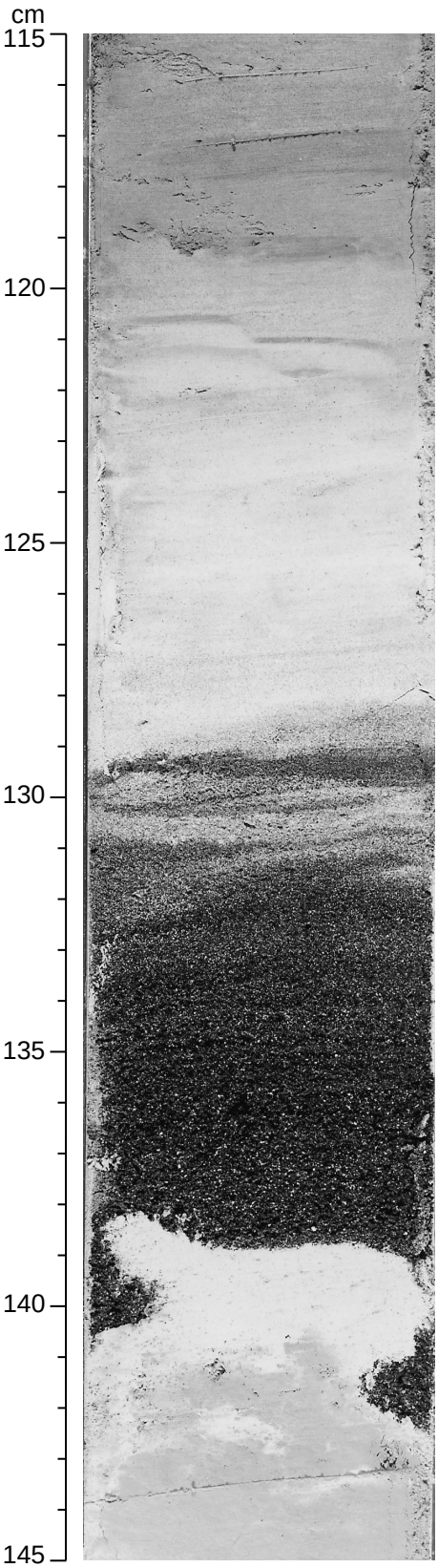

Figure F10. Smoothed (5-point average) magnetic susceptibility data for the upper 250 mcd at Site 1090. Holes 1090A (left curve), 1090B (second from left curve), 1090C (middle curve), 1090D (second from right curve), and 1090E (right curve) are horizontally offset from each other by a constant (15 × 10^{-5} SI units). Data from the top 20 cm of each core have been removed.

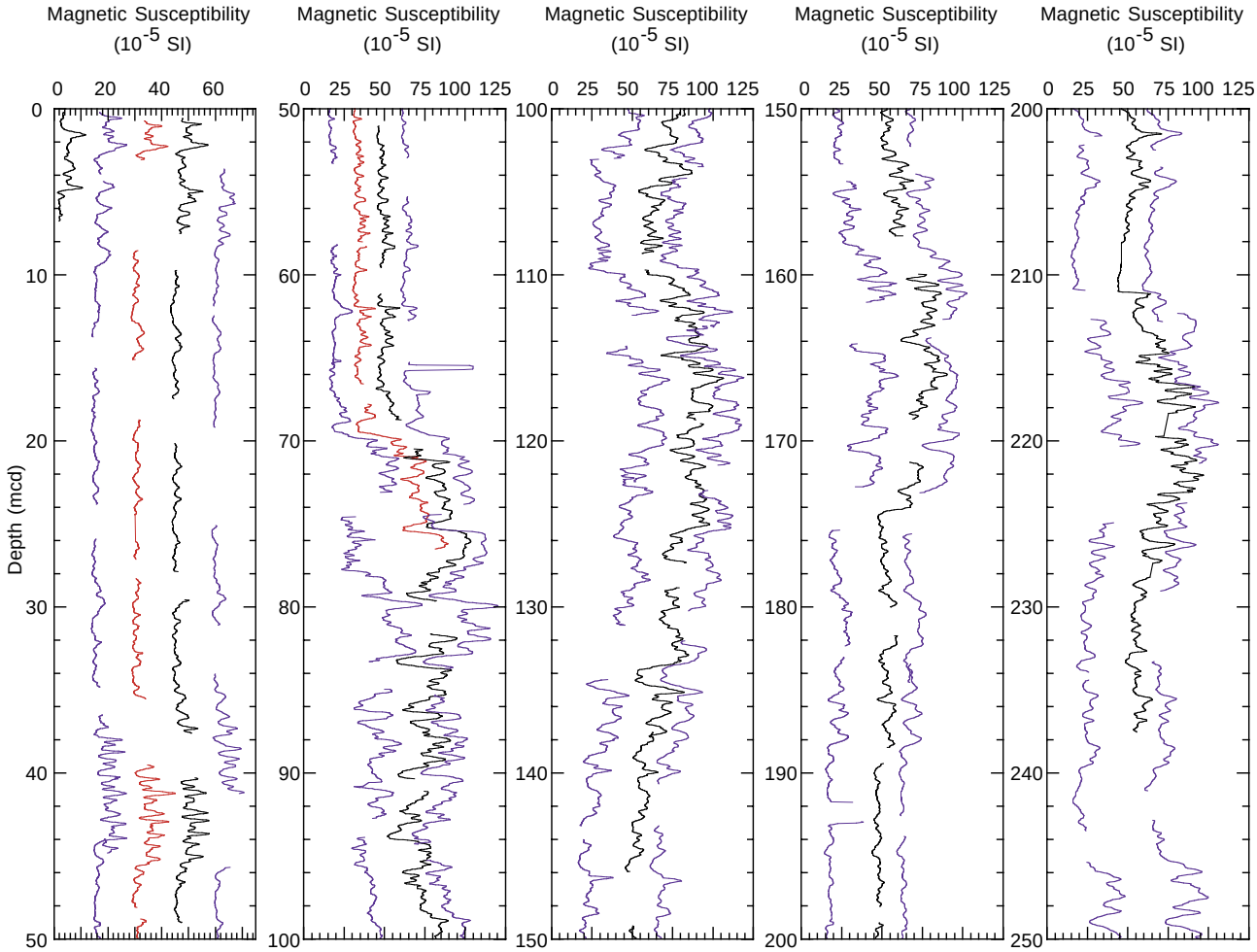

Figure F11. Smoothed (5-point average) GRA bulk density data for the upper 250 mcd at Site 1090. Holes 1090A (left curve), 1090B (second from left curve), 1090C (middle curve), 1080D (second from right curve), and 1090E (right curve) are horizontally offset from each other by a constant (0.15 g/cm³). Data from the top 20 cm of each core have been removed.

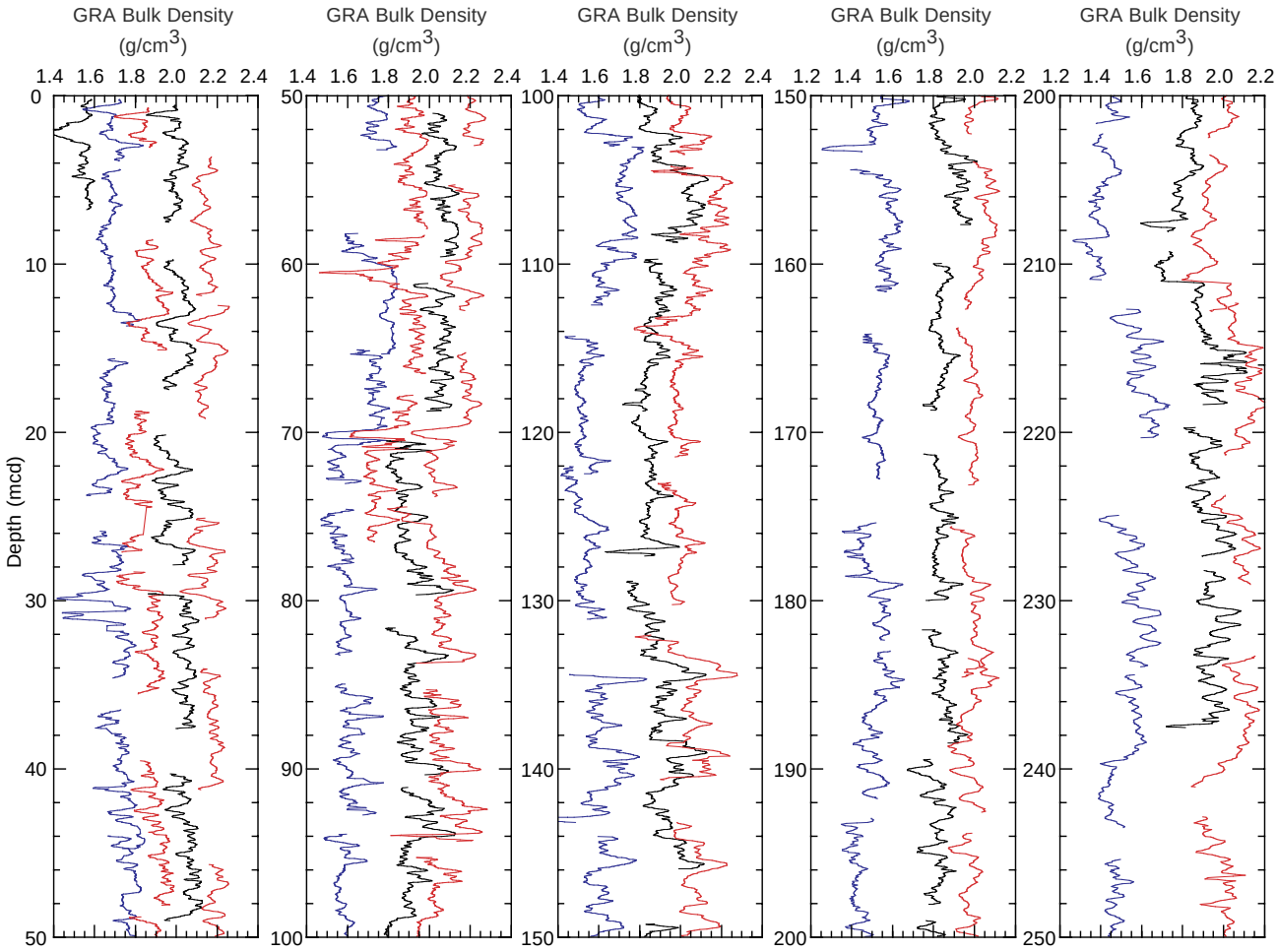

Figure F12. Smoothed (5-point average) color reflectance data (650–750 nm) for the upper 250 mcd at Site 1090. Holes 1090A (left curve), 1090B (second from left curve), 1090D (second from right curve), and 1090E (right curve) are horizontally offset from each other by a constant (15%). Data from the top 20 cm of each core have been removed.

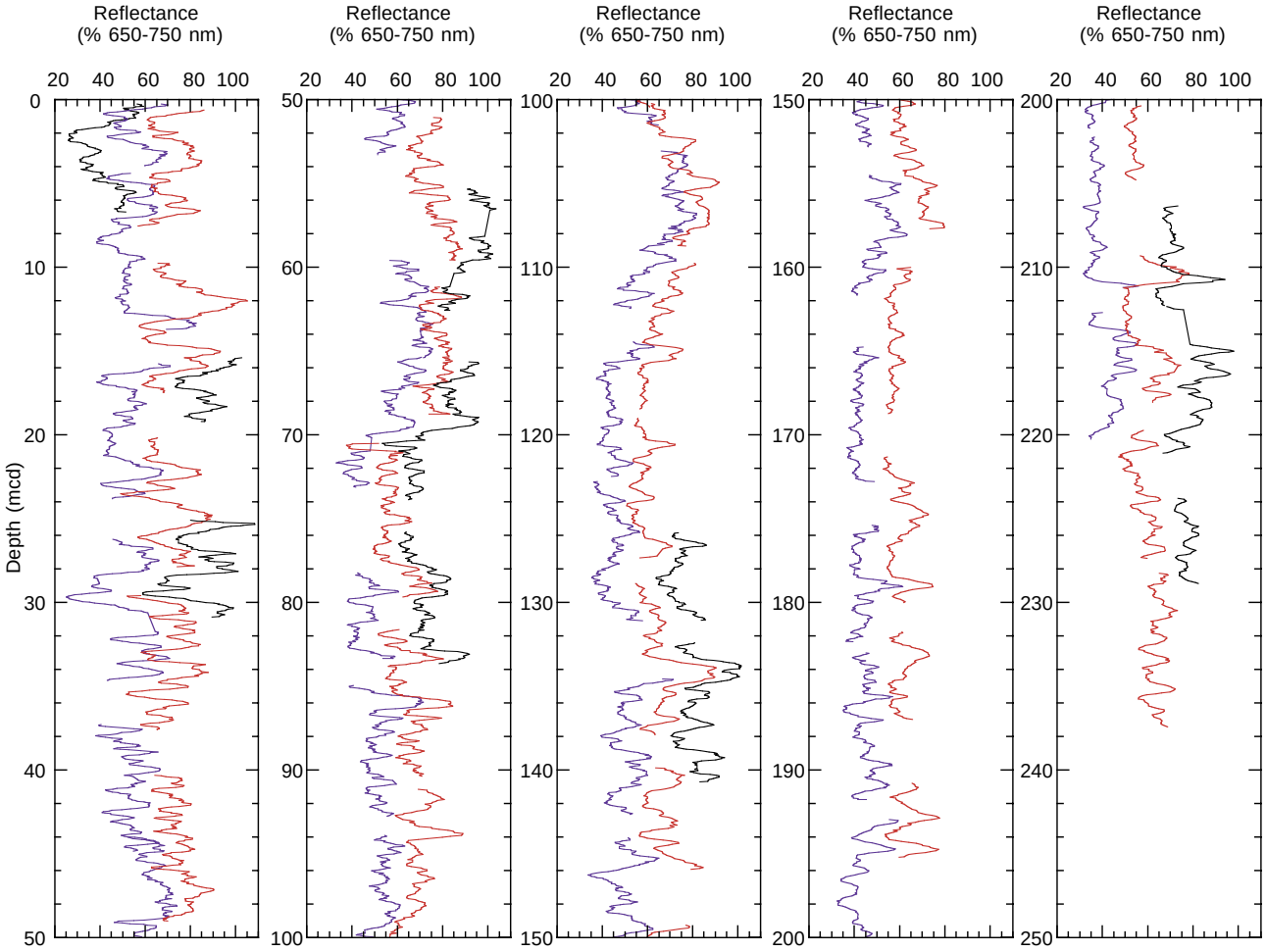

Figure F13. Spliced record of magnetic susceptibility for (**A**) the upper 245 mcd and (**B**) the upper 70 mcd at Site 1090. Both data sets were smoothed with a 5-point running mean. The horizontal lines in each plot identify the splice tie points.

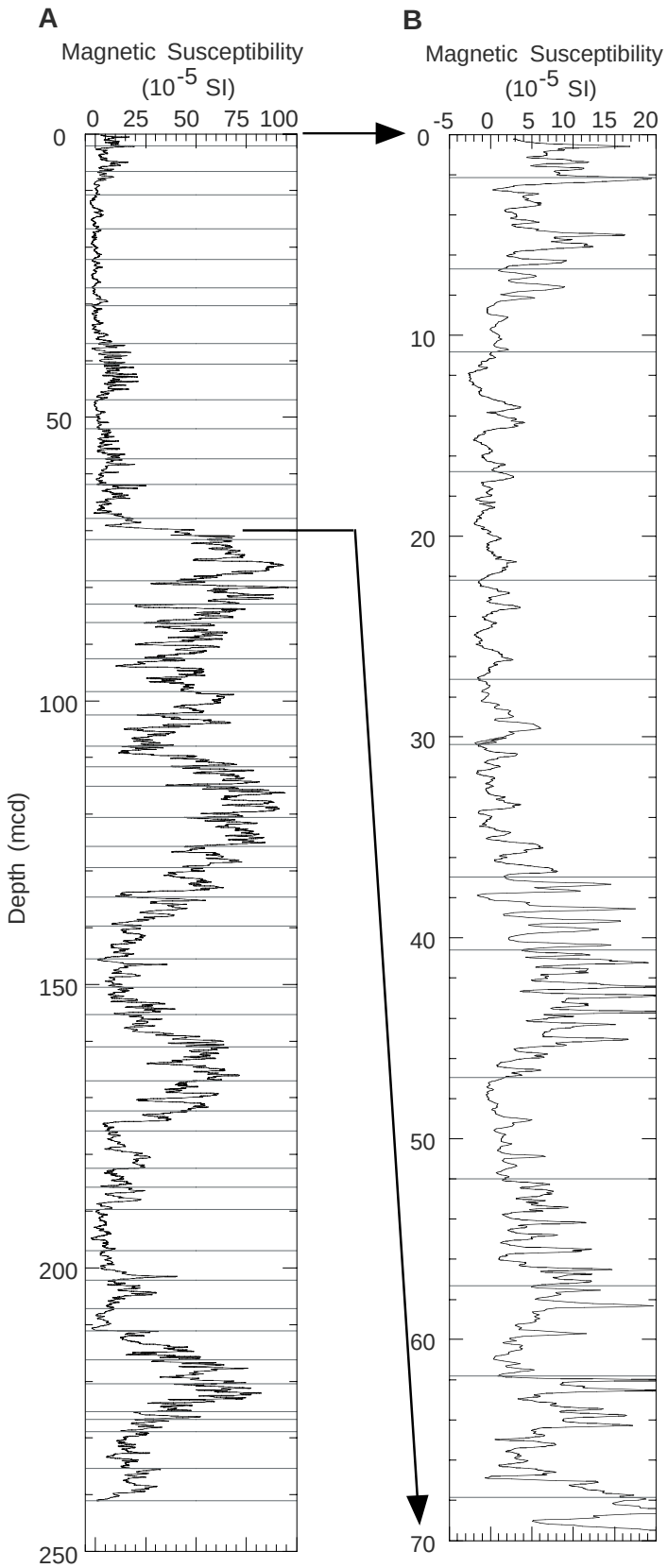

Figure F14. Spliced record of GRA bulk density for (**A**) the upper 245 mcd and (**B**) the upper 70 mcd at Site 1090. Both data sets were smoothed with a 5-point running mean. The horizontal lines in each plot identify the splice tie points.

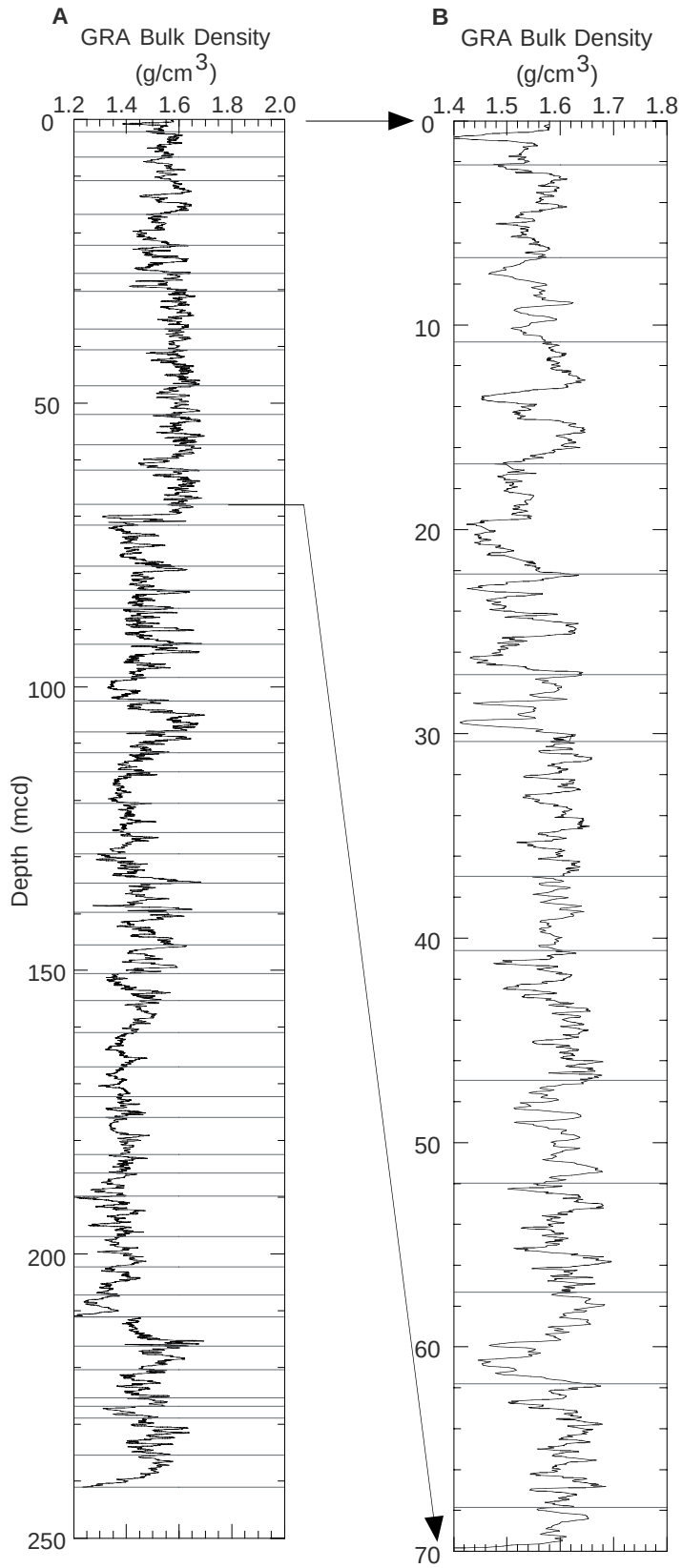

Figure F15. Biostratigraphic and magnetostratigraphic (only upper 60 mcd) correlation chart for Site 1090, and selected absolute age designations. (Continued on next page.)

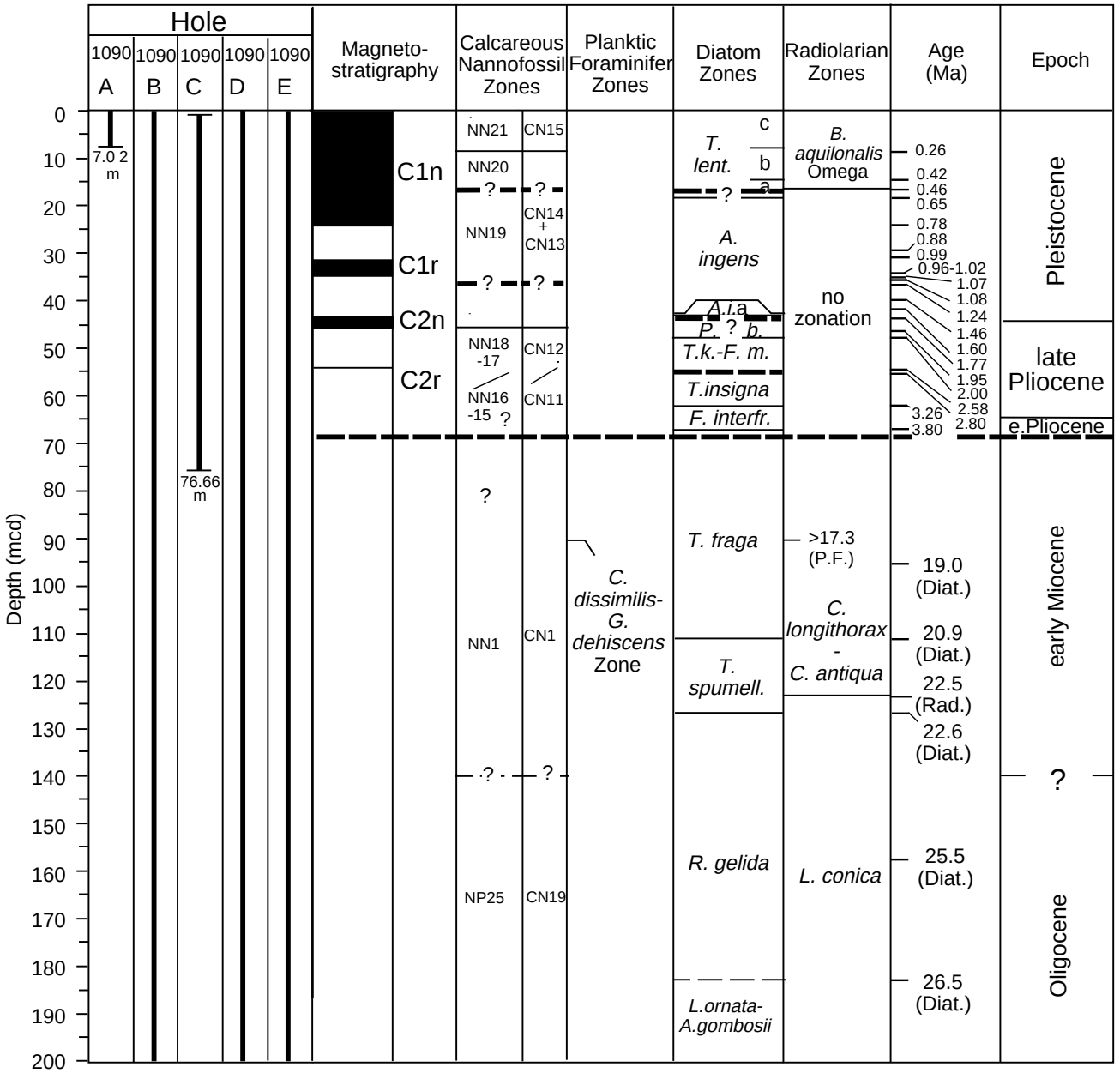

Figure F15 (continued).

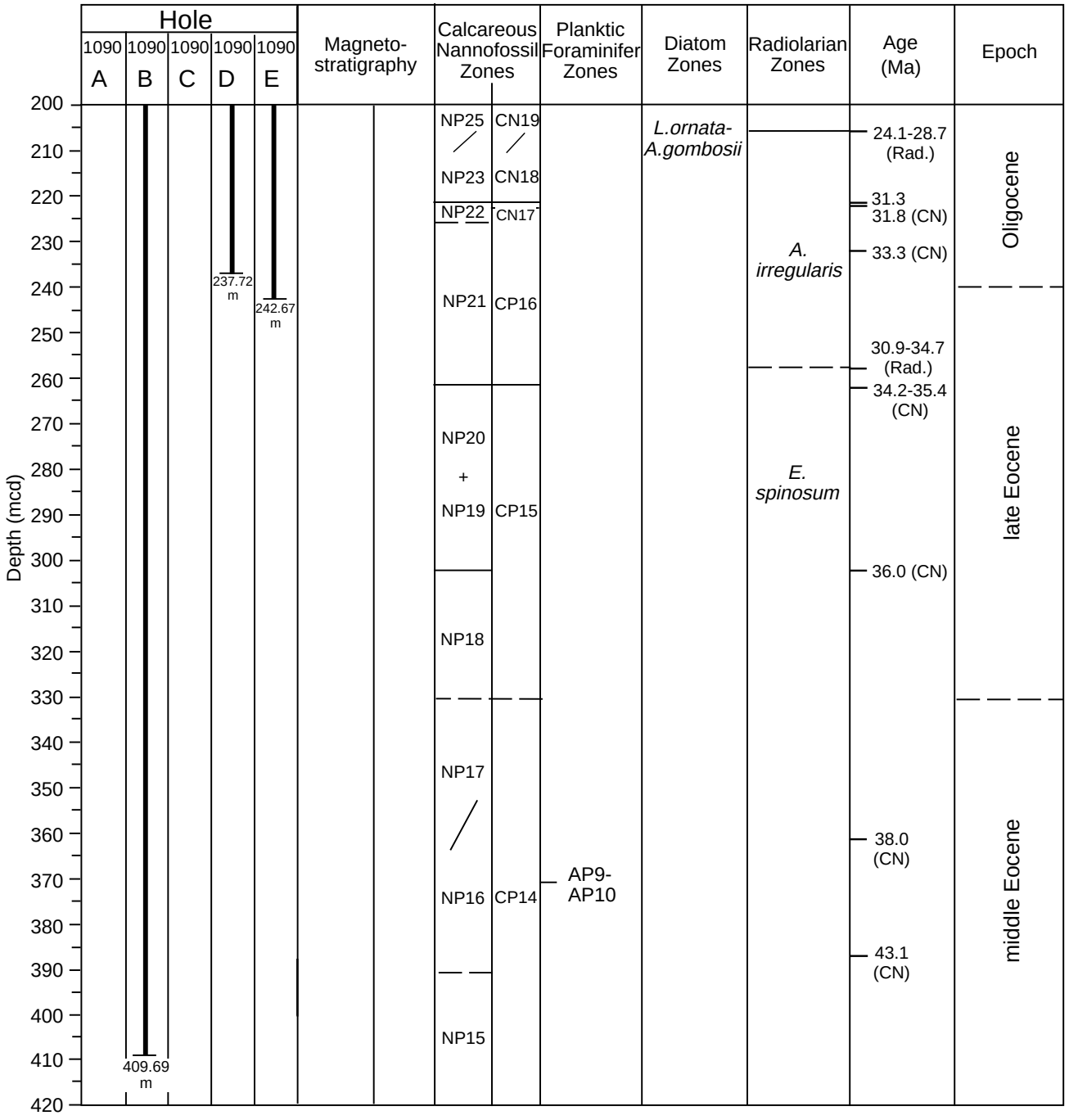

Figure F16. Smoothed (solid line = locally weighted least-squares fit, incorporating a sliding window that includes 7% of the data) and measured (points) $CaCO_3$ concentrations plotted vs. the number of specimens/cm³, the number of species, and the ratio of agglutinated to calcareous taxa in each sample studied for Hole 1090B.

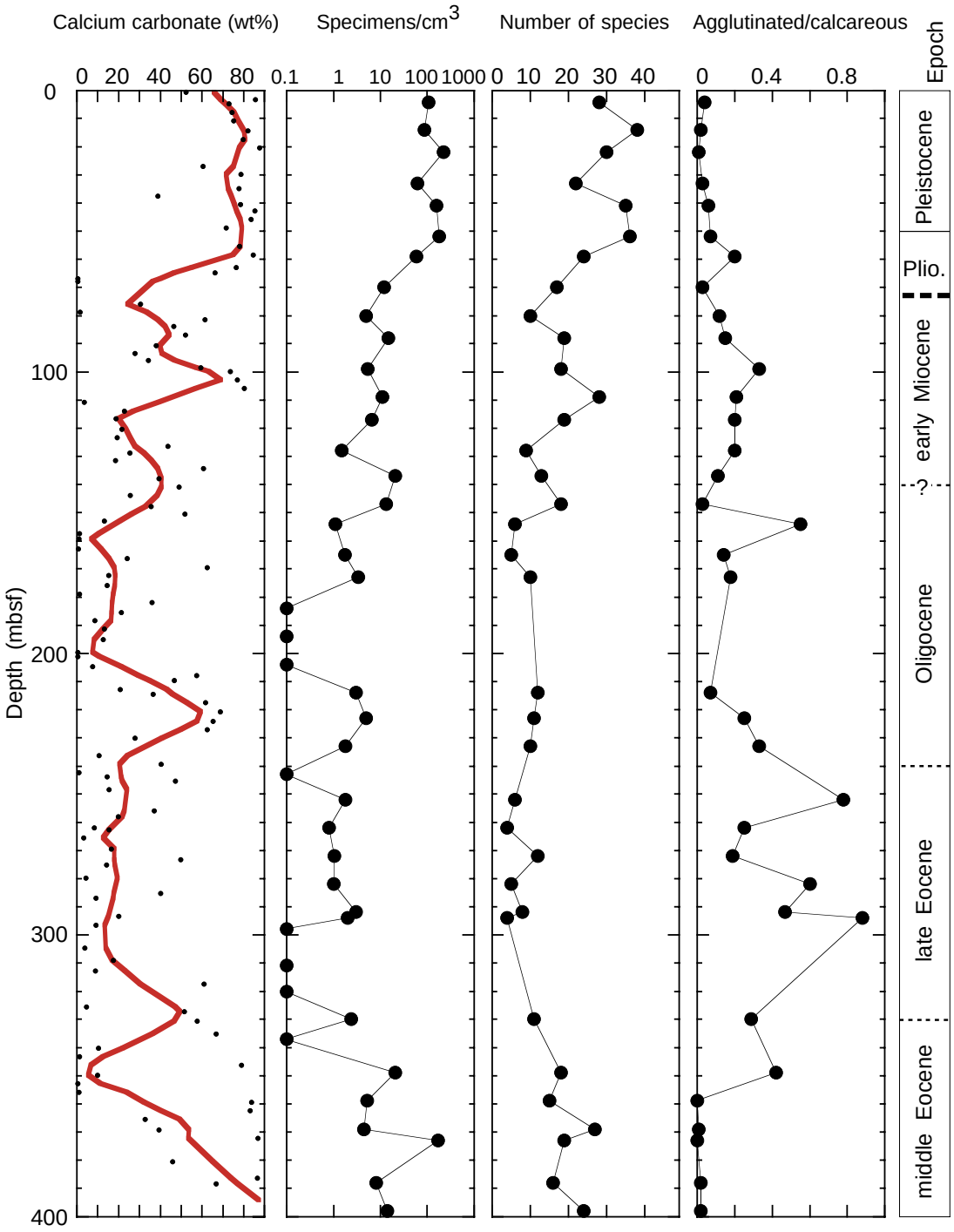

Figure F17. Inclination of the remanent magnetization after alternating-field demagnetization at peak fields of 20 mT of the 0- to 70-mbsf interval from Holes 1090B–1090E. The Brunhes, Matuyama, and Gauss Chrons are identified based on Hole 1090C data. Magnetic polarity shading: black = normal, white = reversed.

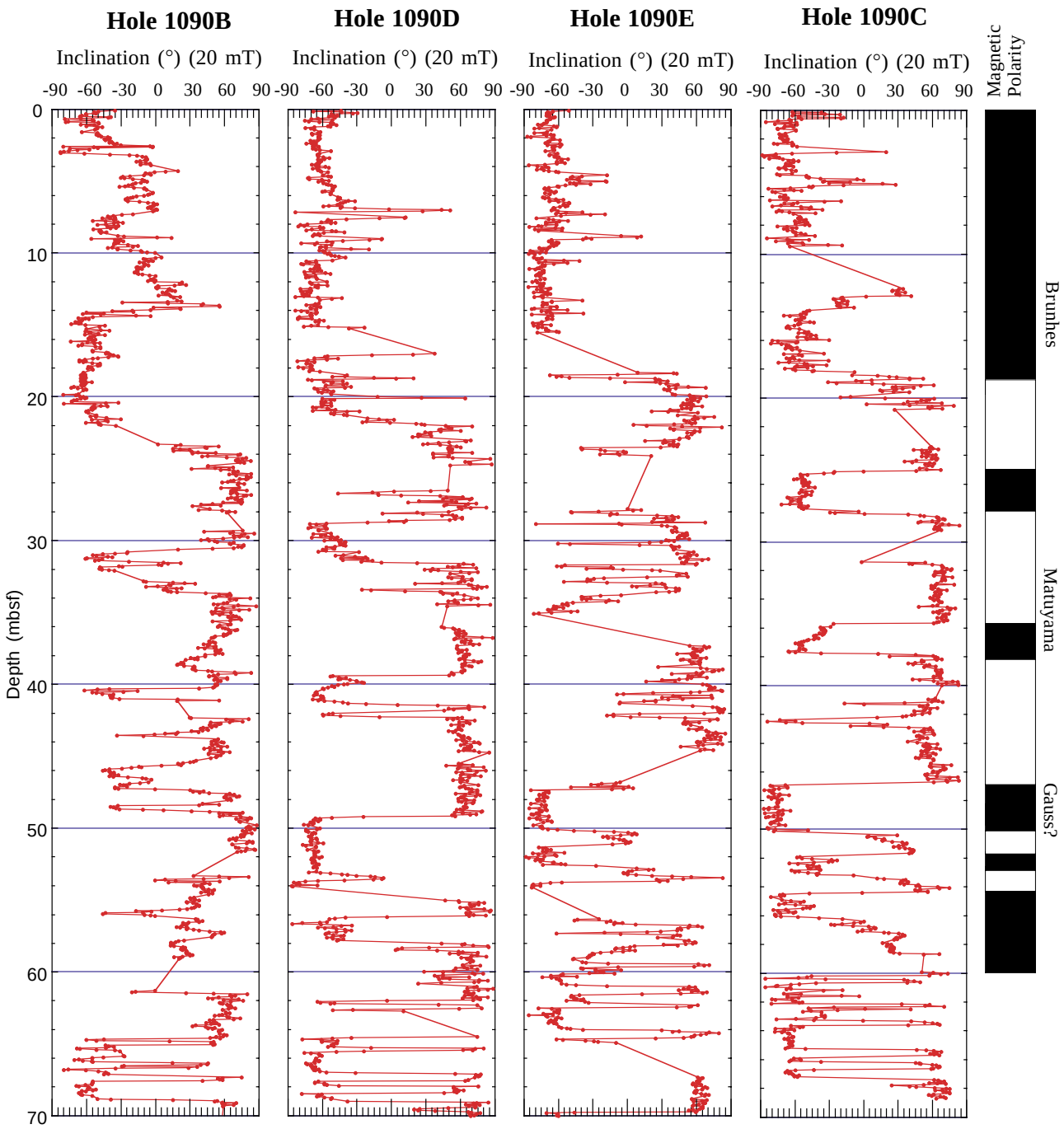

Figure F18. Inclination of the remanent magnetization after alternating-field demagnetization at peak fields of 20 mT of the 60- to 370-mbsf interval from Holes 1090B, 1090D, and 1090E.

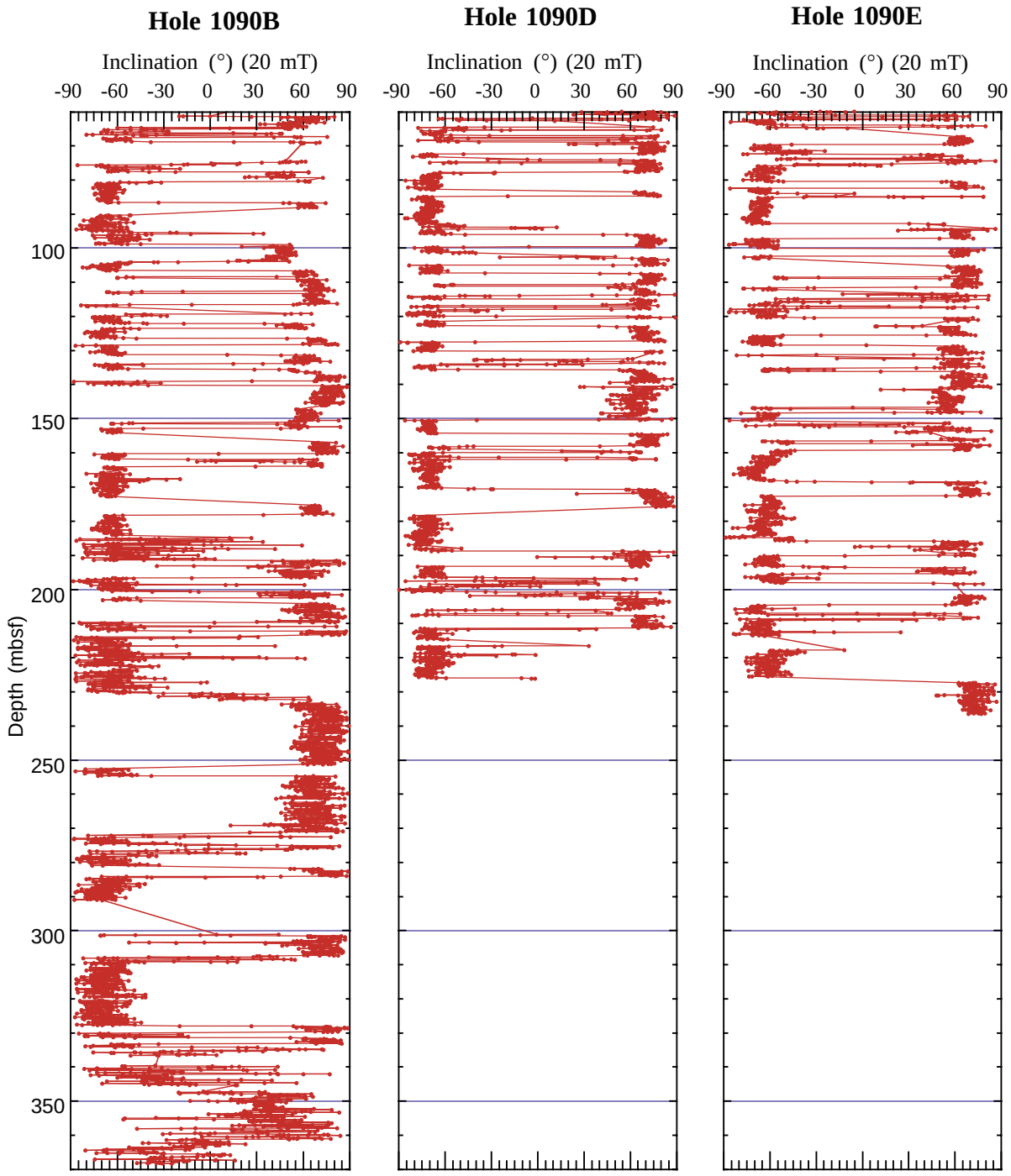

Figure F19. Age-depth relationship integrating biostratigraphic and geomagnetic polarity data for **(A)** the entire sedimentary section and **(B)** a close-up of the upper 70 mcd at Site 1090. The solid lines indicate a visual best fit through the age-depth control points (Table **T9**, p. 89). Corresponding sedimentation rate averages are given in parentheses.

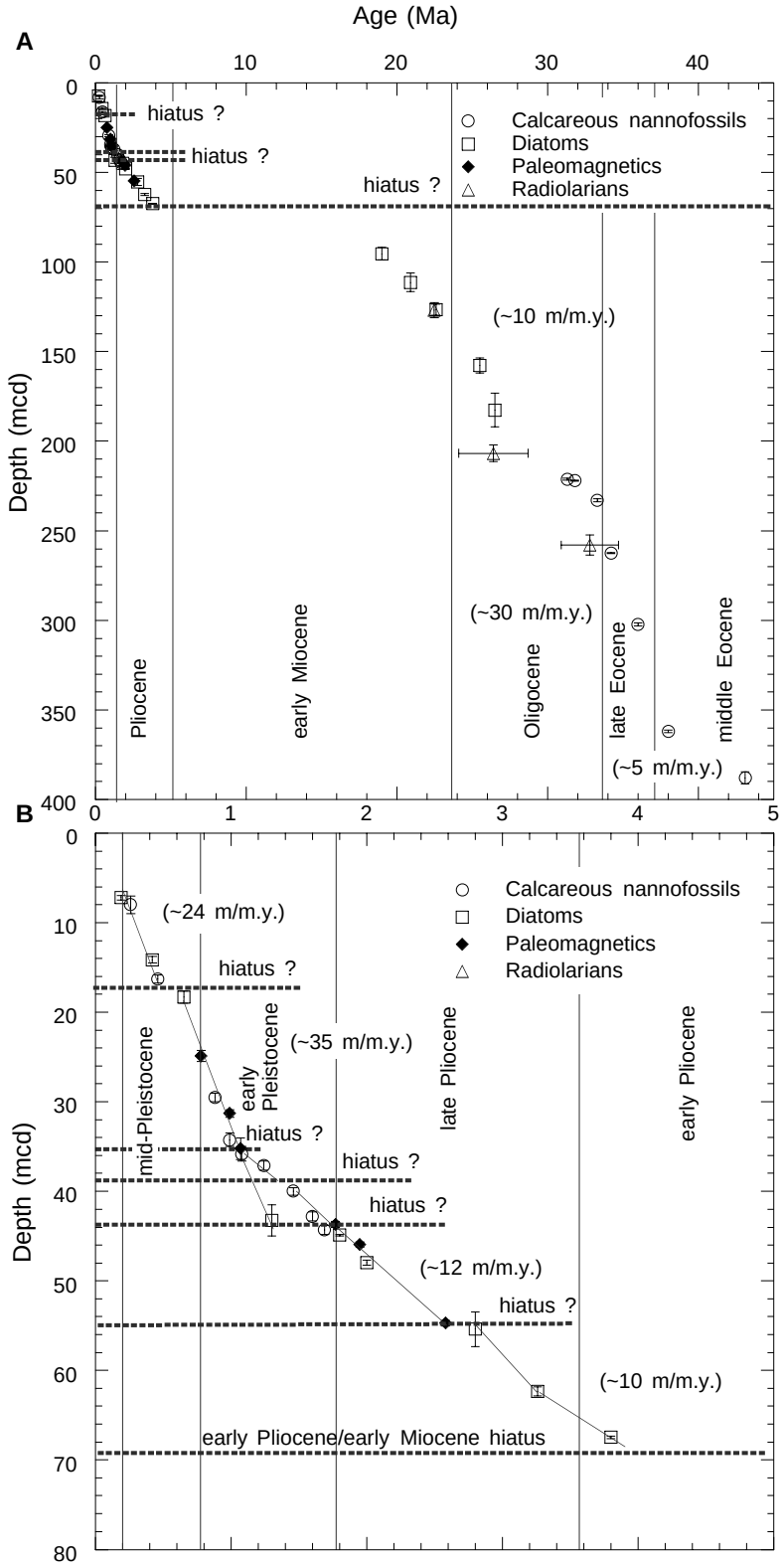

Figure F20. Concentration of methane in sediments vs. depth at Site 1090. Data are reported in Tables T11, p. 93, and T12, p. 94.

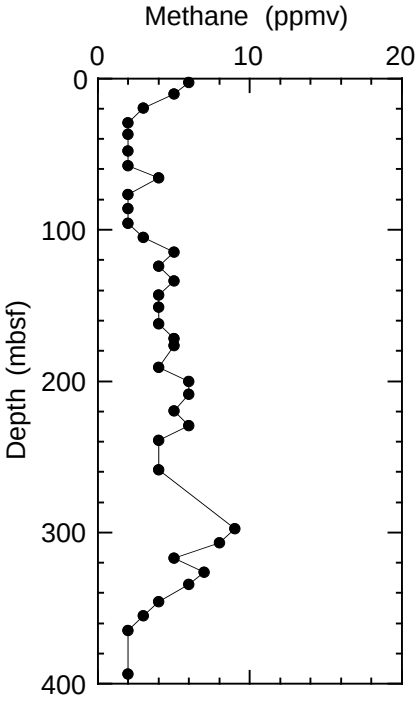

Figure F21. Interstitial water chemistry profiles vs. depth for chlorinity, alkalinity, pH, sodium, sulfate, calcium, magnesium, potassium, strontium, lithium, ammonium, phosphate, silica, manganese, and iron at Site 1090. Data are reported in Table T12, p. 94. Solid and dashed horizontal lines in each plot represent approximate locations of the chert layers at ~290 and 340 mbsf, respectively, in Hole 1090B.

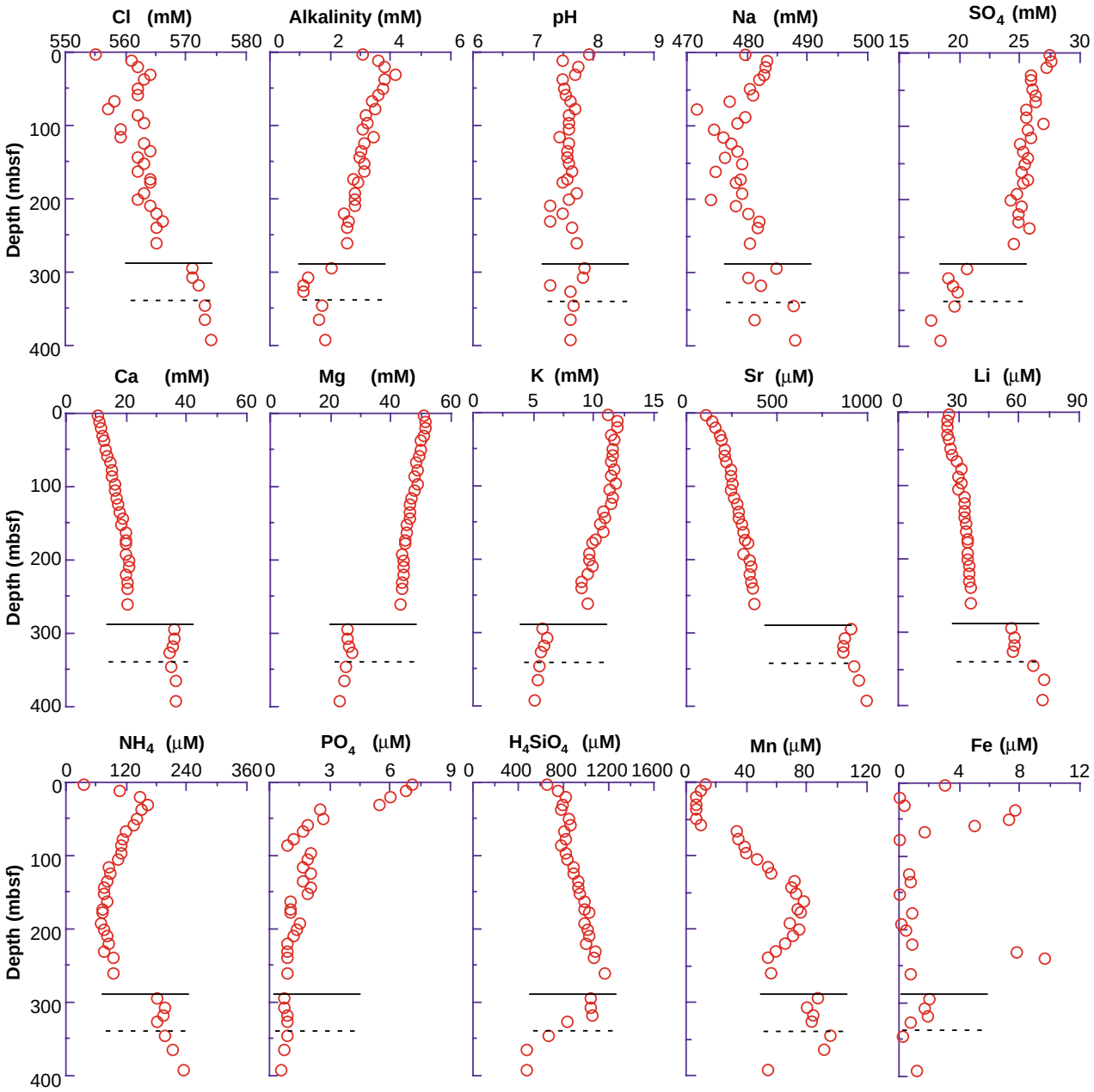

Figure F22. Comparison of profiles of interstitial water Cl^-, Ca^{+2}, Mg^{+2}, and Sr^{+2} from Sites 1088 and 1090. Solid and dashed horizontal lines in each plot represent locations of the chert layers at ~290 and 340 mbsf, respectively, in Hole 1090B.

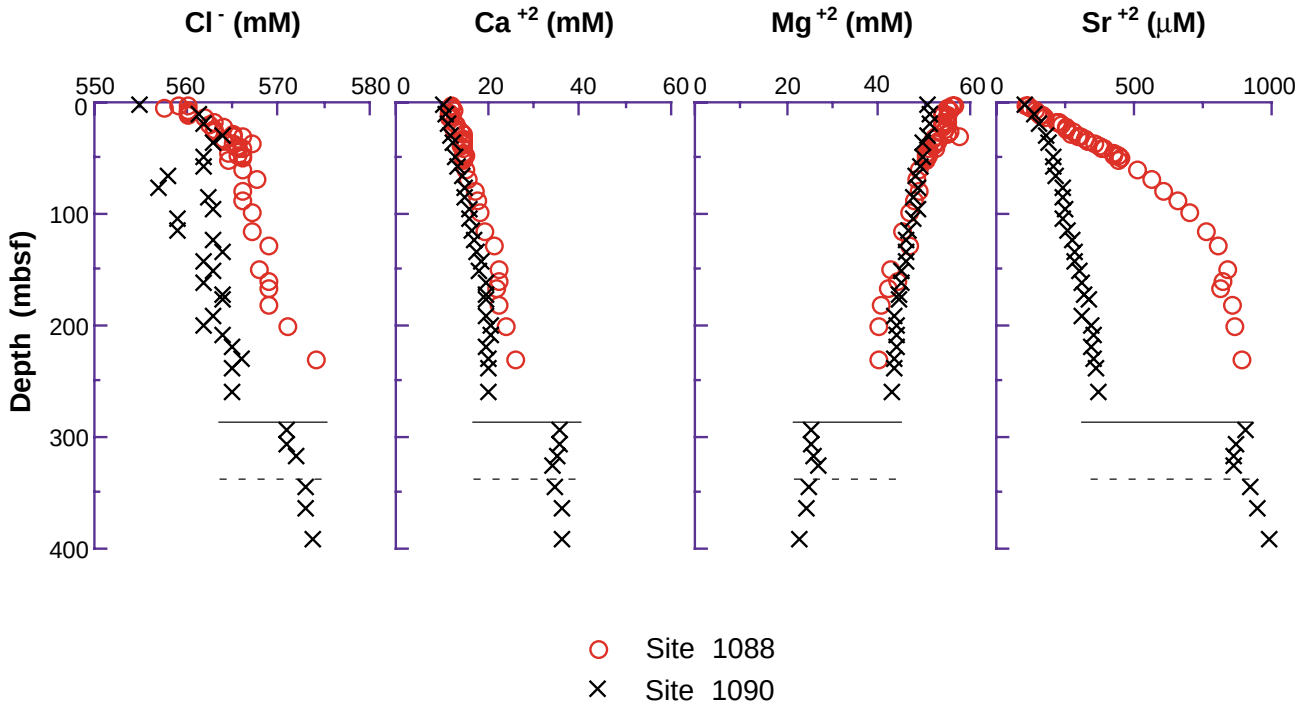

Figure F23. Plots of Mg^{+2} vs. Ca^{+2}, Mg^{+2}/Ca^{+2} vs. depth, Sr^{+2} vs. Ca^{+2}, and Sr^{+2} vs. Mg^{+2} at Sites 1088 and 1090.

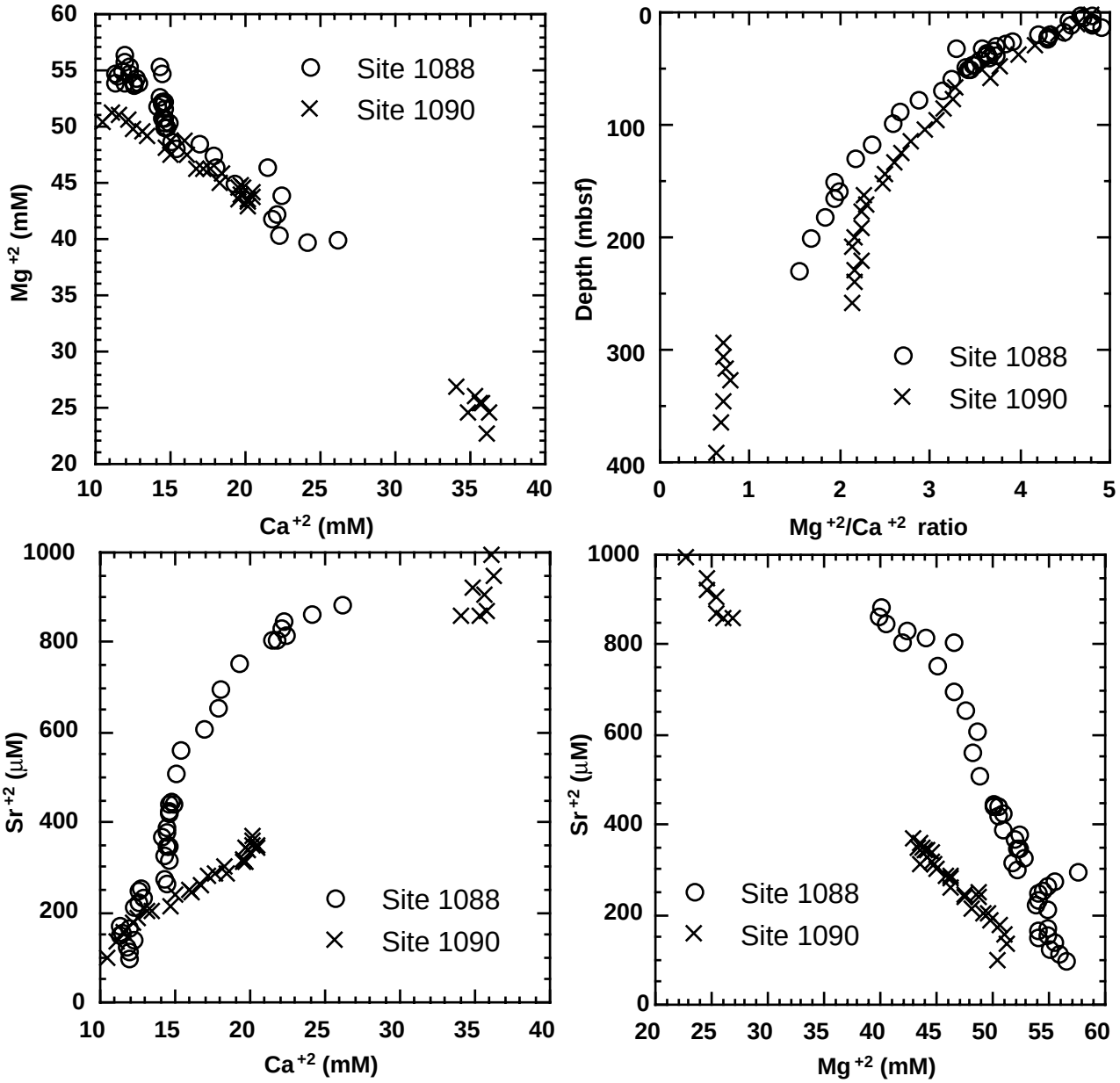

Figure F24. Concentration of calcium carbonate ($CaCO_3$), total organic carbon (TOC), total nitrogen (TN), total sulfur (TS), and TOC/TN vs. depth at Site 1090; the data are reported in Table **T13**, p. 96. The solid line in $CaCO_3$ concentrations shows a long-term trend, which was smoothed with a 7-point running mean.

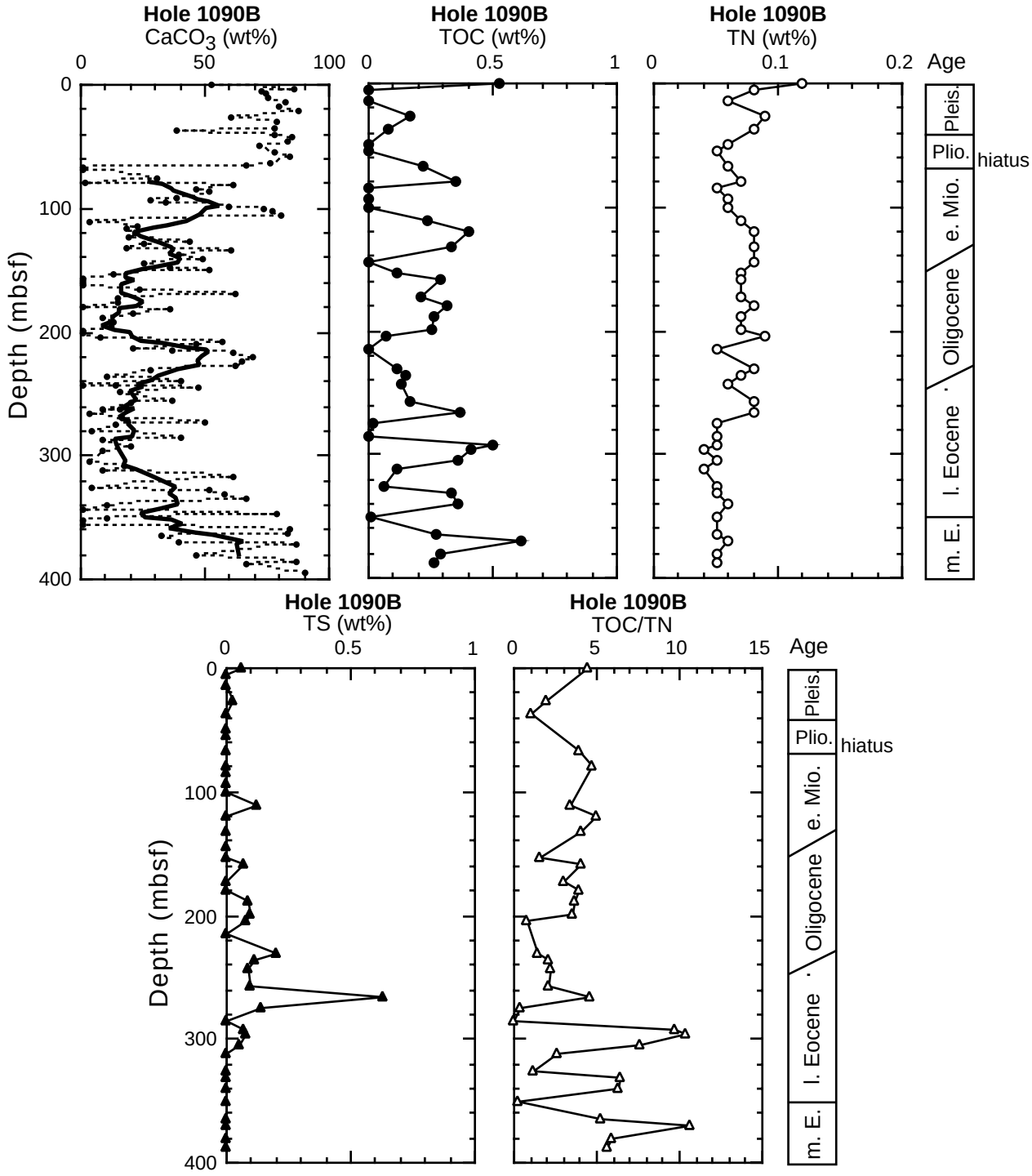

Figure F25. Site 1090 downhole variations of porosity (open circles; MAD method) and OSU-SCAT resistivity (solid line), *P*-wave velocities (small dots = PWL, solid circles = PWS3), GRA (solid line = smoothed data) and MAD bulk density (open circles), volume-specific magnetic susceptibility, and NGR (smoothed data: Holes 1090B and 1090E). H = hiatus.

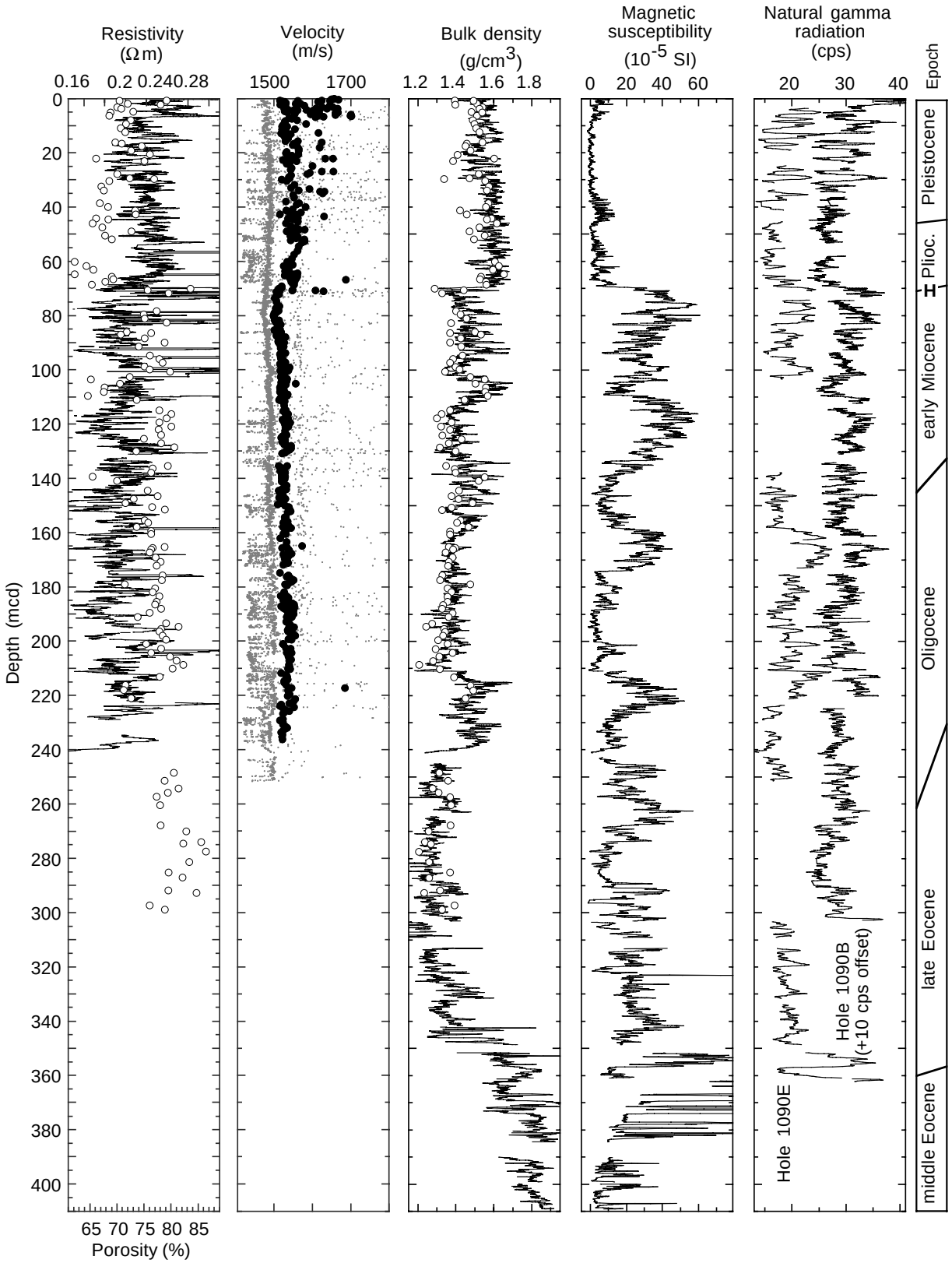

Figure F26. Covariance between resistivity, GRA (solid line) and MAD bulk density (open circles), magnetic susceptibility, NGR emission, and reflectance in the upper 70 mcd of Site 1090. All properties show cyclicity with a period of ~5 m in the uppermost 30 mcd, and a smaller period of ~2 m below. H = hiatus, B/M = Brunhes/Matuyama boundary.

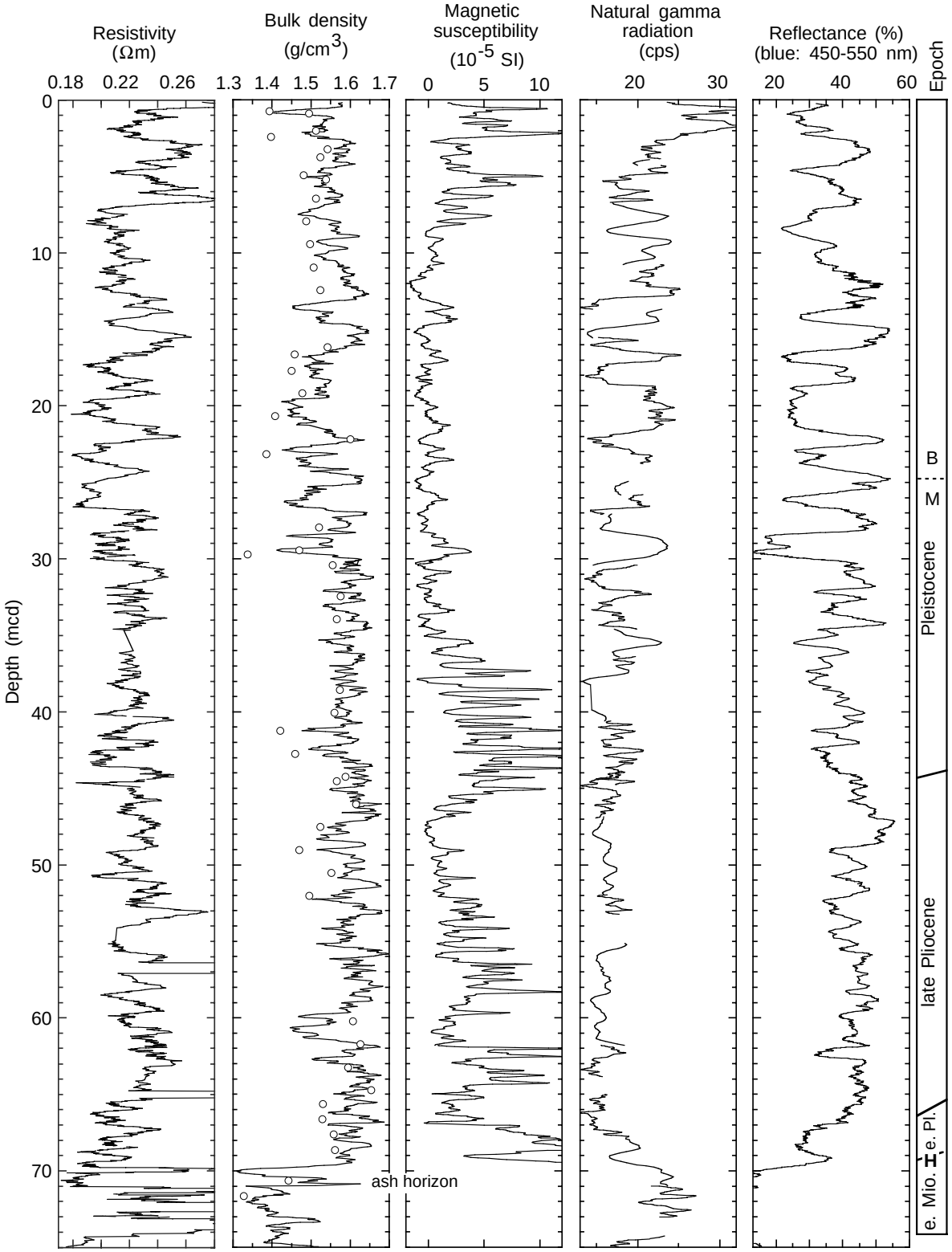

Figure F27. Relationship between GRA and gravimetric (MAD) bulk density at Site 1090.

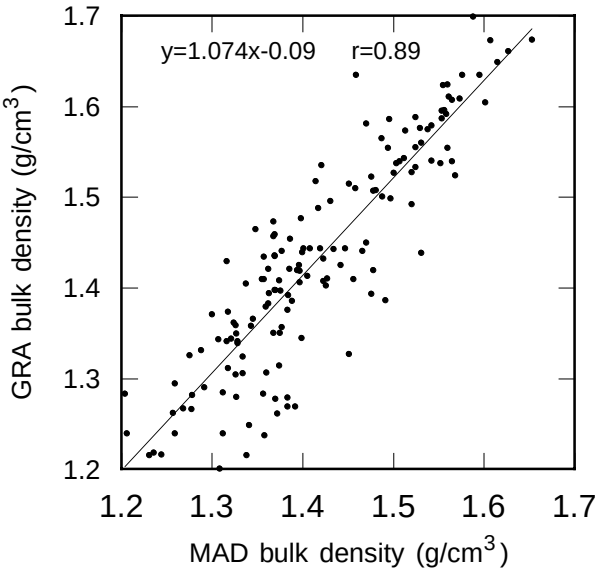

Figure F28. Minolta CM-2002 spectral reflectance in the red band from Hole 1090B.

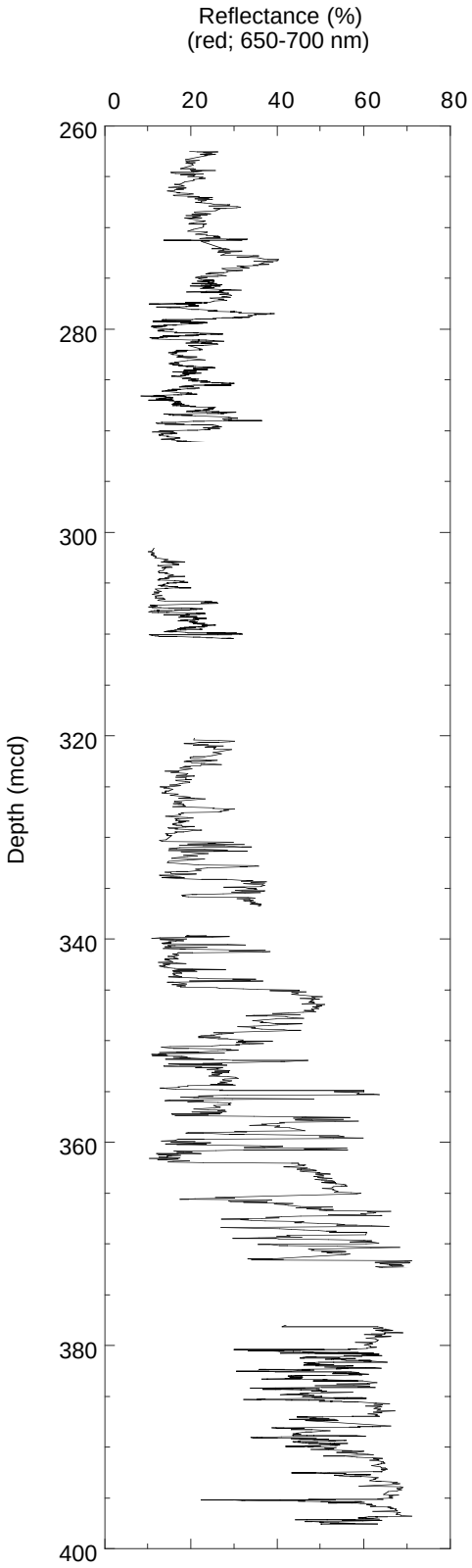

Figure F29. Comparison of OSU-SCAT blue (450–550) and red (650–750) reflectance to carbonate measurements from Sites 1088–1090 indicates a clear relationship between these variables.

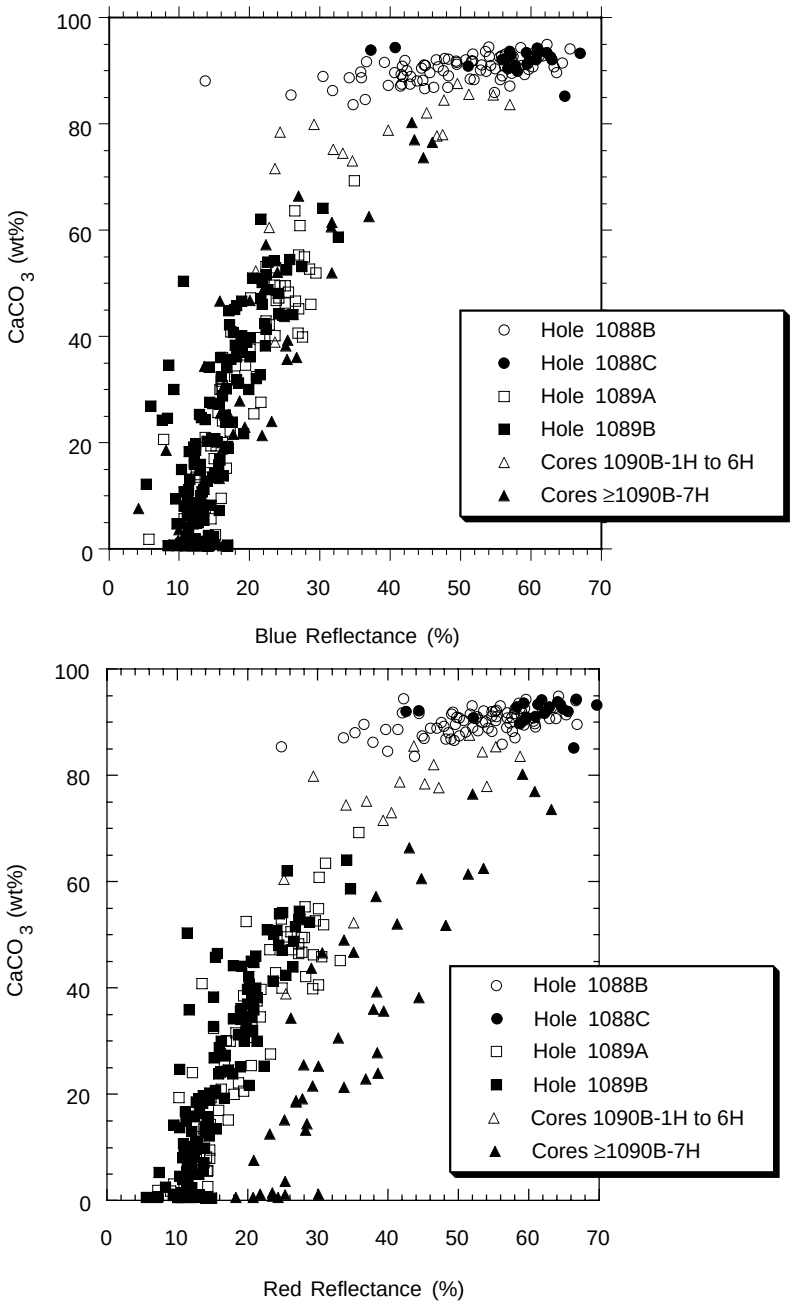

Figure F30. Site 1090 blue (450–550 nm) and red (650–750 nm) reflectance. Sediments above the hiatus (H) exhibit a smaller red/blue contrast than those below as a result of the significant red-clay component of the sediment at this depth.

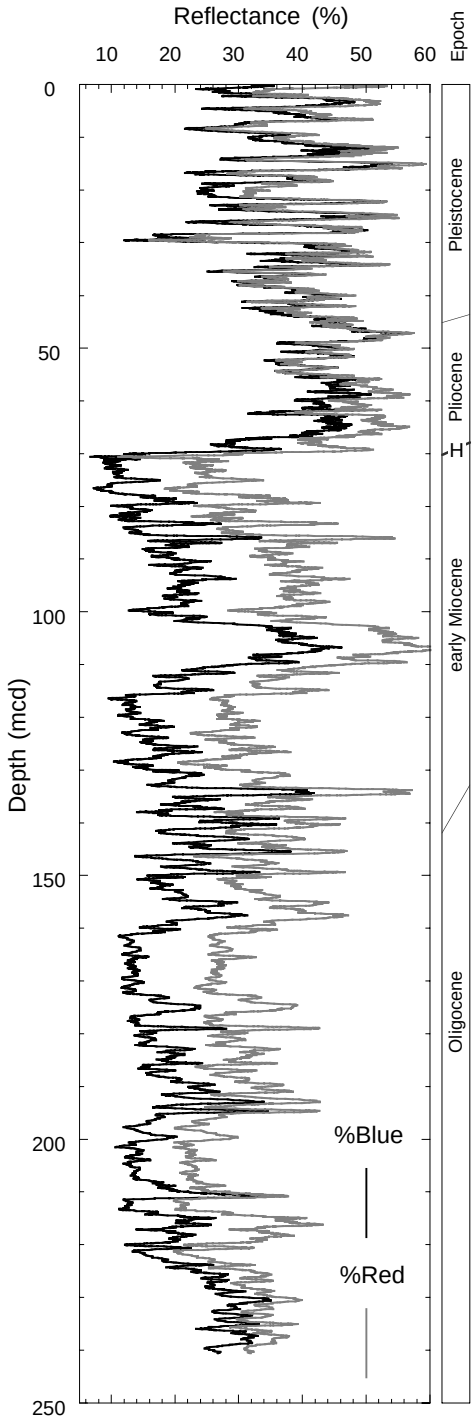

Figure F31. Thermal conductivity measurements of sediment cores at Site 1090. **A.** Frequency distribution of measured values. **B.** Correlation of measured values with interpolated GRA bulk density values. **C.** Thermal conductivity (solid circles) compared to interpolated GRA bulk density (open squares).

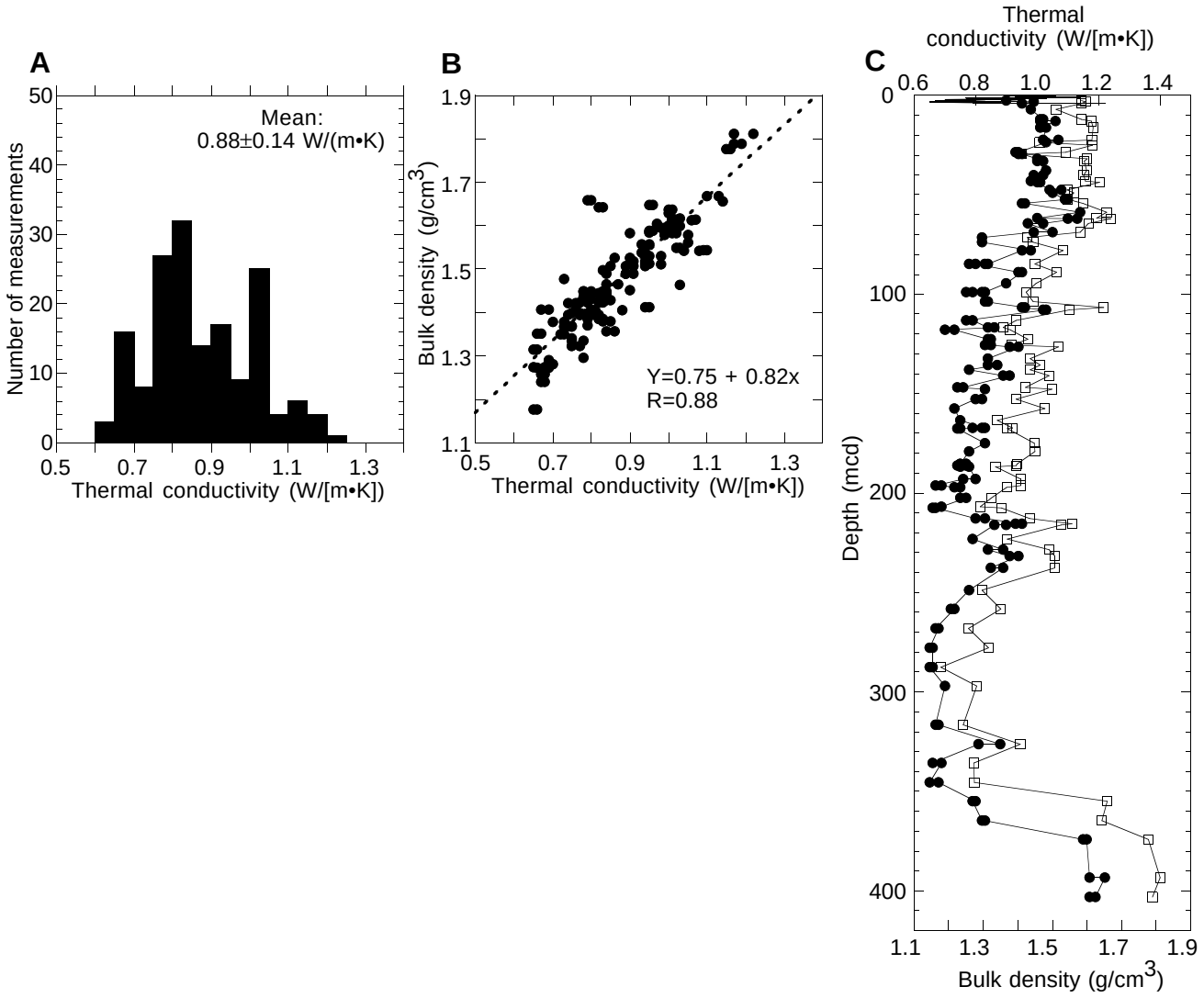

Table T1. X-ray diffraction estimates of opal and terrigenous sediment abundances for Site 1090. (Continued on next page.)

Core, section, interval (cm)	Depth (mbsf)	Depth (mcd)	Quartz/ feldspar (XRD peak area ratio)	Clay/ (quartz + feldspar) (XRD peak area ratio)	Opal carbonate-free fraction (wt%; XRD peak intensity)
177-1090B-					
1H-1, 74-75	0.75	0.75	1.1	0.188	
177-1090A-					
1H-1, 91-93	0.92	0.92	1.29	0.154	17.2
1H-2, 91-93	2.42	2.42	1.39	0.106	10.7
177-1090B-					
1H-3, 74-76	3.25	3.25	1.97	0.219	
2H-1, 76-77	4.97	4.97	1.3	0.23	18.2
177-1090A-					
1H-4, 72-74	5.23	5.23	1.76	0.203	
177-1090B-					
2H-3, 76-77	7.97	7.97	1.55	0.246	
2H-5, 76-77	10.97	10.97	1.29	0.19	18.2
3H-1, 71-73	14.42	16.17	1.56	0.275	15.7
3H-3, 72-73	17.43	19.18	1.33	0.202	
3H-6, 75-78	21.97	23.72	1.66	0.254	
4H-3, 76-77	26.97	29.48	1.7	0.141	16.7
4H-5, 75-77	29.96	32.47	1.55	0.211	13.7
5H-4, 76-77	37.67	41.28	1.42	0.148	15.7
6H-3, 76-78	45.97	47.57	0.92	0.288	26.1
6H-4, 74-76	47.45	49.05	2.36	0.129	15.4
7H-3, 74-76	55.45	61.75	1.01	0.275	
7H-5, 74-76	58.45	64.75	0.91	0.129	
8H-2, 22-24	62.93	66.64	1.49	0.219	17.2
8H-3, 76-77	64.97	68.68	1.37	0.29	22.2
9H-4, 72-73	75.93	79.62	0.65	0.359	
9H-6, 72-73	78.93	82.62	0.85	0.378	18.7
10H-3, 74-76	83.95	88.52	0.6	0.218	19.7
10H-5, 74-76	86.95	91.52	0.67	0.244	
11H-4, 72-73	94.93	98.92	0.69	0.247	34.6
11H-6, 20-21	96.81	100.8	0.62	0.277	
13H-2, 76-77	111	116.4	0.44	0.215	27.6
13H-6, 53-54	116.7	122.2	0.63	0.276	31.6
14H-2, 72-73	120.4	124.1	0.78	0.232	26.6
14H-3, 72-73	121.9	125.6	0.7	0.315	
15H-3, 72-73	131.4	137.9	0.97	0.306	29.1
15H-5, 71-73	134.4	140.9			89.9
16H-2, 119-121	139.9	146.6	0.97	0.418	28.1
16H-5, 73-77	144	150.6	1.01	0.229	14.7
17H-3, 74-76	150.5	158	0.95	0.283	23.6
17H-5, 35-37	153.1	160.6	0.79	0.313	
18H-5, 75-76	163	170.7	0.97	0.276	31.6
19H-5, 72-74	172.4	181.9	1.33	0.326	33.6
20H-2, 122-125	177.9	185.6	0.93	0.351	177.9
21X-1, 72-73	185.4	193.5	0.68	0.367	53.5
21X-3, 72-73	188.4	196.5	0.95	0.368	37.1
22X-3, 73-74	198.1	205.8	0.83	0.282	44.6
22X-5, 73-74	201.1	208.8	0.99	0.341	
23X-1, 72-73	204.8	213.2	0.76	0.289	29.6
23X-5, 72-73	209.7	218.1	0.72	0.184	26.1
23X-7, 72-73	212.7	221.1	0.7	0.363	
24X-1, 70-71	214.5	225.5	0.38	0.294	35.6
24X-5, 86-87	220.7	231.6	0.33	0	12.7
25X-1, 61-62	224.1	234.8	0.3	0.265	53
25X-5, 61-62	230.1	240.8	0.51	0	68.5
26X-3, 21-23	236.4	248.4	0.29	0.362	36.1
26X-5, 23-26	239.4	251.4	0.5	0.17	43.1
26X-7, 17-20	242.4	254.4	0.32	0.21	45.6
27X-2, 97-100	245.4	257.4	0.96	0.159	46.6
27X-4, 100-102	248.4	260.4	0.42	0.389	28.1

Table T1 (continued).

Core, section, interval (cm)	Depth (mbsf)	Depth (mcd)	Quartz/ feldspar (XRD peak area ratio)	Clay/ (quartz + feldspar) (XRD peak area ratio)	Opal carbonate-free fraction (wt%; XRD peak intensity)
28X-4, 93-95	258	270	0.43	0.083	80.4
29X-3, 23-25	265.5	277.5	0.53		
29X-5, 109-111	269.4	281.4	0.29	0.198	
30X-1, 124-126	273.2	285.2	0.55	0.281	56.5
30X-6, 30-32	279.8	291.8	0.18	0.167	
31X-3, 64-66	285.4	297.3	0.35	0.121	36.1
31X-4, 72-74	286.9	298.9	0.32	0.152	31.6
32X-1, 46-47	291.9	303.9	0.54	0.206	46.1
32X-2, 46-47	293.4	305.4	0.61	0.287	70.5
33X-2, 91-92	296.7	308.7	0.49	0.2	33.6
34X-3, 60-61	304.7	316.7	0.42	0.155	42.1
34X-6, 43-44	309	321	0.49	0.22	49
35X-2, 47-48	312.8	324.8	0.39	0.263	36.6
35X-5, 60-61	317.4	329.4	0.2	0.264	27.1
36X-4, 70-71	325.6	337.6	0.19	0.317	23.1
36X-5, 91-92	327.3	339.3	0.15	0.268	24.1
37X-1, 71-72	330.7	342.7	0.18	0.191	24.6
37X-4, 71-72	335.2	347.2	0.24	0.348	19.7
38X-3, 71-72	343.3	355.3	0.26	0.517	13.2
38X-5, 71-73	346.3	358.3	0.42	0.431	
39X-3, 71-72	352.9	364.9	0.53	0.531	0.7
39X-5, 71-72	355.9	367.9	0.71	0.613	9.7
40X-3, 71-73	362.5	374.5	0.87	0.566	
40X-5, 71-72	365.5	377.5	0.65	0.425	5.2
41X-1, 84-86	369.2	381.2	0.73	0.461	1.2
41X-3, 85-87	372.3	384.3	1.86	0.65	
42X-2, 94-96	380.6	392.5	0.79	0.66	4.2
42X-6, 84-86	386.5	398.4	0.81	0.685	1.7
43X-1, 65-67	388.5	400.4	1.05	0.727	6.7
43X-5, 55-57	394.4	406.4	0.84	0.597	8.2

Notes: XRD = X-ray diffraction. This table is also available in ASCII format in the **TABLES** directory.

Table T2. Composite depths for Site 1090. (Continued on next page.)

Core, section	Depth (mbsf)	Offset (m)	Depth (mcd)
177-1090A-			
1H	0.00	0.00	0.00
177-1090B-			
1H	0.00	0.00	0.00
2H	4.20	0.00	4.20
3H	13.70	1.75	15.45
4H	23.20	2.51	25.71
5H	32.70	3.61	36.31
6H	42.20	1.60	43.80
7H	51.70	6.30	58.00
8H	61.20	3.71	64.91
9H	70.70	3.69	74.39
10H	80.20	4.57	84.77
11H	89.70	3.99	93.69
12H	99.20	3.67	102.87
13H	108.70	5.41	114.11
14H	118.20	3.65	121.85
15H	127.70	6.49	134.19
16H	137.20	6.65	143.85
17H	146.70	7.50	154.20
18H	156.20	7.78	163.98
19H	165.70	9.49	175.19
20H	175.20	7.61	182.81
21X	184.70	8.05	192.75
22X	194.40	7.61	202.01
23X	204.10	8.40	212.50
24X	213.80	10.96	224.76
25X	223.50	10.71	234.21
26X	233.20	11.99	245.19
27X	242.90	11.99	254.89
28X	252.60	11.99	264.59
29X	262.30	11.99	274.29
30X	272.00	11.99	283.99
31X	281.70	11.99	293.69
32X	291.40	11.99	303.39
33X	294.90	11.99	306.89
34X	301.10	11.99	313.09
35X	310.80	11.99	322.79
36X	320.40	11.99	332.39
37X	330.00	11.99	341.99
38X	339.60	11.99	351.59
39X	349.20	11.99	361.19
40X	358.80	11.99	370.79
41X	368.40	11.99	380.39
42X	378.10	11.99	390.09
43X	387.80	11.99	399.79
177-1090C-			
1H	0.00	0.50	0.50
2H	2.80	5.57	8.37
3H	12.30	6.25	18.55
4H	21.80	6.31	28.11
5H	31.30	8.05	39.35
6H	40.80	7.82	48.62
7H	50.30	7.82	58.12
8H	59.80	7.81	67.61
177-1090D-			
1H	0.00	0.34	0.34
2H	7.40	2.15	9.55
3H	16.90	3.07	19.97
4H	26.40	2.99	29.39
5H	35.90	4.21	40.11
6H	45.40	5.46	50.86
7H	54.90	6.08	60.98
8H	64.40	5.91	70.31
9H	73.90	7.53	81.43
10H	83.40	7.53	90.93

Table T2 (continued).

Core, section	Depth (mbsf)	Offset (m)	Depth (mcd)
11H	92.90	7.13	100.03
12H	102.40	7.13	109.53
13H	111.90	6.89	118.79
14H	121.40	7.25	128.65
15H	130.90	6.47	137.37
16H	140.40	8.64	149.04
17H	149.90	9.88	159.78
18H	159.40	11.70	171.10
19H	168.90	12.65	181.55
20H	178.40	10.85	189.25
21H	187.90	10.93	198.83
22H	197.40	11.70	209.10
23H	206.90	12.63	219.53
24H	216.40	11.64	228.04
177-1090E-			
1H	0.00	3.38	3.38
2H	8.70	3.59	12.29
3H	18.20	6.71	24.91
4H	27.70	6.15	33.85
5H	37.20	8.29	45.49
6H	46.70	8.42	55.12
7H	56.20	8.89	65.09
8H	65.70	8.55	74.25
9H	75.20	9.91	85.11
10H	84.70	10.37	95.07
11H	94.20	9.81	104.01
12H	103.70	9.21	112.91
13H	113.20	9.61	122.81
14H	122.70	9.15	131.85
15H	132.20	10.81	143.01
16H	141.70	12.06	153.76
17H	151.20	12.43	163.63
18H	160.70	14.73	175.43
19H	170.20	13.06	183.26
20H	179.70	13.94	193.64
21H	189.20	14.12	203.32
22H	198.70	13.44	212.14
23H	208.20	15.36	223.56
24H	217.70	15.41	233.11
25H	227.20	15.47	242.67

Note: This table is also available in ASCII format in the **TABLES** directory.

Table T3. Site 1090 splice tie points.

Core, section, interval (cm)	Depth (mbsf)	Depth (mcd)		Core, section, interval (cm)	Depth (mbsf)	Depth (mcd)
177-				177-		
1090B-1H-2, 66	2.16	2.16	tie to	1090D-1H-2, 32	1.82	2.16
1090D-1H-5, 36	6.36	6.70	tie to	1090E-1H-3, 32	3.32	6.70
1090E-1H-5, 144	7.44	10.82	tie to	1090D-2H-1,127	8.67	10.82
1090D-2H-5, 124	14.64	16.79	tie to	1090B-3H-1, 134	15.04	16.79
1090B-3H-5, 74	20.44	22.19	tie to	1090D-3H-2, 72	19.12	22.19
1090D-3H-5, 114	24.04	27.11	tie to	1090E-3H-2, 69	20.40	27.11
1090E-3H-4, 96	23.66	30.37	tie to	1090D-4H-1, 66	27.06	30.05
1090D-4H-6, 8	33.98	36.97	tie to	1090E-4H-3, 12	30.82	36.97
1090E-4H-5, 76	34.46	40.61	tie to	1090D-5H-1, 50	36.40	40.61
1090D-5H-5, 84	42.74	46.95	tie to	1090E-5H-1, 146	38.66	46.95
1090E-5H-5, 80	43.70	51.99	tie to	1090D-6H-1, 112	46.53	51.99
1090D-6H-5, 48	51.88	57.34	tie to	1090E-6H-2, 72	48.92	57.34
1090E-6H-5, 68	53.38	61.80	tie to	1090D-7H-1, 82	55.72	61.80
1090D-7H-5, 88	61.78	67.86	tie to	1090E-7H-2, 127	58.97	67.86
1090E-7H-5, 44	62.64	71.53	tie to	1090D-8H-1, 122	65.62	71.53
1090D-8H-6, 96	72.86	78.77	tie to	1090E-8H-4, 1	70.22	78.77
1090E-8H-6, 122	74.42	82.97	tie to	1090D-9H-2, 4	75.44	82.97
1090D-9H-4, 28	78.68	86.21	tie to	1090E-9H-1, 110	76.30	86.21
1090E-9H-5, 144	82.64	92.55	tie to	1090D-10H-2, 12	85.02	92.55
1090D-10H-5, 142	90.82	98.35	tie to	1090E-10H-3, 28	87.98	98.35
1090E-10H-5, 144	92.14	102.51	tie to	1090D-11H-2, 98	95.38	102.51
1090D-11H-6, 48	100.88	108.01	tie to	1090E-11H-3, 100	98.20	108.01
1090E-11H-6, 14	101.84	111.65	tie to	1090D-12H-2, 62	104.52	111.65
1090D-12H-4, 102	107.92	115.05	tie to	1090E-12H-2, 64	105.84	115.05
1090E-12H-6, 12	111.32	120.53	tie to	1090D-13H-2, 24	113.64	120.53
1090D-13H-5, 92	118.82	125.71	tie to	1090E-13H-2, 140	116.10	125.71
1090E-13H-5, 60	119.80	129.41	tie to	1090D-14H-1, 76	122.16	129.41
1090D-14H-4, 144	127.34	134.59	tie to	1090E-14H-2, 124	125.44	134.59
1090E-14H-6, 40	130.60	139.75	tie to	1090D-15H-2, 120	133.61	140.08
1090D-15H-6, 96	139.01	145.48	tie to	1090E-15H-2, 95.5	134.67	145.48
1090E-15H-6, 4	139.74	150.55	tie to	1090D-16H-1, 151	141.91	150.55
1090D-16H-5, 26	146.66	155.30	tie to	1090E-16H-2, 2	143.24	155.30
1090E-16H-5, 124	148.94	161.00	tie to	1090D-17H-1, 122	151.12	161.00
1090D-17H-5, 124	157.14	167.02	tie to	1090B-18H-3, 3	159.24	167.02
1090B-18H-6, 80	164.50	172.28	tie to	1090D-18H-1, 118	160.58	172.28
1090D-18H-4, 28	164.18	175.88	tie to	1090E-18H-1, 43.5	161.15	175.88
1090E-18H-5, 104	167.74	182.47	tie to	1090D-19H-1, 91	169.82	182.47
1090D-19H-3, 118	173.08	185.73	tie to	1090E-19H-2, 95.5	172.67	185.73
1090E-19H-5, 48	176.68	189.74	tie to	1090D-20H-1, 48.5	178.89	189.74
1090D-20H-6, 20	186.10	196.95	tie to	1090E-20H-3, 30.5	183.01	196.95
1090E-20H-6, 104	188.24	202.18	tie to	1090D-21H-3, 34.5	191.25	202.18
1090D-21H-6, 86	196.26	207.19	tie to	1090E-21H-3, 86.5	193.07	207.19
1090E-21H-6, 28	196.98	211.10	tie to	1090D-22H-2, 50	199.40	211.10
1090D-22H-5, 106	204.46	216.16	tie to	1090E-22H-3, 101	202.72	216.16
1090E-22H-6, 76	206.96	220.40	tie to	1090D-23H-1, 86.5	207.77	220.40
1090D-23H-4, 128	212.68	225.31	tie to	1090E-23H-2, 23.5	209.95	225.31
1090E-23H-3, 20	211.40	226.76	tie to	1090B-24X-2, 49	215.80	226.76
1090B-24X-3, 112	217.92	228.88	tie to	1090D-24H-1, 84	217.24	228.88
1090D-24H-5, 136	223.76	235.40	tie to	1090E-24H-2, 78.5	219.99	235.40
1090E-24H-6, 48	225.68	241.09				

Note: This table is also available in ASCII format in the **TABLES** directory.

Table T4. Distribution of main calcareous nannofossil species in Hole 1090B. (Continued on next two pages.)

Core, section, interval (cm)	Depth (mbsf)	Depth (mcd)	Abundance	Preservation	*Reticulofenestra umbilica*	*Nannotetrina cristata*	*Discoaster saipanensis*	*Reticulofestra reticulata*	*Reticulofenestra bisecta*	*Chiasmolithus oamaruensis*	*Reticulofenestra oamaruensis*	*Ismolithus recurvus*	*Chiasmolithus* spp.	*Clausicoccus* spp.	*Cyclicargolithus abisectus*	*Cyclicargolithus floridanus*	*Coccolithus miopelagicus*	*Discoaster deflandrei* gr.	*Sphenolithus belemnos*	*Sphenolithus belemnos-dissimilis*	*Calcidiscus* sp.	*Discoaster pentaradiatus*	*Discoaster brouweri*	*Reticulofenestra pseudoumbilicus*	*Pseudoemiliania lacunosa*	*Calcidiscus macintyrei*	*Gephyrocapsa* medium (4-5.5 µm)	*Gephyrocapsa* large (>5.5 µm)	*Gephyrocapsa* sp. 3	*Reticulofenestra asanoi*	*Emiliania huxleyi*
177-1090B-																															
1H-3, 30-30	3.80	2.80	A	G																											D
1H-CC, 20-25	4.20	4.20	A	G																							C				A
2H-1, 130-130	5.80	5.50	A	M																							C				C
2H-2, 30-30	6.00	6.00	A	M																							A				
2H-2, 130-130	7.00	7.00	A	M																							C				?
2H-4, 30-30	7.50	9.00	A	M																											
2H-CC, 0-10	13.80	13.80	A	G																											
3H-1, 40-40	14.10	15.85	A	M																											
3H-1, 130-130	15.00	16.75	A	G																					F						
3H-2, 130-130	16.50	18.25	F	G																					C						
3H-3, 130-130	18.00	19.75	A	G																					C						
3H-4, 130-130	19.50	21.25	A	M																					F						
3H-CC, 13-18	22.28	24.03	A	M																					A						
4H-3, 30-30	26.50	29.01	A	M																					C						
4H-3, 130-130	27.50	30.01	A	M																					C					C	
4H-4, 130-130	29.00	31.51	A	M																					C					C	
4H-5, 30-30	29.50	32.01	A	G																					C				C	F	
4H-5, 130-130	30.50	33.01	A	M																					F				F	F	
4H-6, 30-30	31.00	33.51	A	M																					C				F	C	
4H-CC, 12-17	32.51	35.02	A	M																					R					F	
5H-1, 35-35	33.05	36.66	A	G																					C						
5H-1, 130-130	34.00	37.61	A	G																					A			F	A		
5H-2, 30-30	34.50	38.11	A	G																					F			F	A		
5H-2, 130-130	35.50	39.11	A	G																					C			C	C		
5H-3, 30-30	36.00	39.61	A	G																					A			F	C		
5H-3, 110-110	36.80	40.41	A	G																					C			C			
5H-4, 30-30	37.50	40.81	A	M																					A			C			
5H-4, 130-130	38.50	41.81	A	G																					A			C			
5H-5, 30-30	39.00	42.31	A	G																					A			C			
5H-5, 130-130	40.30	43.31	A	G																					C	R		R			
5H-6, 30-30	40.50	43.81	A	G																					C	F		R			
5H-6, 130-130	41.50	44.81	A	G																					C	R					
5H-CC, 14-19	41.40	45.01	A	M																				R	A	F					
6H-1, 30-30	42.50	44.10	A	M																					C	R					
6H-2, 130-130	45.00	46.60	A	M																				R	C	R					
6H-6, 130-130	51.00	52.60	A	P																				R	C						
6H-7, 30-30	51.50	53.10	A	M																				R	C						
6H-CC, 9-14	51.84	53.44	A	M																		R			C						
7H-CC, 12-17	59.29	65.59	A	M																		R	R		C	F					
8H-1, 30-30	61.50	65.21	A	M																		R	R		F	R					
8H-1, 120-120	62.40	66.11	A	M																					F						
8H-2, 140-140	64.10	67.81	A	M																		R	R	C		R					
8H-4, 30-30	66.00	69.71	A	M																		R									
8H-5, 30-30	67.50	71.21	A	P														A													
8H-CC, 18-23	69.63	73.34	F	P														F													
9H-3, 140-140	75.10	78.79	A	M											F	R	F				R										
9H-5, 30-30	77.00	80.69	A	P											F		C				R										
9H-6, 30-30	78.50	82.19	A	P											F		C														
9H-6, 100-100	79.20	82.89	A	P											C						R										
9H-CC, 13-18	79.99	83.68	F	P											F		F				R										

Table T4 (continued).

Core, section, interval (cm)	Depth (mbsf)	Depth (mcd)	Abundance	Preservation	*Reticulofenestra umbilica*	*Nannotetrina cristata*	*Discoaster saipanensis*	*Reticulofestra reticulata*	*Reticulofenestra bisecta*	*Chiasmolithus oamaruensis*	*Reticulofenestra oamaruensis*	*Ismolithus recurvus*	*Chiasmolithus* spp.	*Clausicoccus* spp.	*Cyclicargolithus abisectus*	*Cyclicargolithus floridanus*	*Coccolithus miopelagicus*	*Discoaster deflandrei* gr.	*Sphenolithus belemnos*	*Sphenolithus belemnos-dissimilis*	*Calcidiscus* sp.	*Discoaster pentaradiatus*	*Discoaster brouweri*	*Reticulofenestra pseudoumbilicus*	*Pseudoemiliania lacunosa*	*Calcidiscus macintyrei*	*Gephyrocapsa* medium (4-5.5 µm)	*Gephyrocapsa* large (>5.5 µm)	*Gephyrocapsa* sp. 3	*Reticulofenestra asanoi*	*Emiliania huxleyi*
10H-1, 140-140	81.60	86.17	A	M												C				R	R										
10H-3, 140-140	84.60	89.17	A	P												C			R	R											
10H-CC, 19-24	88.41	92.98	C	P									R			F		F													
11H-1, 30-30	90.00	93.99	C	P																											
11H-4, 30-30	94.50	98.49	C	P																											
11H-CC, 10-15	99.16	103.15	F	P									F			F		F													
12H-2, 30-30	101.00	104.67	A	P																											
12H-5, 130-130	106.50	110.17	A	P													F														
12H-CC, 6-11	108.89	112.56	A	M												C	F														
13H-2, 130-130	111.50	116.91	C	P																											
13H-6, 90-90	117.10	122.51	C	P																											
13H-CC, 0-5	117.12	122.53	B																												
14H-2, 30-30	120.00	123.65	C	P																											
14H-5, 130-130	125.50	129.15	A	P																											
14H-CC, 0-5	127.51	131.16	C	P											?	C															
15H-1, 130-130	129.00	135.49	A	P											R	A															
15H-6, 130-130	136.50	142.99	A	M											A	C															
15H-CC, 0-10	136.73	143.22	A	M											F	C		C													
16H-1, 30-30	137.50	144.15	C	M											C	A		F													
16H-4, 30-30	142.00	148.65	C	M											C	A	C	F													
16H-6, 130-130	146.00	152.65	C	P											C		R	C													
16H-CC, 0-10	146.75	153.40	C	M											F	C		F													
17H-1, 30-30	147.00	154.50	C	P											F	C	R														
17H-CC, 14-24	154.36	161.86	B																												
18H-CC, 6-16	165.37	173.15	C	P											F	C		F													
19H-1, 30-30	166.00	175.49	C	P											A	C															
19H-1, 120-120	166.90	176.39	B																												
19H-2, 30-30	167.50	176.99	B																												
19H-2, 130-130	168.50	177.99	B																												
19H-3, 30-30	169.00	178.49	B																												
19H-3, 130-130	170.00	179.49	F	P									R		C			F													
19H-4, 120-120	171.40	180.89	A	M					F									C													
19H-5, 30-30	172.00	181.49	C	P					R						C	C		R													
19H-5, 110-110	172.80	182.29	B																												
19H-CC, 24-34	173.14	182.63	A	M					F						C	F															
20H-1, 30-30	175.50	183.11	B															F													
20H-1, 120-120	176.40	184.01	A	M											C		F														
20H-2, 120-120	177.90	185.51	C	M					F				R		C																
20H-3, 120-120	179.40	187.01	C	P											C																
20H-4, 30-30	180.00	187.61	B																												
20H-4, 120-120	180.90	188.51	B																												
20H-5, 30-30	181.50	189.11	F	P					F																						
20H-CC, 22-32	184.42	192.03	A	M					F						C																
21X-1, 30-30	185.00	193.05	A	M					R						A		R														
21X-2, 130-130	187.50	195.55	C	P					R				R		A																
21X-3, 30-30	188.00	196.05	C	M					R						A			C													
21X-3, 130-130	189.00	197.05	F	P					C						F																
21X-4, 130-130	190.50	198.55	A	M					C				R		C																
21X-6, 30-30	192.50	200.55	F	P					F						A																
21X-6, 130-130	193.50	201.55	B																												
21X-7, 10-10	193.80	201.85	B																												
21X-CC, 15-25	194.09	202.14	B																												
22X-1, 30-30	194.70	202.31	B																												
22X-1, 130-130	195.70	203.31	B																												
22X-4, 130-130	200.20	207.81	B																												
22X-6, 130-130	203.20	210.81	B																												

Table T4 (continued).

Core, section, interval (cm)	Depth (mbsf)	Depth (mcd)	Abundance	Preservation	*Reticulofenestra umbilica*	*Nannotetrina cristata*	*Discoaster saipanensis*	*Reticulofestra reticulata*	*Reticulofenestra bisecta*	*Chiasmolithus oamaruensis*	*Reticulofenestra oamaruensis*	*Ismolithus recurvus*	*Chiasmolithus* spp.	*Clausicoccus* spp.	*Cyclicargolithus abisectus*	*Cyclicargolithus floridanus*	*Coccolithus miopelagicus*	*Discoaster deflandrei* gr.	*Sphenolithus belemnos*	*Sphenolithus belemnos-dissimilis*	*Calcidiscus* sp.	*Discoaster pentaradiatus*	*Discoaster brouweri*	*Reticulofenestra pseudoumbilicus*	*Pseudoemiliania lacunosa*	*Calcidiscus macintyrei*	*Gephyrocapsa* medium (4-5.5 µm)	*Gephyrocapsa* large (>5.5 µm)	*Gephyrocapsa* sp. 3	*Reticulofenestra asanoi*	*Emiliania huxleyi*
22X-CC, 0-10	203.69	211.30	B																												
23X-1, 30-30	204.40	212.80	C	P					C								R														
23X-2, 30-30	205.90	214.30	A	P					C						F																
23X-4, 30-30	208.90	217.30	A	P					C						F			F													
23X-6, 130-130	212.90	220.20	C	P					C																						
23X-7, 30-30	213.40	220.70	A	M					C						F	C															
23X-7, 130-130	214.40	221.70	A	M	A				A																						
23X-CC, 26-36	213.76	222.16	A	M	A				F			A				F															
24X-1, 30-30	214.10	225.06	A	M	C				C			F																			
24X-1, 130-130	215.10	226.06	A	C	A				R			C	F	F																	
24X-3, 130-130	218.10	229.06	A	M	A				C		cf.	C	F	C																	
24X-4, 30-30	218.60	229.56	A	M	A				C			F	R																		
24X-5, 130-130	221.10	232.06	A	M	A				F			C	R	A																	
24X-7, 10-10	222.90	233.86	A	M	A				C			C	R	F																	
24X-CC, 18-28	223.35	234.21	A	M	C				F	F		A																			
25X-CC, 19-27	233.01	243.72	C	P	A				A	R	R	A			F																
26X-1, 30-30	233.50	245.49	C	M	A				F			C	F																		
26X-CC, 10-15	242.73	254.72	B																												
27X-4, 120-120	248.60	260.59	F	P	A				C			C																			
27X-5, 30-30	249.20	261.19	C	P	A				C		R	C					R														
27X-5, 120-120	250.10	262.09	C	P	A				C			F																			
27X-6, 30-30	250.70	262.69	A	P	A		R		C			R																			
27X-CC, 13-18	251.53	263.52	A	P	C		F		F			C																			
28X-CC, 16-21	262.19	274.18	F	P	F				F	R		R				R															
29X-CC, 17-22	271.87	283.86	C	P	F				F			F																			
30X-CC, 21-34	281.69	293.68	F	P	F				F			F																			
31X-1, 120-120	282.90	294.89	C	P	A				C			A				F															
31X-2, 120-120	284.40	296.39	A	P	A		R		C			C				R															
31X-4, 30-30	286.50	298.49	C	P	C				C			R																			
31X-4, 130-130	287.50	299.49	A	P	C		R		C			F				R															
31X-6, 30-30	289.50	301.49	A	P	C		R		C			C																			
31X-7, 30-30	291.00	302.99	A	M	A		F		C							R	R				R										
31X-CC, 21-26	291.50	303.43	C	M	F				F						R	F															
32X-CC, 27-32	294.38	306.37	B																												
33X-CC, 13-18	297.73	309.39	F	P	F		F	R	F																						
35X-CC, 17-20	319.91	331.90	A	M	C			C	F	R																					
36X-CC, 26-34	330.12	342.11	R*	P	R			R																							
37X-CC, 40-45	337.16	349.15	C	P	C		R	F	R																						
38X-4, 130-130	345.40	357.39	C	M	C			F	F																						
38X-7, 10-10	348.70	360.69	C	M	C			F	R																						
38X-CC, 8-18	349.12	361.11	A	M	F				R																						
39X-1, 130-130	350.50	362.49	F	P	F																										
39X-2, 130-130	352.00	363.99	C	M	C		R		?																						
39X-CC, 12-22	358.78	370.77	A	M	F																										
40X-CC, 21-31	368.55	380.54	A	M	C									R																	
41X-CC, 0-5	372.58	384.57	A	M	F																										
42X-1, 30-30	378.40	390.39	A	M	F	C																									
42X-1, 120-120	379.30	391.29	C	M	F	F																									
42X-3, 30-30	381.40	393.39	C	M	C	F																									
42X-CC, 22-27	387.50	399.49	C	P	R	A																									
43X-CC, 29-39	397.59	409.58	A	M	R	C																									

Notes: Abundance abbreviations: D = dominant, A = abundant, C = common, F = few, R = rare, R* = almost barren, B = barren. Preservation abbreviations: G = good, M = moderate, P = poor. For more specific definitions, refer to the **"Explanatory Notes"** chapter. Information about taxon distribution is mainly centered upon stratigraphic intervals where events are identified. This table is also available in ASCII format in the **TABLES** directory.

Table T5. Summary of biostratigraphic age assignments for Site 1090. (Continued on next five pages.)

Core, section, interval (cm)	Depth (mbsf)	Depth (mcd)	Calcareous nannofossil zone	Calcareous nannofossil age (Ma)	Diatom zone	Diatom age (Ma)	Radiolaria zone	Radiolaria age (Ma)	Benthic foraminifer zone	Planktic foraminifer age (Ma)	Comment
177-1090A-											
1H-CC, 10-15	6.97	6.97	NN21	0-0.26	*T. lentiginosa* Subzone c	0-0.18					
177-1090B-											
1H-CC, 20-25	4.20	4.20	NN21	0-0.26	*T. lentiginosa* Subzone c	0-0.18	*B. aquilonalis*/Omega	0-0.46			
2H-1, 130-130	5.50	5.50	NN21	0-0.26							
2H-2, 30-30	6.00	6.00	NN20	>0.26							Not well defined
2H-CC, 0-10	13.80	13.80	NN20	>0.26?	*T. lentiginosa* Subzone b	0.18-0.42					
3H-1, 40-40	14.10	15.85	NN19	<0.46							
3H-1, 70-70	14.40	16.15			*T. lentiginosa* Subzone a	0.42-0.65					
3H-1, 100-100	14.70	16.45			*T. lentiginosa* Subzone a	0.42-0.65					
3H-1, 130-130	15.00	16.75	NN19	0.46-0.88							
3H-1, 140-140	15.10	16.85			*T. lentiginosa* Subzone a	0.42-0.65					
3H-6, 50-50	21.70	23.45			*A. ingens* Subzone c	0.65-1.07					Warm-water diatom assemblage ?MIS 17
3H-6, 70-70	21.90	23.65			*A. ingens* Subzone c	0.65-1.07					Cold-water diatom assemblage ?MIS 18
3H-6, 92-92	22.12	23.87			*A. ingens* Subzone c	0.65-1.07					Cold-water diatom assemblage ?MIS 18
3H-CC, 13-18	22.28	24.03	NN19	0.46-0.88	*A. ingens* Subzone c	0.65-1.07					
4H-3, 30-30	26.50	29.01	NN19	0.46-0.88							
4H-3, 130-130	27.50	30.01	NN19	0.88-0.96							
4H-4, 40-40	28.10	30.61			*A. ingens* Subzone c	0.65-1.07					
4H-5, 10-10	29.30	31.81			*A. ingens* Subzone c	0.65-1.07					
4H-6, 30-30	31.00	33.51		0.88-0.96							
4H-6, 130-130	32.00	34.51	NN19	0.96-1.08							
4H-CC, 12-17	32.51	35.02	NN19	0.96-1.08	*A. ingens* Subzone c	0.65-1.07	?	<2.61	>0.6-0.9		
5H-1, 35-35	33.05	36.66	NN19	1.08-1.24							
5H-1, 130-130	34.00	37.61	NN19	1.24-1.46							
5H-3, 30-30	36.00	39.61	NN19	1.24-1.46							
5H-3, 110-110	36.80	40.41	NN19	1.46-1.6							
5H-5, 30-30	39.00	42.31	NN19	1.46-1.6							
5H-5, 130-130	40.00	43.31	NN19	1.6-1.69							
5H-6, 30-30	40.50	43.81	NN19	>1.69							
5H-6, 130-130	41.50	44.81	NN19	1.69-1.95	*A. ingens* Subzone a	1.3-1.8					
5H-CC, 14-19	41.40	45.01	NN18	1.95-2.45	*P. barboi*	1.8-2.0					
6H-1, 30-30	42.50	45.11	NN18	1.95-2.45	*P. barboi*	1.8-2.0					
6H-7, 30-30	51.50	53.10	NN18	1.95-2.45							
6H-CC, 9-14	51.84	53.44	NN17	>2.45	*T. kolbei*/ *F. matuyamae*	2-2.5					

Table T5 (continued).

Core, section, interval (cm)	Depth (mbsf)	Depth (mcd)	Calcareous nannofossil zone	Calcareous nannofossil age (Ma)	Diatom zone	Diatom age (Ma)	Radiolaria zone	Radiolaria age (Ma)	Benthic foraminifer zone	Planktic foraminifer age (Ma)	Comment
7H-CC, 12-17	59.29	65.59	NN17	>2.45	*F. interfrigidaria*	3.3-3.8	?	>2.61			
8H-1, 120-120	62.40	66.11	NN16	2.45-3.66							
8H-2, 30-30	63.30	66.71			*F. interfrigidaria*	3.3-3.8					
8H-2, 90-90	63.90	67.31			*F. interfrigidaria*	3.3-3.8					
8H-2, 120-120	63.90	67.61			pre *F. interfrigidaria*	early Pliocene, >3.8					
8H-2, 140-140	64.10	67.81	NN14-15?	>3.66							
8H-3, 90-90	65.10	68.81			pre *F. interfrigidaria*	early Pliocene, >3.8					
8H-3, 120-120	65.40	69.11			No zonation	mixed ages					Warm-water diatom assemblage
8H-4, 30-30	66.00	69.71	?		No zonation	mixed ages					early Matuyama/late Gauss + early Miocene
8H-4, 60-60	66.30	70.01			No zonation	mixed ages					early Matuyama/late Gauss + early Miocene
8H-4, 90-90	66.60	70.31			No zonation	early Miocene					
8H-5, 30-30	67.50	71.21		Miocene							CN: no markers
8H-CC, 18-23	69.63	73.34			No zonation		*C. longithorax/ C. antiqua*	19.11-22.48			Mixed diatom assemblage Neogene/Paleogene; CN: no markers
9H-3, 140-140	75.10	78.79		Miocene							CN: no markers
9H-CC, 13-18	79.99	83.68			No zonation	early Miocene					CN: no markers
10H-CC, 19-24	88.41	92.98									CN: no markers
11H-CC, 10-15	99.16	103.15			middle-lower *T. fraga*	19-20.8	*C. longithorax/ C. antiqua*	19.11-22.48			CN: no markers
12H-CC, 6-11	108.89	112.56		early Miocene?			*C. longithorax/ C. antiqua*	19.11-22.48			
13H-CC, 0-5	117.12	122.53					*C. longithorax/ C. antiqua*	19.11-22.48			CN: barren
14H-CC, 0-5	127.51	131.16		e. Mioc./l. Oligoc.			*L. conica*	22.48-(24.1-?28.7)			
15H-CC, 0-10	136.73	143.22	?	<23.9	*R. gelida*	22.6-26.5	*L. conica*	22.48-(24.1-?28.7)			
16H-CC, 0-10	146.75	153.40		<23.9	*R. gelida*	22.6-26.5					
17H-CC, 14-24	154.36	161.86			lower *R. gelida*	25.5-26.5					CN: barren
18H-CC, 6-16	165.37	173.15	NN1?	<23.9	lower *R. gelida*	25.5-26.5					
19H-CC, 24-34	173.14	182.63		>23.9			*L. conica*	22.48-(24.1-?28.7)			
20H-CC, 22-32	184.42	192.03		>23.9	*A. gombosii* + *L. ornata*	26.5-28					
21X-3, 30-30	188.00	196.05		>23.9							
21X-3, 130-130	189.00	197.05	NP25	>23.9							
21X-CC, 15-25	194.09	202.14					*L. conica*	22.48-(24.1-?28.7)			CN: barren
22X-CC, 0-10	203.69	211.30			*A. gombosii* + *L. ornata*	26.5-28.3	*A. irregularis*	(24.1-?28.7)-(30.9-34.7)			CN: barren
23X-7, 30-30	213.40	220.70	NP23	<31.3							
23X-7, 130-130	214.40	221.70	NP22	>31.3							

Table T5 (continued).

Core, section, interval (cm)	Depth (mbsf)	Depth (mcd)	Calcareous nannofossil zone	Calcareous nannofossil age (Ma)	Diatom zone	Diatom age (Ma)	Radiolaria zone	Radiolaria age (Ma)	Benthic foraminifer zone	Planktic foraminifer age (Ma)	Comment
23X-CC, 26-36	213.76	222.16	NP22	>31.8-33.1		? late Eocene	*A. irregularis*	(24.1-?28.7)-(30.9-34.7)			
24X-1, 30-30	214.10	225.06	NP22	>31.8							
23X-7, 130-130	214.40	221.70	NP22	>31.3							
24X-4, 30-30	218.6	229.56	NP21	31.8-33.3							
24X-5, 130-130	221.1	232.06	NP21	33.3-35.4							
24X-7, 110-110	222.9	233.86	NP21	33.3-35.4							
24X-CC, 18-28	223.25	234.21	NP21	33.3-35.4							
25X-CC, 19-27	233.01	243.72	NP21	33.3-35.4							
26X-CC, 10-15	242.73	254.72									CN: barren
27X-5, 120-120	250.10	262.09	NP21	33.7-35.4							
27X-6, 30-30	250.70	262.69	NP19-20	33.7-35.4							
27X-CC, 13-18	251.53	263.52	NP19-20	35.4-36.0			*E. spinosum*	>30.9-34.7			
28X-CC, 16-21	262.19	274.18	NP19-20	<36.0							
29X-CC, 17-22	271.87	283.86	NP19-20	<36.0							
30X-CC, 21-34	281.60	293.68	NP19-20	<36.0							
31X-6, 30-30	289.50	301.49	NP19-20	<36.0							
31X-7, 30-30	291.00	302.99	NP19-20	36.0-37.0			*E. spinosum*	>30.9-34.7			
31X-CC, 21-26	291.50	303.43	NP19-20	>36.0?							
33X-CC, 13-18	297.73	309.39	NP18	36.1-37.0							
35X-CC, 17-20	319.91	331.90	NP18	36.1-37.0			*E. spinosum*	>30.9-34.7			
36X-CC, 26-34	330.12	342.11									CN: barren
37X-CC, 40-45	337.16	349.15	NP17	<38.0							Diatom: barren
38X-4, 130-130	346.90	357.39	NP17	36.0-38.0							
38X-7, 10-10	348.70	360.69	NP17	38.0-42.0							
38X-CC, 8-18	349.12	361.11	NN17	<38.0							Diatom: barren
39X-1, 130-130	350.50	362.49	NP16	>38.0							
39X-CC, 12-22	358.78	370.77	NP16	38.0-42.0							Diatom: barren
40X-CC, 21-31	368.55	380.54	NP16	38.0-42.0							
41X-CC, 0-5	372.58	384.57	NP16	42.0-43.1							
42X-1, 30-30	378.40	390.39	NP15	43.1-43.7							
42X-CC, 22-27	387.50	399.49	NP15	43.1-43.7					P12-P14		
43X-CC, 29-39	397.59	409.58	NP15	43.1-43.7							
177-1090C-											
1H-CC, 14-19	2.80	3.16	NN21	0-0.26?	*T. lentiginosa* Subzone c	0-0.18	*B. aquilonalis*/Omega	0-0.46			
2H-CC, 11-16	10.06	15.63	NN19	0.46-0.88	*T. lentiginosa* Subzone a	0.42-0.65					
3H-CC, 9-19	21.01	27.26	NN19	<0.96	*A. ingens* Subzone c	0.65-1.07					
4H-CC, 8-13	30.28	36.59	NN19	<1.95?	*A. ingens* Subzone c	0.65-1.07					
5H-CC, 9-14	40.19	48.24	NN18	>1.95?	*T. kolbei/ F. matuyamae*	2-2.5					
6H-CC, 17-22	50.41	58.23	?	Pliocene	*T. insiga* Subzone a	2.8-3.3					
7H-CC, 8-13	58.88	66.62	NN15-14	3.66-4.0	*F. interfrigidaria*	3.3-3.8	?	>2.61			Diatom: no markers

Table T5 (continued).

Core, section, interval (cm)	Depth (mbsf)	Depth (mcd)	Calcareous nannofossil zone	Calcareous nannofossil age (Ma)	Diatom zone	Diatom age (Ma)	Radiolaria zone	Radiolaria age (Ma)	Benthic foraminifer zone	Planktic foraminifer age (Ma)	Comment
8H-CC, 0-5	68.80	76.61	?				?	early Miocene			CN: no markers; Diatom: barren
177-1090D-											
1H-CC, 12-17	7.37	7.71	NN21	0-0.26	*T. lentiginosa* Subzone b	0.18-0.42	*B. aquilonalis*/Omega	<0.46			
2H-CC, 9-14	15.46	17.61	NN19	0.46-0.88	*T. lentiginosa* Subzone a	0.42-0.65					
3H-CC, 8-13	24.94	28.01	NN19	<0.96?	*A. ingens* Subzone c	0.65-1.07					
4H-CC, 9-14	34.79	37.78	NN19	>1.24	*A. ingens* Subzone c	0.65-1.07	?	<2.61			
5H-CC, 7-12	44.95	49.16	NN19	1.46-1.6	*T. kolbei*/ *F. matuyamae*	2-2.5					
6H-CC, 7-12	54.23	59.69	NN19	<1.6	*T. insigna* Subzone a	2.8-3.3					No *T. vulnifica*, warm-water diatom assemblage
7H-CC, 17-22	62.90	68.98		?	pre *F. interfrigidaria*	early Pliocene, >3.8	?	>2.61			No *T. vulnifica*, warm-water diatom assemblage
8H-CC, 17-22	73.97	79.88					?	<22.48			CN: barren
9H-CC, 7-12	82.95	90.48								>17.3	
10H-CC, 20-25	93.16	100.69									CN: no markers
11H-CC, 20-25	101.84	108.97									CN: no markers
13H-CC, 0-10	120.54	127.43									CN: no markers
14H-CC, 0-10	130.66	137.91									CN: no markers
15H-CC, 17-22	140.06	146.53									CN: no markers
16H-CC, 0-5	149.51	158.15	NN1?	<23.9			*L. conica*	22.48-(24.1-?28.7)			
17H-CC, 16-21	159.33	169.21		<23.9							
18H-CC, 9-14	168.46	180.16	NP25	>23.9							
20H-CC, 17-22	187.47	198.32		>23.9			*L. conica*	22.48-(24.1-?28.7)			
21H-CC, 0-10	197.25	208.18		>23.9							
22H-CC, 51-56	207.21	218.91	?	>23.9							
23H-CC, 33-38	215.14	227.77	NP21-NP22	31.8-33.3							
24H-CC, 0-6	226.02	237.66	NP21	33.3-33.7			*A. irregularis*	(24.1-?28.7)-(30.9-34.7)			
177-1090E-											
1H-1, 110-110	1.10	4.48			*T. lentiginosa* Subzone c	0-0.18					
1H-3, 110-110	4.10	7.48			*T. lentiginosa* Subzone b	0.18-0.42					
1H-6, 100-100	8.50	11.88			*T. lentiginosa* Subzone b	0.18-0.42					
1H-CC, 8-13	8.65	12.03	NN21	0-0.26	*T. lentiginosa* Subzone b	0.18-0.42	*B. aquilonalis*/Omega	0-0.46			
2H-2, 70-70	10.90	14.49			*T. lentiginosa* Subzone a	0.42-0.65					
2H-4, 70-70	13.90	17.49			*T. lentiginosa* Subzone a	0.42-0.65					

Table T5 (continued).

Core, section, interval (cm)	Depth (mbsf)	Depth (mcd)	Calcareous nannofossil zone	Calcareous nannofossil age (Ma)	Diatom zone	Diatom age (Ma)	Radiolaria zone	Radiolaria age (Ma)	Benthic foraminifer zone	Planktic foraminifer age (Ma)	Comment
2H-5, 70-70	15.40	18.99			*A. ingens* Subzone c	0.65-1.07					
2H-CC, 8-13	15.75	19.34	NN19	>0.46	*A. ingens* Subzone c	0.65-1.07					
3H-2, 70-70	20.40	27.11			*A. ingens* Subzone c	0.65-1.07					
3H-4, 70-70	23.40	30.11			*A. ingens* Subzone c	0.65-1.07					
3H-CC, 10-15	24.56	31.27	NN19	0.88-0.96	*A. ingens* Subzone c	0.65-1.07					
4H-2, 70-70	29.90	36.05			*A. ingens* Subzone c	0.65-1.07					
4H-4, 70-70	32.90	39.05			*A. ingens* Subzone c	0.65-1.07					
4H-5, 70-70	34.40	40.55			*A. ingens* Subzone c	0.65-1.07					
4H-CC, 15-20	35.35	41.50	NN19	?	*A. ingens* Subzone c	0.65-1.07	?	<2.61			
5H-1, 70-70	37.90	46.19			*P. barboi*	1.8-2.0					
5H-2, 70-70	39.40	47.69			*P. barboi*	1.8-2.0					
5H-3, 70-70	40.60	48.89			*T. kolbei*/ *F. matuyamae*	2-2.5					
5H-4, 70-70	42.10	50.39			*T. kolbei*/ *F. matuyamae*	2-2.5					
5H-6, 30-30	45.10	52.99			*T. kolbei*/ *F. matuyamae*	2-2.5					
5H-CC, 13-18	44.85	53.14	?	?	*T. kolbei*/ *F. matuyamae*	2-2.5					
6H-2, 70-70	48.90	57.32			*T. insigna* Subzone a	2.8-3.3					No *T. vulnifica*
6H-4, 70-70	51.90	60.32			*T. insigna* Subzone a	2.8-3.3					No *T. vulnifica*
6H-5, 70-70	53.40	61.82			*T. insigna* Subzone a	2.8-3.3					No *T. vulnifica*
6H-6, 20-20	54.90	62.82			*F. interfrigidaria*	3.3-3.8					Warm-water diatom assemblage
6H-CC, 10-15	54.54	62.96	?	?	*F. interfrigidaria*	3.3-3.8	?				
7H-2, 70-70	58.40	67.29			*F. interfrigidaria*	3.3-3.8					Warm-water diatom assemblage
7H-3, 70-70	59.90	68.79			No zonation	Mixed ages					
7H-CC, 17-22	65.19	74.08	?				?	early Miocene			CN: no markers
8H-CC, 9-14	75.31	83.86									CN: no markers
9H-1, 70-70	75.90	85.81			upper *T. fraga*	17.8-19					
9H-5, 70-70	81.90	91.81			upper *T. fraga*	17.8-19					
9H-CC, 8-13	84.53	94.44									CN: no markers
10H-3, 70-70	88.40	98.77			middle-lower *T. fraga*	19-20.8					
10H-CC, 18-23	93.38	103.75									CN: no markers
11H-2, 70-70	96.40	106.21			middle-lower *T. fraga*	19-20.8					
11H-4, 70-70	99.40	109.21									
11H-6, 70-70	102.40	112.21									
11H-CC, 0-10	103.40	113.21					*C. longithorax*/ *C. antiqua*	19.11-22.48			CN: no markers
12H-3, 70-70	107.40	116.61			*T. spumellaroides*	20.8-22.6					
12H-CC, 0-5	112.32	121.53	NN1?	<23.9							
13H-1, 70-70	113.90	123.51			*T. spumellaroides*	20.8-22.6					
13H-5, 70-70	119.90	129.51			*R. gelida*	22.6-26.5					

Table T5 (continued).

Core, section, interval (cm)	Depth (mbsf)	Depth (mcd)	Calcareous nannofossil zone	Calcareous nannofossil age (Ma)	Diatom zone	Diatom age (Ma)	Radiolaria zone	Radiolaria age (Ma)	Benthic foraminifer zone	Planktic foraminifer age (Ma)	Comment
13H-6, 70-70	121.40	131.01									
13H-CC, 12-17	121.65	131.26									CN: dissolution
14H-4, 70-70	127.90	137.05			*R. gelida*	22.6-26.5					
14H-CC, 14-19	131.74	140.89									CN: dissolution
15H-CC, 0-10	141.53	152.34	?	<23.9			*L. conica*	22.48-(24.1-?28.7)			
16H-CC, 29-39	150.99	163.05									CN: barren
17H-CC, 0-10	160.78	173.21									CN: no markers
18H-CC, 14-24	170.04	184.77									
19H-CC, 12-22	179.72	192.78	?	>23.9			*L. conica*	22.48-(24.1-?28.7)			
20H-CC, 14-24	188.76	202.70									CN: barren
21H-CC, 0-10	198.78	212.90									CN: barren
22H-CC, 0-10	208.00	221.44	NP22	>31.3							
23H-CC, 20-27	213.94	229.30	NP22	>31.8			*A. irregularis*	(24.1-?28.7)-(30.9-34.7)			
24H-CC, 11-16	225.84	241.25	NP21	<36.0							
25H-CC, 12-17	236.74	252.21					*A. irregularis*	(24.1-?28.7)-(30.9-34.7)			CN:barren

Notes: CN = calcareous nannofossil; MIS = marine isotope stage. This table is also available in ASCII format in the **TABLES** directory.

Table T6. Distribution of major planktic foraminifer species at Site 1090. (Continued on next page.)

Core, section, interval (cm)	Depth (mbsf)	Depth (mcd)	Abundance	Preservation	*Globigerina bulloides*	*Globigerina quinqueloba*	*Globigerinella aequilateralis*	*Globigerinita glutinata*	*Globigerinita uvula*	*Globorotalia inflata*	*Globorotalia puncticulata*	*Globorotalia puncticuloides*	*Globorotalia scitula*	*Globorotalia truncatulinoides*	*Neogloboquadrina pachyderma* (sinistral)	*Neogloboquadrina pachyderma* (dextral)	*Orbulina universa*	*Acarinina primitiva*	*Acarinina matthewsae*	*Acarinina wilcoxensis*	*Catapsydrax dissimilis*	*Catasydrax stainforthi*	*Chiloguembelina cubensis*	*Globigerina woodi*	*Globorotalia miozea*	*Mazzovella spinulosa*	*Pseudohastigerina micra*	*Subbotina angiporoides*	*Subbotina brevis*	*Subbotina higginsi*	*Subbotina linaperta*	*Truncorotaloides* spp.	*Globoquadrina aehiscens*
177-1090A-																																
1H-CC, 10-15	6.97	6.97	A	G	D	A		A	A	A				A	A	F	F															
177-1090B-																																
1H-CC, 20-25	4.20	4.20	A	G	D	A		A		A				A	A	A	F															
2H-CC, 0-10	13.80	13.80	A	G	A	A		A	A	A		F		F	A	F	R															
3H-CC, 13-18	22.28	24.03	A	P	A						A	A			D																	
4H-CC, 12-17	32.51	35.02	A	M	D	A	P	A	A		A	A	P		A	F																
5H-CC, 14-19	41.40	45.01	A	M	A	F					A	A			D	F																
6H-CC, 9-14	51.84	53.44	A	M							A	A			D																	
7H-CC, 12-17	59.29	65.59	A	M				F			F	A			D																	
8H-CC, 18-23	69.63	73.34	T	P																												
9H-CC, 13-18	79.99	83.68	T	P																												
10H-CC, 19-24	88.41	92.98	R	P																	D	F		R								
11H-CC, 10-15	99.16	103.15	T	P																												
12H-CC, 6-11	108.89	112.56	R	P																				P								
13H-CC, 0-5	117.12	122.53	B																													
14H-CC, 0-5	127.51	131.16	B																													
15H-CC, 0-10	136.73	143.22	R	P																	D			P	P							
16H-CC, 0-10	146.75	153.40	R	P																				D								
17H-CC, 14-24	154.36	161.86	B																													
18H-CC, 6-16	165.37	173.15	B																													
19H-CC, 24-34	173.14	182.63	B																													
20H-CC, 22-32	184.42	192.03	B																													
21X-CC, 15-25	194.09	202.14	B																													
22X-CC, 0-10	203.69	211.30	B																													
23X-CC, 26-36	213.76	222.16	B																													
24X-CC, 18-28	223.25	234.21	R	P																								D				
25X-CC, 19-27	233.01	243.72	B																													
26X-CC, 10-15	242.73	254.72	B																													
27X-CC, 13-18	251.53	263.52	B																													
28X-CC, 16-24	262.19	274.18	B																													
29X-CC, 17-22	271.87	283.86	B																													
31X-CC, 21-26	281.69	303.43	B																													
32X-CC, 27-32	291.50		B																													
33X-CC, 13-18	294.38	309.39	B																													
34X-CC, 46-54	297.73		B																													
35X-CC, 17-20	319.91	331.90	B																													
36X-CC, 26-34	330.12	342.11	B																													
37X-CC, 40-45	337.16	349.15	B																													
38X-CC, 8-18	349.12	361.11	R	M																						A	R				D	
39X-CC, 12-22	358.78	370.77	R	M														A								F	R		D	P		
40X-CC, 21-31	368.55	380.54	R	M														A											A			
41X-CC, 0-5	372.58	384.57	R	M																A	A			P			P				A	
42X-CC, 22-27	387.50	399.49	R	P																												
43X-CC, 29-39	397.59	409.58	F	M																												

Table T6 (continued).

Core, section, interval (cm)	Depth (mbsf)	Depth (mcd)	Abundance	Preservation	*Globigerina bulloides*	*Globigerina quinqueloba*	*Globigerinella aequilateralis*	*Globigerinita glutinata*	*Globigerinita uvula*	*Globorotalia inflata*	*Globorotalia puncticulata*	*Globorotalia puncticuloides*	*Globorotalia scitula*	*Globorotalia truncatulinoides*	*Neogloboquadrina pachyderma* (sinistral)	*Neogloboquadrina pachyderma* (dextral)	*Orbulina universa*	*Acarinina primitiva*	*Acarinina matthewsae*	*Acarinina wilcoxensis*	*Catapsydrax dissimilis*	*Catasydrax stainforthi*	*Chiloguembelina cubensis*	*Globigerina woodi*	*Globorotalia miozea*	*Mozozovella spinulosa*	*Pseudohastigerina micra*	*Subbotina angiporoides*	*Subbotina brevis*	*Subbotina higginsi*	*Subbotina linaperta*	*Truncorotaloides* spp.	*Globoquadrina dehiscens*
177-1090C-																																
1H-CC, 14-19	2.80	3.30	A	G	D	A		F	A	A		F		F	A	F																
2H-CC, 11-16	10.06	15.63	A	G	D	F		F	F	A		A			D	F																
3H-CC, 9-19	21.01	27.26	A	G	A	A		F	A			A			D	F																
4H-CC, 8-13	30.28	36.59	A	M	F	R		R			F	A			D	R																
5H-CC, 9-14	40.19	48.24	A	M	A	R			R		A	A			D	R																
6H-CC, 17-22	50.41	58.23	A	P	A			R	R		F	A			D	R																
7H-CC, 0-5	68.80	66.62	A	P	F						F	A			F																	
8H-CC, 0-5	68.80	76.61	A	P	F						F	A			F																	
177-1090D-																																
1H-CC, 12-17	7.37	7.71	A	M	D	A		F	A	F		F		F	D	F																
2H-CC, 9-14	15.46	17.61	A	M	D	A		F	F			F			D																	
3H-CC, 8-13	24.94	28.01	A	M	D	A		A	A		F	A	P		D																	
4H-CC, 9-14	34.79	37.78	A	M	A	A		A			F	A			D																	
5H-CC, 7-12	44.95	49.16	A	M				P	P		F	A			D																	
6H-CC, 7-12	54.23	59.69	A	P	A				R		F	A			D																	
7H-CC, 17-22	62.90	68.98	A	P	A				P		F	A			D																	
8H-CC, 17-22	73.97	79.88	B																													
9H-CC, 7-12	82.95	90.48	R	P																	D											F
10H-CC, 20-25	93.16	100.69	T	P																												
11H-CC, 20-25	101.84	108.97	R	P																	D			A								
13H-CC, 0-10	120.54	127.43	B																													
14H-CC, 0-10	130.66	137.91	B																													
15H-CC, 17-22	140.06	146.53	B																													
16H-CC, 0-5	149.51	158.15	R	P																				D								
17H-CC, 16-21	159.33	169.21	R	P																				D								
18H-CC, 9-14	168.46	180.16	B																													
20H-CC, 17-22	187.47	198.32	B																													
21H-CC, 0-10	197.25	208.18	B																													
22H-CC, 51-56	207.21	218.91	B																													
23H-CC, 33-38	215.14	227.77	R	P																								D				
24H-CC, 0-6	226.02	237.66	R	P																								D		F		
177-1090E-																																
1H-CC, 8-13	8.65	12.03	A	G	A	A		F	A	A		F			D	F																
2H-CC, 8-13	15.75	19.34	A	M	F	A		F	A	A		F	P	R	D	A																
3H-CC, 10-15	24.56	31.27	A	M	A	A		F	C		F	A	P		D																	
4H-CC, 15-20	35.35	41.50	A	M	A	F		F	F		F	A			D																	
5H-CC, 13-18	44.85	53.14	A	P	F	R		R	R		F	A			D																	
6H-CC, 10-15	54.54	62.96	A	M	F	F		R			F	D			A	F																
7H-CC, 17-22	65.19	74.08	F	M	F						F	A			R																	
8H-CC, 9-14	75.31	83.86	T	P																												
9H-CC, 8-13	84.53	94.44	C	M																	D	F										
10H-CC, 18-23	93.38	103.75	R	P																	F	F						A				
11H-CC, 0-10	103.40	113.21	R	P																								P				
12H-CC, 0-5	112.32	121.53	B																													
13H-CC, 12-17	121.65	131.26	B																													
14H-CC, 14-19	131.74	140.89	R	M																												
15H-CC, 0-10	141.53	152.34	B																													

Table T6 (continued).

Core, section, interval (cm)	Depth (mbsf)	Depth (mcd)	Abundance	Preservation	*Globigerina bulloides*	*Globigerina quinqueloba*	*Globigerinella aequilateralis*	*Globigerinita glutinata*	*Globigerinita uvula*	*Globorotalia inflata*	*Globorotalia puncticulata*	*Globorotalia puncticuloides*	*Globorotalia scitula*	*Globorotalia truncatulinoides*	*Neogloboquadrina pachyderma* (sinistral)	*Neogloboquadrina pachyderma* (dextral)	*Orbulina universa*	*Acarinina primitiva*	*Acarinina matthewsae*	*Acarinina wilcoxensis*	*Catapsydrax dissimilis*	*Catasydrax stainforthi*	*Chiloguembelina cubensis*	*Globigerina woodi*	*Globorotalia miozea*	*Mozozovella spinulosa*	*Pseudohastigerina micra*	*Subbotina angiporoides*	*Subbotina brevis*	*Subbotina higginsi*	*Subbotina linaperta*	*Truncorotaloides* spp.	*Globoquadrina dehiscens*
16H-CC, 29-39	150.99	163.05	B																													
17H-CC, 0-10	160.78	173.21	B																													
18H-CC, 14-24	170.04	184.77	B																													
19H-CC, 12-22	179.72	192.78	R																													
20H-CC, 14-24	188.76	202.70	B																													
21H-CC, 0-10	198.78	212.90	B																													
22H-CC, 0-10	208.00	221.44	B																													
23H-CC, 20-27	213.94	229.30	R	M																							D					
24H-CC, 11-16	225.84	241.25	R	P																							D					
25H-CC, 12-17	236.74	252.21	B																													

Notes: Abundance abbreviations: D = dominant, A = abundant, C = common, F = few, R = rare, T = trace, P = present, B = barren. Preservation abbreviations: M = moderate, P = poor. For more specific definition, refer to the **"Explanatory Notes"** chapter. This table is also available in ASCII format in the **TABLES** directory.

Table T7. Distribution of benthic foraminifers in Hole 1090B. (Continued on next three pages.)

Core, section, interval (cm)	Depth (mbsf)	Depth (mcd)	Abundance	Preservation	*Abyssamina* sp.	*Alabamina aissonata*	*Alabaminella weadelensis*	*Anomalinoides capitatus*	*Anomalinoides semicribratus*	*Anomalinoides* sp.	*Aragonia aragonensis*	*Astrononion* sp.	*Bolivina* spp.	*Bulimina semicostata*	*Bulimina* sp.	*Cassidulina obtusa*	*Cassidulina reniforme*	*Cassidulinoides* spp.	*Cibicidoides* spp.	*Cibicidoides mexicanus*	*Cibicidoides micrus*	*Cibicidoides mundulus*	*Cibicidoides praemundulus*	*Cibicidoides wuellerstorfi*	*Cribrostomoides* sp.	*Cyclammina* sp.	*Dentalina* sp.	*Eggerella bradyi*	*Ehrenbergina* sp.	*Epistominella exigua*	*Fissurina* spp.	*Francesita* sp.	*Globobulimina* sp.	*Gyroidinoides soldanii*	*Gyroidinoides* spp.	*Haplophragmoides* sp.	*Hormosina globulifera*	Indeterminates (agg.)	Indeterminates (calc.)	*Islandiella* sp.	*Karreriella bradyi*	*Lagena* spp.	*Laticarinina pauperata*	*Lenticulina* sp.	*Martinottiella* sp.	*Melonis barleeanum*	*Melonis pompilioides*	*Miliolinella* sp.	*Nodosaria* spp.
177-1090B-																																																	
1H-CC, 20-25	4.2	4.20	C	G		3						8			1		1		1								3	1	14	1	4							3		2			3					
2H-CC, 0-10	13.8	13.80	C	G		8						5			8	1	2	3	2				15				1		22	3			2	3			4	12		2			2			1	
3H-CC, 13-18	22.28	24.03	C	G		55						4					6						1				1		15	6	1	8	1	8			4	11		8				42			
4H-CC, 12-17	32.51	35.02	C	M		2						10					2						1				2		5	1			3	7			2			2				6			
5H-CC, 14-19	41.4	45.01	C	M							1								2								4	1	4	3	3		5	5			9	4			1		3	4	20		
6H-CC, 9-14	51.84	53.44	C	M		3						11					2									1	8		8	3	4		1			7	13		17			1	3	8		2
7H-CC, 12-17	59.29	65.59	C	M								2							5								10		1	2			2	2		1	6	4			1	2	1	13			
8H-CC, 18-23	69.63	73.34	F	P															2		6									1	1		1	1				1	1									
9H-CC, 13-18	79.99	83.68	F	P																										1			3			4										
10H-CC, 19-24	88.41	92.98	C	P															3		2					1	2			1					3	1		1									
11H-CC, 10-15	99.16	103.15	F	M															1		2						1						1		1	6	2		2			3					
12H-CC, 6-11	108.89	112.56	F	P															3		1				1	1	1	5	2	3	1		3			2	6	2			1	1	1				
13H-CC, 0-5	117.12	122.53	F	P								1									2													3		5	2		2	1	1	1	5				
14H-CC, 0-5	127.51	131.16	F	P						1											1															2											
15H-CC, 0-10	136.73	143.22	F	M															6										1					15				1					1				
16H-CC, 0-10	146.75	153.40	F	M																	4												2	1					1					1			
17H-CC, 14-24	154.36	161.86	R	P																					1											1							3				
18H-CC, 6-16	165.37	173.15	R	P														1																													
19H-CC, 24-34	173.14	182.63	F	P																	1												1				1	1					2				
20H-CC, 22-32	184.42	192.03	B																																												
21X-CC, 15-25	194.09	202.14	B																																												
22X-CC, 0-10	203.69	211.30	B																																												
23X-CC, 26-36	213.76	222.16	F	P						1								1													1				1					1				1				
24X-CC, 18-28	223.25	234.21	F	P														1															1				5		3			1						
25X-CC, 19-27	233.01	243.72	F	P					1											1						1				1										1				1				
26X-CC, 10-15	242.73	254.72	B																																												
27X-CC, 13-18	251.53	263.52	F	P					1																											14											
28X-CC, 16-21	262.19	274.18	F	P																														1													
29X-CC, 17-22	271.87	283.86	F	P														1									2				1				1		4	1								1	
30X-CC, 21-26	281.69	293.68	F	P																										1						1	1									
31X-CC, 27-32	291.5	303.43	F	P	1																				1											4	1									
32X-CC, 13-18	294.38		F	P																						1										3										
33X-CC, 46-54	297.73	309.39	B																																											
34X-CC, 12-20	310.7		B																																											
35X-CC, 17-20	319.91	331.90	B																																											

Table T7 (continued).

Core, section, interval (cm)	Depth (mbsf)	Depth (mcd)	Abundance	Preservation	*Nonionella iridea*	*Nonionella* sp.	*Nuttalides truempyi*	*Nuttalides umbonifera*	*Oolina* spp.	*Ophthalmidium* spp.	*Oridorsalis umbonatus*	*Orthomorphina* sp.	*Parafissurina* sp.	*Pleurostomella* sp.	*Pullenia bulloides*	*Pullenia quinqueloba*	*Pullenia subcarinata*	*Pullenia* sp.	*Pyrgo murrhina*	*Pyrgo* spp.	*Quinqueloculina* sp.	*Reophax* sp.	*Siphotextularia* sp.	*Sphaeroidina bulloides*	*Stainforthia loeblichi*	*Stainforthia* sp.	*Stilostomella lepidula*	*Stilostomella subspinosa*	*Stilostomella* sp.	*Textularia* sp.	*Triloculina trihedra*	*Triloculina* sp.	*Uvigerina hispidicostata*	Sample sum	Number of species	Abundance (specimens/cm³)
177-1090B-																																			
1H-CC, 20-25	4.2	4.20	C	G	1			1		2			1		1	4	1			2	2		3		1	2						2	71	28	106.5
2H-CC, 0-10	13.8	13.80	C	G				1		1	7		1	2		22	5	7			5		4		4						4	159	38	87.5
3H-CC, 13-18	22.28	24.03	C	G	1										5	1	3						1		6					2	2	192	30	220.8
4H-CC, 12-17	32.51	35.02	C	M							2					11							2		3		1					62	22	62.0
5H-CC, 14-19	41.4	45.01	C	M				1		2	3				2	1	6		11				2	1		5	5				1	11	120	35	160.0
6H-CC, 9-14	51.84	53.44	C	M							6		3		9	6	5		1		1		7		4				1			135	36	180.0
7H-CC, 12-17	59.29	65.59	C	M							4		2		3	1	1						1		2		1				2	14	83	24	58.1
8H-CC, 18-23	69.63	73.34	F	P							5	3		1	1	3											3	3	7				40	17	12.0
9H-CC, 13-18	79.99	83.68	F	P							3			2	1	2												7	10				33	10	5.0
10H-CC, 19-24	88.41	92.98	C	P					2		10	1		3	2	1						1				11				2			47	19	14.7
11H-CC, 10-15	99.16	103.15	F	M						1	4			3		2									1	5		1					36	18	5.4
12H-CC, 6-11	108.89	112.56	F	P						6	6		1	6	1	4					1	1						8		5			73	28	11.0
13H-CC, 0-5	117.12	122.53	F	P							5			3	5	1						2				4				1			44	19	6.6
14H-CC, 0-5	127.51	131.16	F	P						1						1						1						1	2				10	9	1.5
15H-CC, 0-10	136.73	143.22	F	M						1	15			2		6					1					8							57	13	20.5
16H-CC, 0-10	146.75	153.40	F	M		1		4		3	6			2	2	3		1										2	5				38	18	13.3
17H-CC, 14-24	154.36	161.86	R	P						4	1																			1			11	6	1.1
18H-CC, 6-16	165.37	173.15	R	P							2			1														2		1			7	5	1.8
19H-CC, 24-34	173.14	182.63	F	P							3						1									1	1	5					17	10	3.4
20H-CC, 22-32	184.42	192.03	B																														0		0.0
21X-CC, 15-25	194.09	202.14	B																														0		0.0
22X-CC, 0-10	203.69	211.30	B																														0		0.0
23X-CC, 26-36	213.76	222.16	F	P						1				3									1				1	2	1				15	12	3.0
24X-CC, 18-28	223.25	234.21	F	P					1		3				1		1										1		2				20	11	5.0
25X-CC, 19-27	233.01	243.72	F	P							6					1		1												4			18	10	1.8
26X-CC, 10-15	242.73	254.72	B																														0		0.0
27X-CC, 13-18	251.53	263.52	F	P										1								1							1				18	6	1.8
28X-CC, 16-21	262.19	274.18	F	P						1																			1	1			4	4	0.8
29X-CC, 17-22	271.87	283.86	F	P						1	1				3		2									1		3					21	12	1.1
30X-CC, 21-26	281.69	293.68	F	P																								2	5				10	5	1.0
31X-CC, 27-32	291.5	303.43	F	P							2																	4	2				15	8	3.0
32X-CC, 13-18	294.38		F	P						1																			3				8	4	2.0
33X-CC, 46-54	297.73	309.39	B																														0		0.0
34X-CC, 12-20	310.7		B																														0		0.0
35X-CC, 17-20	319.91	331.90	B																														0		0.0

Table T7 (continued).

Core, section, interval (cm)	Depth (mbsf)	Depth (mcd)	Abundance	Preservation	*Abyssamina* sp.	*Alabamina dissonata*	*Alabaminella weddelensis*	*Anomalinoides capitatus*	*Anomalinoides semicribratus*	*Anomalinoides* sp.	*Aragonia aragonensis*	*Astrononion* sp.	*Bolivina* spp.	*Bulimina semicostata*	*Bulimina* sp.	*Cassidulina obtusa*	*Cassidulina reniforme*	*Cassidulinoides* spp.	*Cibicidoides* spp.	*Cibicidoides mexicanus*	*Cibicidoides micrus*	*Cibicidoides mundulus*	*Cibicidoides praemundulus*	*Cibicidoides wuellerstorfi*	*Cribrostomoides* sp.	*Cyclammina* sp.	*Dentalina* sp.	*Eggerella bradyi*	*Ehrenbergina* sp.	*Epistominella exigua*	*Fissurina* spp.	*Francesita* sp.	*Globobulimina* sp.	*Gyroidinoides soldanii*	*Gyroidinoides* spp.	*Haplophragmoides* sp.	*Hormosina globulifera*	Indeterminates (agg.)	Indeterminates (calc.)	*Islandiella* sp.	*Karreniella bradyi*	*Lagena* spp.	*Laticarinina pauperata*	*Lenticulina* sp.	*Martinotiella* sp.	*Melonis barleeanum*	*Melonis pompilioides*	*Miliolinella* sp.	*Nodosaria* spp.
36X-CC, 26-34	330.12	342.11	F	P					1																									1			7	2											
37X-CC, 40-45	337.16	349.15	B																																															
38X-CC, 8-18	349.12	361.11	F	M									1	1	3			1				2								1				2			25		4									1	
39X-CC, 12-22	358.78	370.77	F	M		1									1			2								3				1								3	1		1								
40X-CC, 21-31	368.55	380.54	F	M	1					6			3		1			3		4													2					14						1					
41X-CC, 0-5	372.58	384.57	A	M									5	2																1				2				7	1		3								
42X-CC, 22-27	387.5	399.49	C	M		1			2		3							5				5											3				1	3			1								
43X-CC, 29-39	397.59	409.58	C	M	3	4		2						2				3		6		4			1					1			7				14			2								

Notes: Abundance abbreviations: A = abundant, C = common, F = few, R = rare, B = barren. Preservation abbreviations: G = good, M = moderate, P = poor. For more specific definitions, refer to **"Biostratigraphy,"** p. 10, in the "Explanatory Notes" chapter. This table is also available in ASCII format in the **TABLES** directory.

Table T7 (continued).

Core, section, interval (cm)	Depth (mbsf)	Depth (mcd)	Abundance	Preservation	*Nonionella iridea*	*Nonionella* sp.	*Nuttalides truempyi*	*Nuttalides umbonifera*	*Oolina* spp.	*Ophthalmidium* spp.	*Oridorsalis umbonatus*	*Orthomorphina* sp.	*Parafissurina* sp.	*Pleurostomella* sp.	*Pullenia bulloides*	*Pullenia quinqueloba*	*Pullenia subcarinata*	*Pullenia* sp.	*Pyrgo murrhina*	*Pyrgo* spp.	*Quinqueloculina* sp.	*Reophax* sp.	*Siphotextularia* sp.	*Sphaeroidina bulloides*	*Stainforthia loeblichi*	*Stainforthia* sp.	*Stilostomella lepidula*	*Stilostomella subspinosa*	*Stilostomella* sp.	*Textularia* sp.	*Triloculina trihedra*	*Triloculina* sp.	*Uvigerina hispidicostata*	Sample sum	Number of species	Abundance (specimens/cm³)
36X-CC, 26-34	330.12	342.11	F	P			3			2	2						3											3						24	11	2.4
37X-CC, 40-45	337.16	349.15	B																														0		0.0
38X-CC, 8-18	349.12	361.11	F	M			13						1		3										1		5		3				67	18	20.6
39X-CC, 12-22	358.78	370.77	F	M			3				1			1			4											13					35	15	5.3
40X-CC, 21-31	368.55	380.54	F	M			18	7	1		4			2				6				1					14	1				89	27	4.5
41X-CC, 0-5	372.58	384.57	A	M			2				1		1	4			1										11						41	19	170.8
42X-CC, 22-27	387.5	399.49	C	M			16				5							5										4					54	16	8.1
43X-CC, 29-39	397.59	409.58	C	M			3		1		10			7				12									4	6	2				94	24	14.1

Table T8. Diatom, silicoflagellate, ebridian, *Actiniscus*, sponge spicule, and phytolith occurrence, Site 1090. (Continued on next five pages.)

Core, section, interval (cm)	Depth (mbsf)	Depth (mcd)	Diatom abundance	Diatom preservation	Silicoflagellate occurrence	Ebridian occurrence	*Actiniscus* occurrence	Sponge spicule occurrence	Opaline phytolith occurrence	*Actinocyclus actinochilus*	*Actinocyclus curvatulus*	*Actinocyclus ingens*	*Actinoptychus senarius*	*Alveolus marinus*	*Asteromphalus parvulus*	*Azpeitia nodulifer*	*Azpeitia tabularis*	*Bogorovia mirabilis*	*Bogorovia veniamini*	*Cavitatus jouseanus*	*Chaetoceros* spp.	*Coscinodiscus marginatus*	*Coscinodiscus radiatus*	*Coscinodiscus rhombicus*	*Ethmodiscus rex*	*Eucampia antarctica*	*Fragilariopsis angulata*	*Fragilariopsis aurica*	*Fragilariopsis barronii*	*Fragilariopsis doliolus*	*Fragilariopsis fossilis*	*Fragilariopsis interfrigidaria*	*Fragilariopsis kerguelensis*	*Fragilariopsis matuyamae*	*Fragilariopsis mat.* var. *heterop.*	*Fragilariopsis praecurta*	*Fragilariopsis praeinterfrigidaria*	*Fragilariopsis reinholdii*	*Fragilariopsis ritscherii*
177-1090A-																																						
1H-CC, 10-15	6.97	6.97	F	M	B	X	B	X	B								F							X								C						
177-1090B-																																						
1H-CC, 20-25	4.2	4.2	F	M	T	B	B	X	B								F															C						
2H-CC, 0-10	13.8	13.8	R	M	R	B	B	X	B								F															F						
3H-1, 50-50	14.2	14.2	F	M	T	B	B	X	B							R	R															A						
3H-1, 70-70	14.4	16.15	F	M	T	B	B	X	B								R							X	R							A						
3H-1, 100-100	14.7	16.45	F	M-P	T	B	B	X	B								F						R									C						
3H-1, 140-140	15.1	16.85	F	M-P	T	B	B	X	B								F						R		R							A						
3H-6, 50-50	21.7	23.45	F	M-P	T	B	B	X	B			R				R	F															C						
3H-6, 70-70	21.9	23.65	A	G	T	B	B	X	B			R					R							X								A			T			
3H-6, 92-92	22.12	23.87	A	G	T	B	B	X	B			R					R							X	R							A						
3H-CC, 13-18	22.28	24.03	A	G-M	T	B	B	X	B			R									R			X	F							C						
4H-4, 40-40	28.1	30.61	C-F	M	T	B	B	X				F					R									R					F	C			R			
4H-5, 10-10	29.3	31.81	F	M	T	B	B	X	B			R												X							F	C			R			
4H-CC, 12-17	32.51	35.02	F	M	B	B	B	X	B			R												X	T						T	C			R			
5H-6, 130-130	41.5	44.81	C	M	B	B	B	B	B																			R				C						
5H-CC, 14-19	41.4	45.01	C	M	T	B	B	X	B			R												X						T		R						
6H-1, 30-30	42.5	44.1	F-R	M	B	B	B	B	B								T											T										
6H-CC, 9-14	51.84	53.44	F	M	T	B	B	X	B													R		X				F		R		R						
7H-CC, 12-17	59.29	65.59	C-F	G	T	B	B	X	B		R	R					F											R			R		R	R			R	
8H-2, 30-30	63.3	66.71	C	M	T	B	B	X	B												R						T			R	F		T				R
8H-2, 120-120	63.9	67.61	A	G	R	B	B	B	B																		R			F					R	R	F	
8H-3, 90-90	65.1	68.81	C	M	T	B	B	X	B		R	R																					F					
8H-3, 120-120	65.4	69.11	F	M	T	B	B	X	B							F	R																		F			
8H-4, 30-30	66	69.71	F	M	T	B	B	X	B							R	R		T								R						F				
8H-4, 60-60	66.3	70.01	F	M	B	B	B	X	B								R	T		F										R							
8H-4, 90-90	66.6	70.31	T	M	B	B	B	X	B														T															
8H-CC, 18-23	69.63	73.34	R	P	B	B	B	X	B		T												T	X											T			
9H-CC, 13-18	79.99	83.68	T	P	B	B	B	B	B											T																		

Table T8 (continued).

Core, section, interval (cm)	Depth (mbsf)	Depth (mcd)	*Fragilariopsis separanda*	*Fragilariopsis weaveri*	*Hemidiscus cuneiformis*	*Hemidiscus karstenii*	*Nitzschia* aff. *januaria*	*Proboscia barboi*	*Rhizosolenia bergonii*	*Rhizosolenia antennata* fo. *semispina*	*Rhizosolenia hebetata* fo. *semispina*	*Rhizosolenia styliformis*	*Roperia tesselata*	*Rouxia antarctica*	*Stellarima stellaris*	*Stephanopyxis turris*	*Thalassionema nitzschioides*	*Thalassionema nitzschioides* fo. 1	*Thalassionema nitzschioides* var. *parva*	*Thalassiosira convexa*	*Thalassiosira convexa* var. *aspinosa*	*Thalassiosira eccentrica*	*Thalassiosira fasciculata*	*Thalassiosira gracilis*	*Thalassiosira inura*	*Thalassiosira kolbei*	*Thalassiosira lentiginosa*	*Thalassiosira leptopus*	*Thalassiosira* aff. *lineata*	*Thalassiosira miocenica*	*Thalassiosira oestrupii*	*Thalassiosira oliverana*	*Thalassiosira tetraoestrupii* var. *reimeri*	*Thalassiosira trifulta*	*Thallassiothrix antarctica-longissima* group	Benthic diatoms, marine	Benthic diatoms, freshwater	Diatom zone	Diatom age (Ma)
177-1090A-																																							
1H-CC, 10-15	6.97	6.97																				R					R			R				F			*T. lentiginosa* Subzone c	0-0.18
177-1090B-																																							
1H-CC, 20-25	4.2	4.2				R							T				T	T									R			R				F			*T. lentiginosa* Subzone c	0-0.18
2H-CC, 0-10	13.8	13.8				C											R																	F			*T. lentiginosa* Subzone b	0.18-0.42
3H-1, 50-50	14.2	14.2																	R											F				R				
3H-1, 70-70	14.4	16.15																				R								R				R			*T. lentiginosa* Subzone a	0.42-0.65
3H-1, 100-100	14.7	16.45																				F					R			F				F		T		
3H-1, 140-140	15.1	16.85																																R				
3H-6, 50-50	21.7	23.45																												R				R			*A. ingens* Subzone c	0.65-1.07
3H-6, 70-70	21.9	23.65																																C				
3H-6, 92-92	22.12	23.87																																C				
3H-CC, 13-18	22.28	24.03																									F			R	R			F				
4H-4, 40-40	28.1	30.61														R											R			R	R							
4H-5, 10-10	29.3	31.81																									R			R				R				
4H-CC, 12-17	32.51	35.02																									R				R			F				
5H-6, 130-130	41.5	44.81														R											F			F	R			F				
5H-CC, 14-19	41.4	45.01				F		R								R											F			R	R			F			*A. ingens* Subzone a *P. barboi*	1.3-1.8 1.8 - 2
6H-1, 30-30	42.5	44.1						F																						R				C				
6H-CC, 9-14	51.84	53.44				T		R																			F				R			F			*T. kolbei/F. matuyamae*	2.0 - 2.5
7H-CC, 12-17	59.29	65.59			F	R																R			R			R		F				F			*F. interfrigidaria*	3.3-3.8
8H-2, 30-30	63.3	66.71				F																					R				R			F				
8H-2, 120-120	63.9	67.61														C		C																F			pre *F. interfrigidaria*	early Pliocene >3.8
8H-3, 90-90	65.1	68.81																										R		F				F				
8H-3, 120-120	65.4	69.11				R		R							R	F																					No zonation	Mixed ages
8H-4, 30-30	66	69.71				F																								R				F			No zonation	Mixed ages
8H-4, 60-60	66.3	70.01				F										F	R																				No zonation	Mixed ages
8H-4, 90-90	66.6	70.31																																			No zonation	early Miocene
8H-CC, 18-23	69.63	73.34																																T			No zonation	Neogene/ Paleogene
9H-CC, 13-18	79.99	83.68																																			No zonation	early Miocene

Table T8 (continued).

Core, section, interval (cm)	Depth (mbsf)	Depth (mcd)	Diatom abundance	Diatom preservation	Silicoflagellate occurrence	Ebridian occurrence	*Actiniscus* occurrence	Sponge spicule occurrence	Opaline phytolith occurrence	*Actinocyclus actinochilus*	*Actinocyclus curvatulus*	*Actinocyclus ingens*	*Actinoptychus senarius*	*Alveolus marinus*	*Asteromphalus parvulus*	*Azpeitia nodulifer*	*Azpeitia tabularis*	*Bogorovia mirabilis*	*Bogorovia veniamini*	*Cavitatus jouseanus*	*Chaetoceros* spp.	*Coscinodiscus marginatus*	*Coscinodiscus radiatus*	*Coscinodiscus rhombicus*	*Ethmodiscus rex*	*Eucampia antarctica*	*Fragilariopsis angulata*	*Fragilariopsis aurica*	*Fragilariopsis barronii*	*Fragilariopsis doliolus*	*Fragilariopsis fossilis*	*Fragilariopsis interfrigidaria*	*Fragilariopsis kerguelensis*	*Fragilariopsis matuyamae*	*Fragilariopsis mat.* var. *heterop.*	*Fragilariopsis praecurta*	*Fragilariopsis praeinterfrigidaria*	*Fragilariopsis reinholdii*	*Fragilariopsis ritscherii*
177-1090C-																																						
1H-CC, 14-19	2.8	3.16	F	M	T	B	B	X	B								F															C						
2H-CC, 11-16	10.06	15.63	F	M	T	B	B	X	B								F															C						
3H-CC, 9-19	21.01	27.26	A	M	B	B	B	X	B			R					R								X	R				T		C						
4H-CC, 8-13	30.28	36.59	F	M	B	X	B	X	B			T					R								X							F		T				
5H-CC, 9-14	40.19	48.24	C	M	B	B	B	X	B			F																	F				R	F					
6H-CC, 17-22	50.41	58.23	F	M	T	X	B	X	B			R					R				R				X										T				
7H-CC, 8-13	58.8	66.62	C	M	R	X	B	B	B			R					R				R				X				T		F	T			F			
8H-CC, 0-5	68.8	76.61	T																																			
177-1090D-																																						
1H-CC, 12-17	7.37	7.71	F	M	T	B	B	X	B								F													R		C						
2H-CC, 9-14	15.46	17.61	C	M	T	X	B	X	B								F								X	R						C						
3H-CC, 8-13	24.94	28.01	C	M	T	B	B	X	B			C		R			R								X					R	T	F						
4H-CC, 9-14	34.79	37.78	R	P	B	B	B	X	B								R					T			X							R			R			
5H-CC, 7-12	44.95	49.16	C	M	T	B	B	X	B			C													X				R					R				
6H-CC, 7-12	54.23	59.69	A	G	R	B	B	X	B			F																							R			
7H-CC, 17-22	62.9	68.98	F	M-P	T	B	B	X	B		R					F												F			R			R		F	R	R
177-1090E-																																						
1H-1, 110-110	1.1	4.48	T-R	P-M	B	B	B	X	B					T			R				R											C						
1H-3, 110-110	4.1	7.48	F	M	B	B	B	X	B					T			R				F		T			F						R						
1H-6, 100-100	8.5	11.88	R	M	T	B	B	X	B								C															C						
1H-CC, 8-13	8.65	12.03	R	P-M	R	B	B	X	B								R													R		C						
2H-2, 70-70	10.9	14.49	C	M	B	B	B	X	B								R				F					R						C						
2H-4, 70-70	13.9	17.49	C	M	T	B	B	X	B			R					C													R		C						
2H-5, 70-70	15.4	18.99	A-C	M	T	B	B	X	B			R			T		R						T			R						A						
2H-CC, 8-13	15.75	19.34	C	M	B	B	B	X	B																							C						
3H-2, 70-70	20.4	27.11	C	M	T	B	B	X	B		T	F					C															C						
3H-4, 70-70	23.4	30.11	C	M	B	B	B	B	B			R					F								X		T			R		C			R			

Table T8 (continued).

Core, section, interval (cm)	Depth (mbsf)	Depth (mcd)	*Fragilariopsis separanda*	*Fragilariopsis weaveri*	*Hemidiscus cuneiformis*	*Hemidiscus karstenii*	*Nitzschia* aff. *januaria*	*Proboscia barboi*	*Rhizosolenia bergonii*	*Rhizosolenia antennata* fo. *semispina*	*Rhizosolenia hebetata* fo. *semispina*	*Rhizosolenia styliformis*	*Roperia tesselata*	*Rouxia antarctica*	*Stellarima stellaris*	*Stephanopyxis turris*	*Thalassionema nitzschioides*	*Thalassionema nitzschioides* fo. 1	*Thalassionema nitzschioides* var. *parva*	*Thalassiosira convexa*	*Thalassiosira convexa* var. *aspinosa*	*Thalassiosira eccentrica*	*Thalassiosira fasciculata*	*Thalassiosira gracilis*	*Thalassiosira inura*	*Thalassiosira kolbei*	*Thalassiosira lentiginosa*	*Thalassiosira leptopus*	*Thalassiosira* aff. *lineata*	*Thalassiosira miocenica*	*Thalassiosira oestrupii*	*Thalassiosira oliverana*	*Thalassiosira tetraoestrupii* var. *reimeri*	*Thalassiosira trifulta*	*Thallassiothrix antarctica-longissima* group	Benthic diatoms, marine	Benthic diatoms, freshwater	Diatom zone	Diatom age (Ma)
177-1090C-																																						
1H-CC, 14-19	2.8	3.16															F										F		R						F			*T. lentiginosa* Subzone c	0-0.18
2H-CC, 11-16	10.06	15.63				T										F					R						R				T				F			*T. lentiginosa* Subzone a	0.42-0.65
3H-CC, 9-19	21.01	27.26																					T				F					R			C			*A. ingens* Subzone c	0.65-1.07
4H-CC, 8-13	30.28	36.59															F										F					T			C				
5H-CC, 9-14	40.19	48.24						F								R										R	F				R	R	R		F			*T. kolbei/F. matuyamae*	2-2.5
6H-CC, 17-22	50.41	58.23		R		F										R	R					T	R		T						R	R			F			lower *T. insigna*	2.8-3.3
7H-CC, 8-13	58.8	66.62				F	T				T					F	R								R		T								F	T		*F. interfrigidaria*	3.3-3.8
8H-CC, 0-5	68.8	76.61																																					
177-1090D-																																							
1H-CC, 12-17	7.37	7.71				T				T																	R					R			F			*T. lentiginosa* Subzone. b	0.18-0.42
2H-CC, 9-14	15.46	17.61									R						F										R								F			*T. lentiginosa* Subzone a	0.42-0.65
3H-CC, 8-13	24.94	28.01														R			T				R				R				T				F			*A. ingens* Subzone c	0.65-1.07
4H-CC, 9-14	34.79	37.78																									R					T			F				
5H-CC, 7-12	44.95	49.16						F			R	R														T	R				R	R	T		F			*T. kolbei/F. matuyamae*	2-2.5
6H-CC, 7-12	54.23	59.69		C	A	R		R			T														T										F			lower *T. insigna*	2.8-3.3
7H-CC, 17-22	62.9	68.98		F	F											F	F								R				T	R					F			pre *F. interfrigidaria*	early Pliocene >3.8
177-1090E-																																							
1H-1, 110-110	1.1	4.48							T							R											R					R			F			*T. lentiginosa* Subzone c	0-0.18
1H-3, 110-110	4.1	7.48				F				F																	R						T		C			*T. lentiginosa* Subzone b	0.18-0.42
1H-6, 100-100	8.5	11.88				R										F															R	T			F				
1H-CC, 8-13	8.65	12.03				R										R						T													F				
2H-2, 70-70	10.9	14.49														R		R									F					R		T	F			*T. lentiginosa* Subzone a	0.42-0.65
2H-4, 70-70	13.9	17.49	T															T									F					F			F			*T. lentiginosa* Subzone a	0.42-0.65
2H-5, 70-70	15.4	18.99									T						T										F								F			*A. ingens* Subzone c	0.65-1.1
2H-CC, 8-13	15.75	19.34	T								T																F					T			F				
3H-2, 70-70	20.4	27.11								T																						R	R			C				
3H-4, 70-70	23.4	30.11																				T		T			R								F				

Table T8 (continued).

Core, section, interval (cm)	Depth (mbsf)	Depth (mcd)	Diatom abundance	Diatom preservation	Silicoflagellate occurrence	Ebridian occurrence	*Actiniscus* occurrence	Sponge spicule occurrence	Opaline phytolith occurrence	*Actinocyclus actinochilus*	*Actinocyclus curvatulus*	*Actinocyclus ingens*	*Actinoptychus senarius*	*Alveolus marinus*	*Asteromphalus parvulus*	*Azpeitia nodulifer*	*Azpeitia tabularis*	*Bogorovia mirabilis*	*Bogorovia veniamini*	*Cavitatus jouseanus*	*Chaetoceros* spp.	*Coscinodiscus marginatus*	*Coscinodiscus radiatus*	*Coscinodiscus rhombicus*	*Ethmodiscus rex*	*Eucampia antarctica*	*Fragilariopsis angulata*	*Fragilariopsis aurica*	*Fragilariopsis barronii*	*Fragilariopsis doliolus*	*Fragilariopsis fossilis*	*Fragilariopsis interfrigidaria*	*Fragilariopsis kerguelensis*	*Fragilariopsis matuyamae*	*Fragilariopsis mat.* var. *heterop.*	*Fragilariopsis praecurta*	*Fragilariopsis praeinterfrigidaria*	*Fragilariopsis reinholdii*	*Fragilariopsis ritscherii*
3H-CC, 10-15	24.56	31.27	C-F	M	T	B	B	X	B		T	R				F													R			C				R	
4H-2, 70-70	29.9	36.05	A	M	B	B	X	B	B			R																	F	T		C					
4H-4, 70-70	32.9	39.05	C	M	B	B	B	X	B			R				R						T		X								F					
4H-5, 70-70	34.4	40.55	F	M	B	X	B	B	B			F				R								X		T						C			T		
4H-CC, 15-20	35.35	41.5	C	M	T	B	X	X	X			R												X						R		F			R		
5H-1, 70-70	37.9	46.19	F	M	B	B	B	B				T																R									
5H-2, 70-70	39.4	47.69	F	M	B	B	B	B	B			R									R			X				R				F					
5H-3, 70-70	40.6	48.89	F	M	B	B	B	B	B	T		F												X				C				R	C	F			
5H-4, 70-70	42.1	50.39	C	M	R	B	X	B	B		T													X								R	C				
5H-6, 30-30	45.1	52.99	F	M	B	B	B	B	B													R		X				F					C	F			
5H-CC, 13-18	44.85	53.14	F	P	T	B	B	X	B			T										R		X				F					R			R	
6H-2, 70-70	48.9	57.32	F	M	B	B	B	B	B																					R						R	
6H-4, 70-70	51.9	60.32	F	M	B	B	B	X	B		T	F				R												R		R	R					R	
6H-5, 70-70	53.4	61.82	F	M-P	B	B	B	B	B																											R	
6H-6, 20-20	54.9	62.82	C	M	T	B	B	X	B																					F	R					R	
6H-CC, 10-15	54.54	62.96	A	M	T	X	B	X	B			T				R					R			X				R			F	R		T		C	
7H-2, 70-70	58.4	67.29	C	G	R	B	B	B	B			R			F	F								X							R	T				R	
7H-3, 70-70	59.9	68.79	F	M	B	B	B	X	B															X							F						
7H-CC, 17-22	65.19	74.08	T	M	B	B	B	B	B													T															
8H-CC, 9-14	75.31	83.86	R-T	P	T	B	B	B	B				F									C						T			T						

Notes: Abundance abbreviations: A = abundant, C = common, F = few, R = rare, T = trace, X = present, B = barren. Preservation abbreviations: G = good, M = moderate, P = poor. For more specific definitions, refer to the **"Explanatory Notes"** chapter. This table is also available in ASCII format in the **TABLES** directory.

Table T8 (continued).

Core, section, interval (cm)	Depth (mbsf)	Depth (mcd)	*Fragilariopsis separanda*	*Fragilariopsis weaveri*	*Hemidiscus cuneiformis*	*Hemidiscus karstenii*	*Nitzschia* aff. *januaria*	*Proboscia barboi*	*Rhizosolenia bergonii*	*Rhizosolenia antennata* fo. *semispina*	*Rhizosolenia hebetata* fo. *semispina*	*Rhizosolenia styliformis*	*Roperia tesselata*	*Rouxia antarctica*	*Stellarima stellaris*	*Stephanopyxis turris*	*Thalassionema nitzschioides*	*Thalassionema nitzschioides* fo. 1	*Thalassionema nitzschioides* var. *parva*	*Thalassiosira convexa*	*Thalassiosira convexa* var. *aspinosa*	*Thalassiosira eccentrica*	*Thalassiosira fasciculata*	*Thalassiosira gracilis*	*Thalassiosira inura*	*Thalassiosira kolbei*	*Thalassiosira lentiginosa*	*Thalassiosira leptopus*	*Thalassiosira* aff. *lineata*	*Thalassiosira miocenica*	*Thalassiosira oestrupii*	*Thalassiosira oliverana*	*Thalassiosira tetraoestrupii* var. *reimeri*	*Thalassiosira trifulta*	*Thallassiothrix antarctica-longissima* group	Benthic diatoms, marine	Benthic diatoms, freshwater	Diatom zone	Diatom age (Ma)
3H-CC, 10-15	24.56	31.27																									F				R			F				
4H-2, 70-70	29.9	36.05																												R	R			C				
4H-4, 70-70	32.9	39.05										T											R							R	R			C				
4H-5, 70-70	34.4	40.55	R			R																								R		T		F				
4H-CC, 15-20	35.35	41.5				R					T						R							R			F			R				C				
5H-1, 70-70	37.9	46.19				T		R									T													R		R		C			*P. barboi*	1.8-2
5H-2, 70-70	39.4	47.69				T		T									T										F			R		R		F				
5H-3, 70-70	40.6	48.89						F			T												T								R		R		F			*T. kolbei/F. matuyamae*	2-2.5
5H-4, 70-70	42.1	50.39						C				T															R							F				
5H-6, 30-30	45.1	52.99						C		T																	F				F			F				
5H-CC, 13-18	44.85	53.14				T		F			R																R				T	T		F				
6H-2, 70-70	48.9	57.32		F	T	C										F		T							T				R				C			lower *T. insigna*	2.8-3.3
6H-4, 70-70	51.9	60.32		F	F	R		R						T				C									F			R	R			F				
6H-5, 70-70	53.4	61.82		R	F																									F				F				
6H-6, 20-20	54.9	62.82			F											C	C								R					F		R				*F. interfrigidaria*	3.3-3.8
6H-CC, 10-15	54.54	62.96		F	R	R					T					R	F		T						R					F			C			*F. interfrigidaria*	3.3-3.8
7H-2, 70-70	58.4	67.29			R												C				R	R								F			C			*F. interfrigidaria*	3.3-3.8
7H-3, 70-70	59.9	68.79				R										R	F																			No zonation	Mixed ages
7H-CC, 17-22	65.19	74.08																																				
8H-CC, 9-14	75.31	83.86						T																														

Table T9. Control points used to calculate sedimentation rates at Site 1090. (Continued on next page.)

Code	Event/Zone/Chron	Depth range of stratigraphic datums: Top Core, section, interval (cm)	Top Depth (mbsf)	Top Depth (mcd)	Base Core, section, interval (cm)	Base Depth (mbsf)	Base Depth (mcd)	Mean Depth (mbsf)	Mean Depth (mcd)	Age (Ma)	Sedimentation rate (m/m.y.)
		177-			177-						
DIAT	TOP *T. lentiginosa* Subzone b	1090A-1H-CC, 10-15	6.97	6.97	1090E-1H-3, 110-110	4.1	7.48	5.54	7.23	0.19	
CN	FO *E. huxleyi*	1090B-2H-1, 130-130	5.50	5.50	1090B-2H-2, 30-30	6.00	6.00	5.75	5.75	0.26	
DIAT	BOT *T. lentiginosa* Subzone b	1090B-2H-CC, 0-10	13.80	13.80	1090E-2H-2, 70-70	10.90	14.49	12.35	14.15	0.42	~24
CN	LO *P. lacunosa*	1090B-3H-1, 40-40	14.10	15.85	1090B-3H-1, 130-130	15.00	16.75	14.55	16.30	0.46	
DIAT	TOP *A. ingens* Subzone c	1090D-2H-CC, 9-14	15.46	17.61	1090E-2H-5, 70-70	15.40	18.99	15.43	18.30	0.65	
PMAG	BOT C1n (Brunhes)	1090C-3H-4, 120-120	18.00	24.25	1090C-3H-5, 90-90	19.20	25.54	18.60	24.89	0.78	
CN	LO *R. asanoi*	1090B-4H-3, 30-30	26.50	29.01	1090B-4H-3, 130-130	27.50	30.01	27.00	29.51	0.88	
PMAG	TOP C1r.1n (Jaramillo)	1090C-4H-2, 130-130	24.60	30.91	1090C-4H-3, 70-?	25.40	31.71	25.00	31.31	0.99	~35
CN	RE *Gephyrocapsa* medium (4-5.5 µm)	1090B-4H-6, 30-30	31.00	33.51	1090B-4H-6, 130-130	32.00	34.51	31.50	34.01	0.96-1.02	
PMAG	BOT C1r.1n (Jaramillo)	1090C-4H-4, 140-140	27.70	34.01	1090C-4H-5, 60-60	28.40	36.45	28.05	35.23	1.07	
CN	FO *R. asanoi*	1090B-4H-CC, 12-17	32.51	35.02	1090B-5H-1, 35-35	33.05	36.66	32.78	35.84	1.08	
CN	LO *Gephyrocapsa* large (>5.5 µm)	1090B-5H-1, 35-35	33.05	36.66	1090B-5H-1, 130-130	34.00	37.61	33.53	37.14	1.24	
CN	FO *Gephyrocapsa* large (>5.5 µm)	1090B-5H-3, 30-30	36.61	39.61	1090B-5H-3, 110-110	36.80	40.41	36.71	40.01	1.46	
CN	LO *C. macintyrei*	1090B-5H-5, 30-30	39.00	42.31	1090B-5H-5, 130-130	40.30	43.31	39.65	42.81	1.60	
DIAT	TOP *A. ingens* Subzone a	1090E-4H-CC, 15-20	35.35	41.50	1090B-5H-CC, 14-19	41.40	45.01	38.38	43.26	1.30	
PMAG	TOP C2n (Olduvai)	1090C-5H-3, 100-100	35.30	43.35	1090C-5H-4, 20-20	36.00	44.05	35.65	43.70	1.77	
CN	FO *Gephyrocapsa* medium (4-5.5 µm)	1090B-5H-6, 30-30	40.50	43.81	1090B-5H-6, 130-130	41.50	44.81	41.00	44.31	1.69	~12
DIAT	TOP *P. barboi* Zone	1090B-5H-6, 130-130	41.50	44.81	1090B-5H-CC, 14-19	41.40	45.01	41.45	44.91	1.80	
PMAG	BOT C2n (Olduvai)	1090C-5H-5, 30-30	37.60	45.65	1090C-5H-5, 90-90	38.20	46.25	37.90	45.95	1.95	
DIAT	TOP *T. kolbei-F. matuyamae* Zone	1090E-5H-2, 70-70	39.40	47.69	1090C-5H-CC, 9-14	40.19	48.24	39.80	47.97	2.00	
PMAG	BOT C2r (Matuyama)	1090C-6H-4, 130-130	46.60	54.42	1090C-6H-5, 40-40	47.20	55.02	46.90	54.72	2.58	
DIAT	TOP *T. insigna* Subzone a	1090B-6H-CC, 9-14	51.84	53.44	1090E-6H-2, 70-70	48.90	57.32	50.37	55.38	2.80	
DIAT	TOP *F. interfrigidara* Zone	1090E-6H-5, 70-70	53.40	61.82	1090E-6H-6, 20-20	54.90	62.82	54.15	62.32	3.26	
DIAT	BOT *F. interfrigidara* Zone	1090B-8H-2, 90-90	63.90	67.31	1090B-8H-2, 120-120	63.90	67.61	63.90	67.46	3.80	
	early Pliocene/early Miocene hiatus	1090D-7H-CC, 17-22	62.90	68.98	1090B-8H-4, 90-90	66.60	70.31	64.75	69.65	—	
DIAT	LO *T. spumellaroides*	1090E-9H-5, 70-70	81.90	91.81	1090B-10H-3, 70-70	88.40	98.77	85.15	95.29	19.0	
DIAT	BOT *T. fraga* Zone	1090E-11H-2, 70-70	96.40	106.21	1090E-12H-3, 70-70	107.40	116.61	101.90	111.41	20.9	
RAD	TOP *L. conica* Zone	1090B-13H-CC, 0-5	117.12	122.53	1090B-14H-CC, 0-5	127.51	131.16	122.32	126.85	22.5	
DIAT	BOT *T. spumellaroides* Zone	1090E-13H-1, 70-70	113.90	123.51	1090E-13H-5, 70-70	119.90	129.51	116.90	126.51	22.6	~10
DIAT	LO *R. vigilans*	1090B-16H-CC, 0-10	146.75	153.40	1090B-17H-CC, 14-24	154.36	161.86	150.56	157.63	25.5	
DIAT	BOT *R. gelida* Zone	1090B-18H-CC, 6-16	165.37	173.15	1090B-20H-CC, 22-32	184.42	192.03	174.90	182.59	26.5	
RAD	TOP *A. irregularis* Zone	1090B-21X-CC, 15-25	194.09	202.14	1090B-22X-CC, 0-10	203.69	211.30	198.89	206.72	24.1-?28.7	
CN	LO *R. umbilica*	1090B-23X-7, 30-30	213.40	220.70	1090B-23X-7, 130-130	214.40	221.70	213.90	221.20	31.3	
CN	LO *I. recurvus*	1090B-23X-7, 130-130	214.40	221.70	1090B-23X-CC, 26-36	213.76	222.16	214.08	221.93	31.8	
CN	Acme *Clausicoccus* spp.	1090B-24X-5, 130-130	221.10	232.06	1090B-24X-7, 110-110	222.90	233.86	222.00	232.96	33.3	
RAD	TOP *E. spinosum* Zone	1090B-25X-CC, 19-27	236.74	252.21	1090B-27X-CC, 13-18	251.53	263.52	244.14	257.87	30.9-34.7	
CN	LO *D. saipanensis*	1090B-27X-5, 120-120	250.10	262.09	1090B-27X-6, 30-30	250.70	262.69	250.40	262.39	34.2	
CN	FO *I. recurvus*	1090B-31X-6, 30-30	289.50	301.49	1090B-31X-7, 30-30	291.00	302.99	290.25	302.24	36.0	~30

Table T9 (continued).

Code	Event/Zone/Chron	Depth range of stratigraphic datums: Top: Core, section, interval (cm)	Top: Depth (mbsf)	Top: Depth (mcd)	Base: Core, section, interval (cm)	Base: Depth (mbsf)	Base: Depth (mcd)	Mean: Depth (mbsf)	Mean: Depth (mcd)	Age (Ma)	Sedimentation rate (m/m.y.)
CN	FO *R. bisecta*	1090B-38X-CC, 8-18	349.12	361.11	1090B-39X-1, 130-130	350.50	362.49	349.81	361.80	38.0	
CN	LO *Nannotetrina* spp.	1090B-41X-CC, 0-5	372.58	384.57	1090B-4-2X-1, 120-120	378.40	390.39	375.49	387.48	43.1	~5

Notes: Code abbreviations: DIAT = diatom, CN = calcareous nannofossil, PMAG = magnetic polarity, RAD = radiolaria. Event abbreviations: FO = first occurrence, LO = last occurrence, RE = reentrance, TOP = top of zone, BOT = bottom of zone. This table is also available in ASCII format in the **TABLES** directory.

Table T10. Main components of the radiolarian assemblage at Site 1090. (Continued on next page.)

Core, section, interval (cm)	Depth (mbsf)	Depth (mcd)	Abundance	Preservation	*Actinomma delicatum*	*Antarctissa deflandrei*	*Antarctissa denticulata*	*Antarctissa longa*	*Axoprunum bispiculum*	*Axoprunum irregularis*	*Axoprunum pierinae*	*Botryostrobus aquilonaris*	*Botryostrobus auritus*	*Calocyclas* cf. *semipoita*	*Calocyclas* sp.	*Cycladophora antiqua*	*Cycladophora bicornis*	*Cycladophora davisiana*	*Cycladophora pliocenica*	*Cymaetron* sp.	*Cytocapsella* aff. *japonica*	*Cytocapsella longithorax*	*Cytocapsella robusta*	*Cytocapsella tetrapera*	*Eucyrtidium antiquum*	*Eucyrtidium calvertense*	*Eucyrtidium cienkowskii*	*Eucyrtidium (?) mariae*	*Eucyrtidium spinosum*	*Eurystomoskevos petrushevskayaae*	*Helothous vema*	*Lamprocyclas margatensis*	*Lamprocyclas* sp.
177-1090A-																																
1H-CC, 10-15	6.97	6.97																														
177-1090B-																																
1H-CC, 20-25	4.20	4.2	C	M			F					A						F	F						F							
2H-CC, 0-10	13.80	13.8																														
3H-CC, 13-18	22.28	24.03																														
4H-CC, 12-17	32.51	35.02	A	G	F		F		F			C	F					C														
5H-CC, 14-19	41.40	45.01																														
6H-CC, 9-14	51.84	53.44																														
7H-CC, 12-17	59.29	65.59	A	E	F		F						F				C								C							
8H-CC, 18-23	69.63	73.34	A	E										R								F	C						R		R	
9H-CC, 13-18	79.99	83.68																														
10H-CC, 19-24	88.41	92.98																														
11H-CC, 10-15	99.16	103.15	A	E												F						F	C				F					
12H-CC, 6-11	108.89	112.56	A	E					F							F					F	F	F				F					F
13H-CC, 0-5	117.12	122.53	A	E					F							F						F	R									F
14H-CC, 0-5	127.51	131.16	A	E					F						R	R					F							F		F		
15H-CC, 0-10	136.73	143.22	A	G					F																							F
16H-CC, 0-10	146.75	153.4																														
17H-CC, 14-24	154.36	161.86																														
18H-CC, 6-16	165.37	173.15																														
19H-CC, 24-34	173.14	182.63	A	E					C					F									F									F
20H-CC, 22-32	184.42	192.03																														
21X-CC, 15-25	194.09	202.14	A	E					F						F								F									F
22X-CC, 0-10	203.69	211.3	A	E					F	C				F									F						F			F
23X-CC, 26-36	213.76	222.16	A	E					F		F			F											F							
24X-CC, 18-28	223.25	234.21																														
25X-CC, 19-27	233.01	243.72																														
26X-CC, 10-15	242.73	254.72																														
27X-CC, 13-18	251.53	263.52	A	E							F			F	F														F	F		
28X-CC, 16-21	262.19	274.18																														
29X-CC, 17-22	271.87	283.86																														
30X-CC, 21-34	281.60	293.68																														
31X-CC, 21-26	291.50	303.43	A	E					F					F															F			
32X-CC, 27-32	294.38																															
33X-CC, 13-18	297.73	309.39																														
34X-CC, 12-20	310.7	322.69																														
35X-CC, 17-20	319.91	331.9	C	G										F	F														F			
36X-CC, 26-34	330.12	342.11																														
37X-CC, 40-45	337.16	349.15																														
38X-CC, 8-18	349.12	361.11	B																													
39X-CC, 12-22	358.78	370.77	B																													
40X-CC, 21-31	368.55	380.49																														
41X-CC, 0-5	372.58	384.57																														
42X-CC, 22-27	387.50	399.49																														
43X-CC, 29-39	397.59	409.58	B																													
177-1090C-																																
1H-CC, 14-19	2.8	3.16	C	M								A	F					C														
2H-CC, 11-16	10.06	15.63																														
3H-CC, 9-19	21.01	27.26																														
4H-CC, 8-13	30.28	36.59																														
5H-CC, 9-14	40.19	48.24																														
6H-CC, 17-22	50.41	58.23																														
7H-CC, 8-13	58.88	66.62	A	E		F							C						F						C							

Table T10 (continued).

Core, section, interval (cm)	Depth (mbsf)	Depth (mcd)	Abundance	Preservation	*Actinomma delicatum*	*Antarctissa deflandrei*	*Antarctissa denticulata*	*Antarctissa longa*	*Axoprunum bispiculum*	*Axoprunum irregularis*	*Axoprunum pierinae*	*Botryostrobus aquilonalis*	*Botryostrobus auritus*	*Calocyclas* cf. *semipolita*	*Calocyclas* sp.	*Cycladophora antiqua*	*Cycladophora bicornis*	*Cycladophora davisiana*	*Cycladophora pliocenica*	*Cymaetron* sp.	*Cyrtocapsella* aff. *japonica*	*Cyrtocapsella longithorax*	*Cyrtocapsella robusta*	*Cyrtocapsella tetrapera*	*Eucyrtidium antiquum*	*Eucyrtidium calvertense*	*Eucyrtidium cienkowskii*	*Eucyrtidium (?) mariae*	*Eucyrtidium spinosum*	*Eurystomoskevos petrushevskayaae*	*Helotholus vema*	*Lamprocyclas margatensis*	*Lamprocyclas* sp.
8H-CC, 0-5	68.8	76.61	A	E					F	F														C								
177-1090D-																																	
1H-CC, 12-17	7.37	7.71	C	M			F		F			F						F															
2H-CC, 9-14	15.46	17.61																															
3H-CC, 8-13	24.94	28.01																															
4H-CC, 9-14	34.79	37.78	A	E			F	F	F			F	F				F	F								F							
5H-CC, 7-12	44.95	49.16																															
6H-CC, 7-12	54.23	59.69																															
7H-CC, 17-22	62.9	68.98	A	E					F								F		F					F		F							
8H-CC, 17-22	73.97	79.88	A	E					F					F										F			F		F				
9H-CC, 7-12	82.95	90.48																															
10H-CC, 20-25	93.16	100.69																															
11H-CC, 20-25	101.84	108.97																															
12H-CC, 0-5	111.65	118.78	A	E					F							R						F		F									F
13H-CC, 0-10	120.54	127.43																															
14H-CC, 0-10	130.66	137.91																															
15H-CC, 17-22	140.06	146.53																															
16H-CC, 0-5	149.51	158.15	A	E					F						F							F	F		F								
17H-CC, 16-21	159.33	169.21																															
18H-CC, 9-14	168.46	180.16																															
20H-CC, 17-22	187.47	198.32	C	E											F																		
21H-CC, 0-10	197.25	208.18																															
22H-CC, 51-56	207.21	218.91																															
23H-CC, 33-38	215.14	227.77																															
24H-CC, 0-6	226.02	237.66	A	E					F					F						F					F								
177-1090E-																																	
1H-CC, 8-13	8.65	12.03	C	M			F					F	F					F															
2H-CC, 8-13	15.75	19.34																															
3H-CC, 10-15	24.56	31.27																															
4H-CC, 15-20	35.35	41.5	A	G			F											F															
5H-CC, 13-18	44.85	53.14																															
6H-CC, 10-15	54.54	62.96	A	E		F													F							F					R		
7H-CC, 17-22	65.19	74.08	A	E					F															F									F
8H-CC, 9-14	75.31	83.86																															
9H-CC, 8-13	84.53	94.44																															
10H-CC, 18-23	93.38	103.75																															
11H-CC, 0-10	103.4	113.21	A	E												F						F		F			F						F
12H-CC, 0-5	112.32	121.53																															
13H-CC, 12-17	121.65	131.26																															
14H-CC, 14-19	131.74	140.89																															
15H-CC, 0-10	141.53	152.34	A	E					F					F						F			F	F									F
16H-CC, 29-39	150.99	163.05																															
17H-CC, 0-10	160.78	173.21																															
18H-CC, 14-24	170.04	184.77																															
19H-CC, 12-22	179.72	192.78	A	E					F																								
20H-CC, 14-24	188.76	202.7																															
21H-CC, 0-10	198.78	212.9																															
22H-CC, 0-10	208	221.44																															
23H-CC, 20-27	213.94	229.3	A	E					F					F						F					F					F			
24H-CC, 11-16	225.84	241.25																															
25H-CC, 12-17	236.74	252.21	A	E					F					F						F					F					F			

Notes: Abundance abbreviations: A = abundant, C = common, F = few, R = rare, B = barren. Preservation abbreviations: E = excellent, G = good, M = moderate. For more specific definitions, refer to **"Biostratigraphy,"** p. 10, in the "Explanatory Notes" chapter. This table is also available in ASCII format in the **TABLES** directory.

Table T11. Concentrations of methane at Site 1090.

Core, section, interval (cm)	Depth (mbsf)	C_1 (ppmv)
177-1090B-		
1H-3, 0-5	2.52	6
2H-5, 0-5	10.22	5
3H-5, 0-5	19.73	3
4H-5, 0-5	29.22	2
5H-4, 0-5	36.93	2
6H-5, 0-5	48.22	2
7H-5, 0-5	57.72	2
8H-4, 0-5	65.72	4
9H-5, 0-5	76.73	2
10H-5, 0-5	86.22	2
11H-5, 0-5	95.72	2
12H-5, 0-5	105.22	3
13H-5, 0-5	114.72	5
14H-5, 0-5	124.22	4
15H-5, 0-5	133.72	5
16H-5, 0-5	143.22	4
17H-4, 0-5	151.22	4
18H-5, 0-5	162.22	4
19H-5, 0-5	171.72	5
20H-2, 0-5	176.72	5
21X-5, 0-5	190.72	4
22X-5, 0-5	200.42	6
23X-4, 0-5	208.62	6
24X-5, 0-5	219.82	5
25X-5, 0-5	229.52	6
26X-5, 0-5	239.22	4
28X-5, 0-5	258.62	4
32X-2, 0-5	292.90	9
34X-5, 0-5	307.12	8
35X-5, 0-5	316.82	5
36X-5, 0-5	326.42	7
37X-4, 0-5	334.52	6
38X-5, 0-5	345.62	4
39X-5, 0-5	355.22	3
40X-5, 0-5	364.82	2
43X-5, 0-5	393.82	2

Note: C_1 = methane.

Table T12. Interstitial water chemistry at Site 1090. (Continued on next page.)

Core, section, interval (cm)	Depth (mbsf)	pH	Method	Alkalinity (mM)	Method	Salinity	Method	Cl (mM)	Method	SO_4 (mM)	Method	Na (mM)	Method	Mg (mM)	Method	Ca (mM)	Method
177-1090B-																	
1H-2, 95-100	2.4	7.91	ISE	3.063	T	35.5	R	555	T	27.44	I	480	CB	50.5	I	10.5	I
2H-4, 145-150	10.2	7.47	ISE	3.576	T	35.5	R	561	T	27.57	I	483	CB	51.3	I	11.1	I
3H-4, 145-150	19.7	7.73	ISE	3.763	T	35.5	R	562	T	27.15	I	483	CB	51.0	I	11.5	I
4H-4, 145-150	29.2	7.68	ISE	4.122	T	35.5	R	564	T	25.89	I	483	CB	50.6	I	12.2	I
5H-3, 115-120	36.9	7.48	ISE	3.766	T	35.5	R	563	T	25.90	I	482	CB	49.9	I	12.5	I
6H-4, 145-150	48.2	7.50	ISE	3.727	T	35.5	R	562	T	26.04	I	480	CB	49.7	I	13.1	I
7H-4, 145-150	57.7	7.53	ISE	3.587	T	35.0	R	562	T	26.27	I	481	CB	49.3	I	13.4	I
8H-3, 140-150	65.7	7.61	ISE	3.341	T	35.0	R	558	T	26.30	I	477	CB	48.0	I	14.6	I
9H-4, 140-150	76.7	7.68	ISE	3.445	T	34.5	R	557	T	25.41	I	471	CB	48.9	I	15.0	I
10H-4, 140-150	86.2	7.58	ISE	3.162	T	34.5	R	562	T	25.41	I	480	CB	47.5	I	15.0	I
11H-4, 140-150	95.7	7.59	ISE	3.212	T	35.0	R	563	T	26.86	I	478	CB	48.8	I	15.9	I
12H-4, 140-150	105.2	7.58	ISE	3.041	T	35.0	R	559	T	25.62	I	474	CB	47.6	I	16.1	I
13H-4, 145-150	114.7	7.43	ISE	3.398	T	35.0	R	559	T	25.82	I	476	CB	46.3	I	16.7	I
14H-4, 145-150	124.2	7.58	ISE	3.112	T	35.5	R	563	T	24.92	I	477	CB	46.2	I	17.2	I
15H-4, 145-150	133.7	7.56	ISE	2.987	T	35.5	R	564	T	25.16	I	478	CB	46.2	I	17.7	I
16H-4, 145-150	143.2	7.56	ISE	2.926	T	35.5	R	562	T	25.59	I	476	CB	45.9	I	18.4	I
17H-3, 145-150	151.2	7.57	ISE	3.129	T	35.5	R	563	T	25.30	I	479	CB	45.0	I	18.3	I
18H-4, 145-150	162.2	7.64	ISE	3.123	T	35.5	R	562	T	25.03	I	475	CB	44.8	I	19.8	I
19H-4, 140-150	171.7	7.54	ISE	2.738	T	35.5	R	564	T	25.54	I	479	CB	44.6	I	19.5	I
20H-4, 140-150	181.1	7.48	ISE	2.901	T	35.5	R	564	T	25.21	I	478	CB	44.7	I	19.9	I
21X-4, 140-150	190.7	7.72	ISE	2.784	T	35.5	R	563	T	24.75	I	479	CB	43.6	I	19.5	I
22X-4, 140-150	200.4	7.57	ISE	2.811	T	35.5	R	562	T	24.20	I	474	CB	44.2	I	20.5	I
23X-3, 140-150	208.6	7.26	ISE	2.780	T	35.5	R	564	T	25.14	I	478	CB	43.8	I	20.5	I
24X-4, 140-150	219.8	7.48	ISE	2.433	T	35.0	R	565	T	24.86	I	480	CB	43.9	I	19.7	I
25X-4, 140-150	229.5	7.27	ISE	2.599	T	35.0	R	566	T	24.81	I	482	CB	43.3	I	20.1	I
26X-4, 140-150	239.2	7.62	ISE	2.530	T	35.0	R	565	T	25.73	I	482	CB	43.6	I	20.2	I
28X-4, 145-150	258.6	7.72	ISE	2.557	T	35.5	R	565	T	24.46	I	480	CB	42.9	I	20.2	I
32X-1, 140-150	292.9	7.85	ISE	2.007	T	35.5	R	571	T	20.61	I	484	CB	25.4	I	35.7	I
34X-4, 140-150	307.1	7.80	ISE	1.267	T	35.0	R	571	T	18.97	I	480	CB	25.5	I	35.8	I
35X-4, 145-150	316.8	7.26	ISE	1.101	T	35.5	R	572	T	19.40	I	482	CB	26.0	I	35.2	I
36X-4, 140-150	326.4	7.60	ISE	1.111	T	35.5	R		T	19.75	I		CB	26.9	I	34.1	I
38X-4, 140-150	345.6	7.65	ISE	1.707	T	35.5	R	573	T	19.51	I	487	CB	24.7	I	34.9	I
40X-4, 140-150	364.8	7.60	ISE	1.623	T	35.5	R	573	T	17.64	I	481	CB	24.5	I	36.3	I
43X-4, 140-150	392.3	7.61	ISE	1.819	T	35.5	R	574	T	18.33	I	487	CB	22.8	I	36.1	I

Note: Method abbreviations: ISE = ion selective electrode, T = titration, R = refractometer, I = ion chromatography, CB = charge balance calculation, S = spectrophotometry, AAS = atomic absorption spectrometry, AES = atomic emission spectrometry.

Table T12 (continued).

Core, section, interval (cm)	Depth (mbsf)	K (mM)	Method	H_4SiO_4 (µM)	Method	NH_4 (µM)	Method	HPO_4 (µM)	Method	Sr (µM)	Method	Fe (µM)	Method	Mn (µM)	Method	Li (µM)	Method
177-1090B-																	
1H-2, 95-100	2.4	11.2	I	653	S	36	S	7.1	S	100	AAS	3.0	AAS	12.9	AAS	24.9	AES
2H-4, 145-150	10.2	12.0	I	740	S	106	S	6.8	S	134	AAS	-0.1	AAS	9.3	AAS	24.0	AES
3H-4, 145-150	19.7	11.9	I	809	S	146	S	5.9	S	157	AAS	0.0	AAS	6.7	AAS	24.1	AES
4H-4, 145-150	29.2	11.3	I	787	S	161	S	5.5	S	178	AAS	0.3	AAS	6.2	AAS	24.1	AES
5H-3, 115-120	36.9	11.6	I	772	S	148	S	2.5	S	188	AAS	7.6	AAS	6.2	AAS	24.8	AES
6H-4, 145-150	48.2	11.5	I	847	S	139	S	2.7	S	206	AAS	7.2	AAS	6.7	AAS	25.5	AES
7H-4, 145-150	57.7	11.5	I	858	S	132	S	1.8	S	206	AAS	4.9	AAS	9.8	AAS	26.6	AES
8H-3, 140-150	65.7	11.4	I	806	S	118	S	1.7	S	214	AAS	1.6	AAS	33.0	AAS	29.0	AES
9H-4, 140-150	76.7	11.7	I	809	S	113	S	1.2	S	241	AAS	0.0	AAS	34.0	AAS	30.9	AES
10H-4, 140-150	86.2	11.4	I	779	S	108	S	0.9	S	240	AAS		AAS	38.6	AAS	29.5	AES
11H-4, 140-150	95.7	11.8	I	819	S	110	S	2.0	S	252	AAS	-0.2	AAS	39.7	AAS	30.9	AES
12H-4, 140-150	105.2	11.2	I	826	S	102	S	1.8	S	246	AAS		AAS	46.4	AAS	29.8	AES
13H-4, 145-150	114.7	11.5	I	888	S	83	S	1.7	S	263	AAS	-0.7	AAS	54.1	AAS	32.2	AES
14H-4, 145-150	124.2	11.4	I	883	S	88	S	2.0	S	280	AAS	0.6	AAS	56.1	AAS	32.3	AES
15H-4, 145-150	133.7	10.8	I	920	S	81	S	1.7	S	288	AAS	0.8	AAS	71.1	AAS	32.7	AES
16H-4, 145-150	143.2	10.8	I	922	S	76	S	2.0	S	288	AAS		AAS	69.0	AAS	32.5	AES
17H-3, 145-150	151.2	10.5	I	933	S	76	S	1.8	S	303	AAS	0.0	AAS	72.1	AAS	33.2	AES
18H-4, 145-150	162.2	10.7	I	986	S	81	S	1.0	S	313	AAS		AAS	77.8	AAS	33.6	AES
19H-4, 140-150	171.7	10.0	I	973	S	73	S	1.0	S	318	AAS	-0.2	AAS	73.6	AAS	34.4	AES
20H-4, 140-150	181.1	9.8	I	1022	S	73	S	1.0	S	338	AAS	0.8	AAS	75.2	AAS	34.2	AES
21X-4, 140-150	190.7	9.6	I	977	S	69	S	1.5	S	313	AAS	0.1	AAS	68.5	AAS	34.0	AES
22X-4, 140-150	200.4	9.5	I	1001	S	74	S	1.3	S	342	AAS	0.4	AAS	74.2	AAS	34.4	AES
23X-3, 140-150	208.6	9.9	I	1027	S	81	S	1.2	S	350	AAS	-0.1	AAS	70.6	AAS	35.3	AES
24X-4, 140-150	219.8	9.4	I	995	S	85	S	0.9	S	342	AAS	0.8	AAS	65.4	AAS	34.9	AES
25X-4, 140-150	229.5	8.9	I	1080	S	76	S	0.9	S	351	AAS	7.7	AAS	59.2	AAS	35.3	AES
26X-4, 140-150	239.2	8.9	I	1069	S	92	S	0.9	S	361	AAS	9.6	AAS	54.1	AAS	35.7	AES
28X-4, 145-150	258.6	9.4	I	1155	S	92	S	0.9	S	370	AAS	0.7	AAS	55.6	AAS	35.5	AES
32X-1, 140-150	292.9	5.7	I	1035	S	180	S	0.7	S	906	AAS	2.0	AAS	86.5	AAS	56.1	AES
34X-4, 140-150	307.1	6.1	I	1039	S	196	S	0.7	S	872	AAS	1.7	AAS	79.3	AAS	57.2	AES
35X-4, 145-150	316.8	5.8	I	1044	S	194	S	0.9	S	859	AAS	1.9	AAS	83.4	AAS	57.2	AES
36X-4, 140-150	326.4	5.6	I	828	S	180	S	0.9	S	860	AAS	0.7	AAS	82.4	AAS	56.4	AES
38X-4, 140-150	345.6	5.4	I	665	S	196	S	0.9	S	921	AAS	0.2	AAS	95.3	AAS	67.0	AES
40X-4, 140-150	364.8	5.4	I	464	S	212	S	0.7	S	950	AAS		AAS	90.6	AAS	72.2	AES
43X-4, 140-150	392.3	5.1	I	467	S	233	S	0.5	S	993	AAS	1.2	AAS	54.1	AAS	71.3	AES

Table T13. Concentrations of IC, $CaCO_3$, TC, TOC, TN, TS, and TOC/TN at Site 1090. (Continued on next page.)

Core, section, interval (cm)	Depth (mbsf)	IC (wt%)	$CaCO_3$ (wt%)	TC (wt%)	TOC (wt%)	TN (wt%)	TS (wt%)	TOC/TN
177-1090B-								
1H-1, 74-75	0.74	6.28	52.3	6.80	0.53	0.12	0.06	4.5
1H-3, 74-75	3.24	10.27	85.6					
2H-1, 72-73	4.92	8.77	73.0	8.55	0.00	0.08	0.00	
2H-3, 72-73	7.92	8.94	74.5					
2H-5, 72-73	10.92	9.03	75.2					
3H-1, 75-76	14.45	9.86	82.1	9.82	0.00	0.06	0.00	
3H-3, 75-76	17.45	9.60	79.9					
3H-5, 75-76	20.45	10.51	87.6					
4H-3, 73-74	26.93	7.26	60.5	7.43	0.17	0.09	0.03	2.0
4H-5, 72-73	29.92	9.46	78.8					
5H-2, 72-73	34.92	9.34	77.8					
5H-4, 72-73	37.62	4.67	38.9	4.75	0.08	0.08	0.00	1.0
5H-6, 73-74	40.63	9.43	78.5					
6H-1, 74-75	42.94	10.26	85.4					
6H-3, 74-75	45.94	10.03	83.6					
6H-5, 74-75	48.94	8.59	71.6	8.52	0.00	0.06	0.00	
7H-3, 74-75	55.44	9.36	78.0	9.23	0.00	0.05	0.00	
7H-5, 74-75	58.44	10.14	84.5					
8H-2, 22-23	62.92	9.18	76.5					
8H-3, 76-77	64.96	7.97	66.4					
8H-4, 123-124	66.93	0.09	0.7	0.30	0.22	0.06	0.00	3.9
8H-5, 75-76	67.95	0.09	0.7					
9H-4, 75-76	75.95	3.67	30.6					
9H-6, 75-76	78.95	0.18	1.5	0.53	0.35	0.07	0.00	4.7
10H-1, 120-121	81.40	7.38	61.5					
10H-3, 72-73	83.92	5.60	46.7	5.49	0.00	0.05	0.00	
10H-5, 72-73	86.92	6.25	52.1					
11H-1, 109-110	90.79	4.59	38.2					
11H-3, 74-75	93.44	3.35	27.9	3.18	0.00	0.06	0.00	
11H-5, 23-24	95.93	4.13	34.4					
11H-7, 46-47	98.56	7.16	59.6					
12H-1, 75-76	99.95	8.85	73.7	8.69	0.00	0.06	0.00	
12H-3, 75-76	102.95	9.24	77.0					
12H-5, 75-76	105.95	9.64	80.3					
13H-2, 72-73	110.92	0.44	3.6	0.67	0.24	0.07	0.12	3.4
13H-4, 72-73	113.92	2.75	22.9					
13H-6, 49-50	116.69	2.26	18.8					
14H-2, 75-76	120.45	2.59	21.6	2.99	0.40	0.08	0.00	5.0
14H-4, 75-76	123.45	2.30	19.2					
14H-6, 75-76	126.45	5.26	43.8					
15H-1, 118-119	128.88	3.05	25.4					
15H-3, 75-76	131.45	2.23	18.6	2.56	0.33	0.08	0.00	4.1
15H-5, 75-77	134.45	7.28	60.7					
16H-1, 74-75	137.94	4.72	39.3					
16H-3, 74-75	140.94	5.90	49.1					
16H-5, 74-75	143.94	3.07	25.6	3.05	0.00	0.08	0.00	
17H-1, 123-124	147.93	4.29	35.7					
17H-3, 73-74	150.43	6.24	51.9					
17H-5, 34-35	153.04	1.60	13.3	1.71	0.11	0.07	0.00	1.6
18H-1, 122-123	157.42	0.14	1.2					
18H-3, 22-23	159.42	0.13	1.1	0.42	0.29	0.07	0.07	4.1
18H-5, 74-75	162.94	0.10	0.9					
19H-1, 60-61	166.30	2.88	24.0					
19H-3, 87-88	169.57	7.50	62.5					
19H-5, 72-73	172.42	1.82	15.2	2.03	0.21	0.07	0.00	3.0
20H-1, 72-73	175.92	1.74	14.5					
20H-3, 74-75	178.94	0.15	1.2	0.47	0.32	0.08	0.00	4.0
20H-5, 74-75	181.94	4.33	36.1					
21X-1, 75-76	185.45	2.56	21.4					
21X-3, 75-76	188.45	1.05	8.8	1.31	0.26	0.07	0.09	3.7
21X-5, 75-76	191.45	1.59	13.2					
22X-1, 75-76	195.15	1.51	12.6					
22X-4, 75-76	199.65	0.07	0.6	0.32	0.25	0.07	0.10	3.6
22X-5, 75-76	201.15	0.07	0.6					
23X-1, 75-76	204.85	0.91	7.6	0.98	0.07	0.09	0.08	0.8
23X-3, 75-76	207.85	6.88	57.3					
23X-5, 75-76	209.75	5.62	46.8					

Table T13 (continued).

Core, section, interval (cm)	Depth (mbsf)	IC (wt%)	$CaCO_3$ (wt%)	TC (wt%)	TOC (wt%)	TN (wt%)	TS (wt%)	TOC/TN
23X-7, 75-76	212.75	2.49	20.8					
24X-1, 69-70	214.49	4.40	36.7	4.35	0.00	0.05	0.00	
24X-3, 69-70	217.49	7.41	61.7					
24X-5, 87-88	220.67	8.28	69.0					
25X-1, 60-61	224.10	7.83	65.2					
25X-3, 60-61	227.10	7.53	62.7					
25X-5, 60-61	230.10	3.37	28.0	3.48	0.11	0.08	0.20	1.4
26X-3, 21-22	236.41	1.28	10.7	1.43	0.15	0.07	0.11	2.1
26X-5, 22-23	239.42	4.85	40.4					
26X-7, 16-17	242.36	0.13	1.1					
27X-1, 96-97	243.86	1.73	14.4	1.86	0.13	0.06	0.09	2.2
27X-2, 97-98	245.37	5.69	47.4					
27X-4, 100-101	248.40	1.87	15.6					
28X-3, 29-30	255.89	4.46	37.1					
28X-4, 93-94	258.03	2.39	19.9	2.56	0.17	0.08	0.10	2.1
28X-7, 34-35	261.94	1.02	8.5					
29X-1, 45-46	262.75	1.88	15.6					
29X-3, 22-23	265.52	0.40	3.3	0.77	0.37	0.08	0.63	4.6
29X-5, 108-109	269.38	1.98	16.5					
30X-1, 125-126	273.25	5.98	49.8					
30X-3, 20-21	275.20	1.71	14.2	1.72	0.02	0.05	0.14	0.4
30X-6, 30-31	279.80	0.53	4.4					
31X-3, 64-65	285.34	4.82	40.1	4.72	0.00	0.05	0.00	0.0
31X-4, 72-73	286.92	1.09	9.1					
32X-2, 47-48	293.37	2.41	20.1	2.91	0.50	0.05	0.06	9.7
33X-2, 90-91	296.67	1.10	9.2	1.50	0.41	0.04	0.08	10.4
34X-3, 61-62	304.71	0.45	3.8	0.81	0.36	0.05	0.05	7.6
34X-6, 44-45	309.04	2.11	17.6					
35X-2, 47-48	312.77	1.08	9.0	1.19	0.11	0.04	0.00	2.6
35X-5, 60-61	317.40	7.32	61.0					
36X-4, 70-71	325.60	0.54	4.5	0.60	0.06	0.05	0.00	1.2
36X-5, 91-92	327.31	6.21	51.7					
37X-1, 70-71	330.70	6.93	57.8	7.26	0.33	0.05	0.00	6.5
37X-4, 70-71	335.20	8.03	66.9					
38X-1, 70-71	340.30	1.27	10.5	1.62	0.36	0.06	0.00	6.3
38X-3, 70-71	343.30	0.14	1.2					
38X-5, 70-71	346.30	9.49	79.0					
39X-1, 70-71	349.90	1.22	10.1	1.23	0.01	0.05	0.00	0.3
39X-3, 70-71	352.90	0.07	0.6					
39X-5, 70-71	355.90	0.13	1.1					
40X-1, 70-71	359.50	10.06	83.8					
40X-3, 70-71	362.50	9.99	83.2					
40X-5, 70-71	365.50	3.94	32.8	4.20	0.27	0.05	0.00	5.2
41X-1, 84-85	369.24	4.74	39.5	5.35	0.61	0.06	0.00	10.7
41X-3, 84-85	372.24	10.44	86.9					
42X-2, 93-94	380.53	5.54	46.1	5.83	0.29	0.05	0.00	5.9
42X-6, 84-85	386.44	10.41	86.7					
43X-1, 67-68	388.47	8.02	66.8	8.28	0.26	0.04	0.00	5.7
43X-5, 57-58	394.37	10.89	90.7					

Note: IC = inorganic carbon, $CaCO_3$ = calcium carbonate, TC = total carbon, TOC = total organic carbon, TN = total nitrogen, TS = total sulfur.

Table T14. Physical properties measurements conducted at Site 1090.

Measurement	Core 177-1090A-	Core 177-1090B-	Core 177-1090C-	Core 177-1090D-	Core 177-1090E-
GRA sample spacing	1H: 2 cm	1H-20H: 2 cm; 21X-43X: 4 cm	1H-8H: 2 cm	1H-24H: 2 cm	1H-8H-2: 4 cm; 8H3-13H-3: 2 cm 13H-4-25H: 4 cm
MS sample spacing	1H: 2 cm	1H-20H: 2 cm; 21X-43X: 4 cm	1H-8H: 2 cm	1H-24H: 2 cm	1H-8H-2: 4 cm; 8H-3-13H-3: 2 cm; 13H-4-25H: 4 cm
NGR sample spacing	—	1H-20H: 2 cm; 21X-31X-2: 4 cm; 31X-3-43X: 8 cm	—	—	1H-25H: 8 cm
PWL sample spacing	—	1H-20H: 2 cm; 21X-24X: 4 cm	—	3H-24H: 2 cm	1H-8H-2: 4 cm; 8H-3-13H-3: 2 cm; 13H-4-25H: 4 cm
OSU-SCAT sample spacing	1H: 4 cm	1H-20H: 4 cm; 21X-23X: 6 cm	—	1H-9H: 4 cm; 10H-24H: 6 cm	Selected sections in 2H, 3H, 6H-8H, 13H, 14H, 21H-24H
CM-2002 sample spacing	—	29X-31X, 34X, 36X-43X: 2-5 cm	—	—	—
PWS3	*N* = 15	*N* = 296	—	*N* = 235	—
MAD	*N* = 4	*N* = 147	—	—	—
TC	—	*N* = 33	*N* = 8	*N* = 24	*N* = 22

Notes: GRA = gamma-ray attenuation, MS = magnetic susceptibility, NGR = natural gamma radiation, PWL = *P*-wave logger, OSU-SCAT = Oregon State University Split Core Analysis Track, CM-2002 = Minolta spectrophotometer, PWS3 = *P*-wave velocity sensor 3 for split cores, MAD = moisture and density, TC = thermal conductivity.

Table T15. Thermal conductivity measurements at Site 1090. (Continued on next two pages.)

Core, section, interval (cm)	Depth (mbsf)	Depth (mcd)	TC (W/[m·K])	Start (s)	Length (s)	End (s)
177-1090B-						
1H-3, 75	3.25	3.25	0.99	25.5	26.5	52
4H-3, 75	26.95	29.46	0.94	109	30.5	140
4H-3, 75	26.95	29.46	0.95	57	25.5	82.5
5H-3, 75	36.45	40.06	1.02	49.5	27	76.5
5H-3, 75	36.45	40.06	0.99	82	25	107
6H-3, 75	45.95	47.55	1.08	78.5	25	104
6H-3, 75	45.95	47.55	1.04	99.5	25	125
7H-3, 75	55.45	61.75	1	43	28.5	71.5
12H-3, 75	103	106.6	0.96	99.5	25	125
12H-3, 75	103	106.6	0.95	75.5	33.5	109
13H-3, 75	112.5	117.9	0.7	122	25	147
13H-3, 75	112.5	117.9	0.73	63.5	25	88.5
14H-3, 75	122	125.6	0.83	116	26	142
14H-3, 75	122	125.6	0.85	63.5	25	88.5
15H-3, 75	131.5	137.9	0.78	105	27	132
16H-3, 75	141	147.6	0.83	124	26	150
16H-3, 75	141	147.6	0.83	117	25	142
18H-3, 75	160	167.7	0.74	122	25.5	148
18H-3, 75	160	167.7	0.75	89	25	114
20H-3, 50	178.7	186.3	0.77	60.5	27.5	88
20H-3, 50	178.7	186.3	0.74	124	25.5	150
21X-3, 50	188.2	196.3	0.67	115	27	142
21X-3, 50	188.2	196.3	0.69	58.5	26	84.5
22X-4, 75	199.7	207.3	0.66	123	25	148
22X-4, 75	199.7	207.3	0.67	92.5	32.5	125
23X-3, 50	207.6	216	0.9	26	25	51
23X-3, 50	207.6	216	0.86	112	25.5	137
24X-3, 70	217.5	228.5	0.84	115	29	144
24X-3, 70	217.5	228.5	0.89	63	28	91
25X-3, 60	227.1	237.8	0.85	96	25	121
25X-3, 60	227.1	237.8	0.89	27	25	52
26X-3, 50	236.7	248.7	0.78	30.5	25	55.5
26X-3, 50	236.7	248.7	0.78	35	27	62
27X-3, 50	246.4	258.4	0.73	86.5	25	112
27X-3, 50	246.4	258.4	0.72	84	25	109
28X-3, 50	256.1	268.1	0.67	91.5	25	117
28X-3, 50	256.1	268.1	0.68	74	33	107
29X-3, 50	265.8	277.8	0.66	96	25	121
29X-3, 50	265.8	277.8	0.65	120	25.5	146
30X-3, 50	275.5	287.5	0.65	124	25.5	150
30X-3, 50	275.5	287.5	0.66	114	25	139
31X-3, 50	285.2	297.2	0.7	95	26	121
34X-3, 50	304.6	316.6	0.68	105	25	130
34X-3, 50	304.6	316.6	0.67	114	25	139
35X-3, 50	314.3	326.3	0.81	121	26.5	148
35X-3, 50	314.3	326.3	0.88	34.5	31.5	66
36X-3, 50	323.9	335.9	0.69	112	25	137
36X-3, 50	323.9	335.9	0.66	120	28.5	149
37X-3, 50	333.5	345.5	0.65	124	25	149
37X-3, 50	333.5	345.5	0.68	63	28.5	91.5
38X-3, 50	343.1	355.1	0.8	120	28	148
38X-3, 50	343.1	355.1	0.79	124	25	149
39X-3, 50	352.7	364.7	0.83	116	25	141
39X-3, 50	352.7	364.7	0.82	124	25.5	150
40X-3, 50	362.3	374.3	1.16	117	25	142
40X-3, 50	362.3	374.3	1.15	77	26	103
42X-3, 50	381.6	393.6	1.22	32.5	25	57.5
42X-3, 50	381.6	393.6	1.17	66	25	91
43X-3, 50	391.3	403.3	1.17	50.5	25	75.5
43X-3, 50	391.3	403.3	1.19	30.5	25.5	56
177-1090C-						
1H-2, 60	2.1	2.6	0.9	121	27	148
1H-2, 60	2.1	2.6	0.9	107	25	132
2H-3, 75	6.55	12.12	1.02	65	25	90
2H-3, 75	6.55	12.12	1.01	75	25	100
3H-3, 75	16.05	22.3	1.07	51.5	34.5	86

Table T15 (continued).

Core, section, interval (cm)	Depth (mbsf)	Depth (mcd)	TC (W/[m·K])	Start (s)	Length (s)	End (s)
3H-3, 75	16.05	22.3	1.02	89	25.5	115
4H-3, 75	25.55	31.86	1	83	25	108
4H-3, 75	25.55	31.86	1	48.5	25.5	74
5H-3, 75	35.05	43.1	1	48.5	27.5	76
5H-3, 75	35.05	43.1	0.98	70.5	25	95.5
6H-3, 75	44.55	52.37	1.09	63.5	25	88.5
6H-3, 75	44.55	52.37	1.1	25.5	25	50.5
7H-3, 75	54.05	61.87	1.1	119	26.5	145
7H-3, 75	54.05	61.87	1.13	38.5	25	63.5
8H-3, 75	63.55	71.36	0.82	85	25	110
177-1090D-						
1H-3, 75	3.75	4.09	0.95	71.5	25	96.5
2H-3, 50	10.9	13.05	1.01	103	25	128
2H-3, 50	10.9	13.05	1.06	53.5	25	78.5
3H-3, 50	20.4	23.47	1.03	32	26.5	58.5
4H-3, 50	29.9	32.89	1	122	26	148
4H-3, 50	29.9	32.89	1.02	73.5	25	98.5
5H-3, 50	39.4	43.61	1	112	25	137
5H-3, 50	39.4	43.61	1.01	119	25	144
6H-3, 50	48.9	54.36	0.95	118	25.5	143
6H-3, 50	48.9	54.36	0.96	111	25	136
7H-3, 50	58.4	64.48	0.97	119	25	144
7H-3, 50	58.4	64.48	1.02	82.5	25	108
8H-3, 50	67.9	73.81	0.82	97	26.5	124
8H-3, 50	67.9	73.81	0.82	59	25	84
9H-3, 50	77.4	84.93	0.83	68.5	25	93.5
9H-3, 50	77.4	84.93	0.84	111	26	137
9H-3, 50	77.4	84.93	0.8	99.5	25	125
9H-3, 50	77.4	84.93	0.78	117	26.5	144
10H-3, 75	87.15	94.68	0.9	117	25	142
11H-3, 75	96.65	103.8	0.84	84	26.5	111
11H-3, 75	96.65	103.8	0.83	111	25	136
12H-3, 75	106.2	113.3	0.77	117	25.5	143
12H-3, 75	106.2	113.3	0.79	41	25	66
13H-3, 75	115.7	122.5	0.84	51	25	76
13H-3, 75	115.7	122.5	0.85	25	27	52
14H-3, 75	125.2	132.4	0.84	46	25	71
14H-3, 75	125.2	132.4	0.84	50.5	27.5	78
15H-3, 75	134.7	141.1	0.91	58.5	26	84.5
15H-3, 75	134.7	141.1	0.89	87	25	112
16H-3, 75	144.2	152.8	0.82	68	25	93
16H-3, 75	144.2	152.8	0.8	122	26	148
17H-3, 75	153.7	163.5	0.75	95	25	120
17H-3, 75	153.7	163.5	0.75	111	25	136
18H-3, 75	163.2	174.9	0.83	81.5	25	107
18H-3, 75	163.2	174.9	0.83	66.5	25	91.5
19H-3, 75	172.7	185.3	0.77	111	25	136
19H-3, 75	172.7	185.3	0.75	121	26	147
20H-3, 75	182.2	193	0.76	97	34	131
20H-3, 75	182.2	193	0.8	26.5	27	53.5
21H-3, 75	191.7	202.6	0.77	55.5	25	80.5
21H-3, 75	191.7	202.6	0.75	89.5	25	115
22H-3, 75	201.2	212.9	0.8	107	28	135
22H-3, 75	201.2	212.9	0.83	45.5	25	70.5
23H-3, 75	210.7	223.3	0.79	105	27	132
23H-3, 75	210.7	223.3	0.79	109	25	134
24H-3, 75	220.2	231.8	0.94	112	25	137
24H-3, 75	220.2	231.8	0.91	117	25	142
177-1090E-						
1H-3, 75	3.75	7.13	0.98	49.5	26	75.5
2H-3, 75	12.45	16.04	1.01	113	25	138
2H-3, 75	12.45	16.04	1.03	115	29	144
3H-3, 75	21.95	28.66	0.93	102	25	127
3H-3, 75	21.95	28.66	0.94	71	33.5	105
4H-3, 75	31.45	37.6	1.03	97	25	122
4H-3, 75	31.45	37.6	1.03	90.5	25	116
5H-3, 75	40.65	48.94	1.05	68.5	25.5	94
5H-3, 75	40.65	48.94	1.05	65.5	25	90.5
6H-3, 75	50.45	58.87	1.14	26	25	51
6H-3, 75	50.45	58.87	1.14	25	26	51

Table T15 (continued).

Core, section, interval (cm)	Depth (mbsf)	Depth (mcd)	TC (W/[m·K])	Start (s)	Length (s)	End (s)
7H-3, 75	59.95	68.84	1.05	33	25	58
7H-3, 75	59.95	68.84	0.99	124	26	150
8H-3, 75	69.45	78	0.95	99.5	25	125
8H-3, 75	69.45	78	0.98	27	25	52
9H-3, 75	78.95	88.86	0.95	99.5	25	125
9H-3, 75	78.95	88.86	0.94	123	25	148
10H-3, 75	88.45	98.82	0.77	116	30	146
10H-3, 75	88.45	98.82	0.79	105	28	133
10H-3, 75	88.45	98.82	0.83	84.5	25	110
10H-3, 75	88.45	98.82	0.82	104	25.5	129
11H-3, 75	97.95	107.8	1.02	43	28	71
11H-3, 75	97.95	107.8	1.03	25	26.5	51.5
12H-3, 75	107.5	116.7	0.84	124	25.5	150
12H-3, 75	107.5	116.7	0.86	93	28.5	122
13H-3, 75	117	126.6	0.94	50	29	79
13H-3, 75	117	126.6	0.91	119	30	149
14H-3, 75	126.5	135.6	0.87	68	27.5	95.5
14H-3, 75	126.5	135.6	0.84	124	25.5	150
15H-3, 75	136	146.8	0.76	59	28.5	87.5
15H-3, 75	136	146.8	0.74	123	25	148
16H-3, 75	145.5	157.5	0.73	52	25	77
17H-3, 60	154.8	167.2	0.82	63	27	90
17H-3, 60	154.8	167.2	0.79	78.5	25	104
17H-3, 60	154.8	167.2	0.83	48.5	25	73.5
18H-3, 75	164.5	179.2	0.78	109	27	136
18H-3, 75	164.5	179.2	0.78	115	29	144
19H-3, 60	173.8	186.9	0.75	110	28	138
19H-3, 60	173.8	186.9	0.78	44.5	25	69.5
20H-3, 50	183.2	197.1	0.75	51	25	76
20H-3, 50	183.2	197.1	0.73	77	25.5	103
21H-3, 50	192.7	206.8	0.69	37	35.5	72.5
22H-3, 50	202.2	215.6	0.93	97	25	122
22H-3, 50	202.2	215.6	0.95	77	25.5	103

Notes: TC = thermal conductivity. Start, Length, and End refer to the interval of the time-temperature series used for the determination of thermal conductivity. This table is also available in ASCII format in the **TABLES** directory.